Mathematical Modeling and Computer Simulation of Mitotic Transition Control Mechanisms

Dissertation
to receive the degree Dr. rer. nat. from the
Department of Mathematics and Computer Science
Friedrich-Schiller-University Jena, Germany
submitted by

Maiko Lohel

born in Wesel, Germany
on September 19th, 1978

Examiners

1. Prof. Dr. Peter Dittrich, Department of Mathematics and Computer Science, Friedrich-Schiller-University Jena, Germany
2. Prof. Dr. habil. Bashar Ibrahim, Umm Al-Qura University, Kingdom of Saudi Arabia, and Department of Mathematics and Computer Science, Friedrich-Schiller-University Jena, Germany
3. Prof. Dr. Elmar Schiebel, Center for Molecular Biology, Ruprecht-Karls-University Heidelberg, Germany

Public defence: January 15th, 2016

Mathematical Modeling and Computer Simulation of Mitotic Transition Control Mechanisms

Dissertation
zur Erlangung des akademischen Grades
doctor rerum naturalium (Dr. rer. nat.)
vorgelegt dem Rat der Fakultät für Mathematik und Informatik
der Friedrich-Schiller-Universität Jena
von

Maiko Lohel

geboren am 19.09.1978 in Wesel

Gutachter

1. Prof. Dr. Peter Dittrich, Fakultät für Mathematik und Informatik, Friedrich-Schiller-Universität Jena
2. Prof. Dr. habil. Bashar Ibrahim, Umm Al-Qura Universität, Königreich Saudi-Arabien, und Fakultät für Mathematik und Informatik, Friedrich-Schiller-Universität Jena
3. Prof. Dr. Elmar Schiebel, Zentrum für Molekulare Biologie, Ruprecht-Karls-Universität Heidelberg

Tag der öffentlichen Verteidigung: 15. Januar 2016

Ehrenwörtliche Erklärung

Hiermit erkläre ich,

- dass mir die Promotionsordnung der Fakultät bekannt ist,

- dass ich die Dissertation selbst angefertigt habe, keine Textabschnitte oder Ergebnisse eines Dritten oder eigenen Prüfungsarbeiten ohne Kennzeichnung übernommen und alle von mir benutzten Hilfsmittel, persönliche Mitteilungen und Quellen in meiner Arbeit angegeben habe,

- dass ich die Hilfe eines Promotionsberaters nicht in Anspruch genommen habe und daß Dritte weder unmittelbar noch mittelbar geldwerte Leistungen von mir für Arbeiten erhalten haben, die im Zusammenhang mit dem Inhalt der vorgelegten Dissertation stehen,

- dass ich die Dissertation noch nicht als Prüfungsarbeit für eine staatliche oder andere wissenschaftliche Prüfung eingereicht habe.

Bei der Auswahl und Auswertung des Materials sowie bei der Herstellung des Manuskripts haben mich folgende Personen unterstützt:

* PD Dr. habil. Bashar Ibrahim, Fakultät für Mathematik und Informatik, Friedrich-Schiller-Universität Jena

* Dr. Gislene Pereira, Molekularbiologie von Zentrosomen und Zilien, Deutsches Krebsforschungszentrum, Heidelberg

Ich habe die gleiche, eine in wesentlichen Teilen ähnliche bzw. eine andere Abhandlung* bereits bei einer anderen Hochschule als Dissertation eingereicht: Ja / Nein*.
(* Zutreffendes unterstreichen)

Wenn Ja, Name der Hochschule: .....

Ergebnis: .....

Köln, den 01.06.2015

Unterschrift

Für Daniela und Emma.

Acknowledgements

I would like to express my gratitude to all the people who supported me in completing this thesis. In particular I wish to thank my advisors Bashar Ibrahim for countless passionate and fruitful discussions and his constant encouragement, and Gislene Pereira, who gave me the great opportunity to perform my thesis work in her lab. Furthermore, I want to thank Peter Dittrich for his valuable advice and continuous support.

I also appreciate the fellowship awarded by the International Graduate School for Cancer Research of the German Cancer Research Center in Heidelberg, which made this work possible.

No words can express my gratitude towards my family for all their love, patience and encouragement.

Abstract

The eukaryotic cell cycle is a tightly regulated sequence of processes leading from cell growth over DNA replication to the physical division of the mother into two daughter cells, each containing a complete set of chromosomes and organelles. Transition from one process to the next is guided by a number of crucial surveillance mechanisms, the so called cell cycle checkpoints. Dis-regulation of the cell cycle through checkpoint malfunction can lead to developmental defects and contribute to the development or progression of tumors. The cell cycle checkpoints are complex biochemical signal transduction networks, and their elaborate spatiotemporal dynamics are challenging to understand intuitively. Mathematical modeling and computer simulation can help to decrypt the underlying principles.

This thesis approaches two important mitotic checkpoints with mathematical modeling and simulation. The highly conserved spindle assembly checkpoint (SAC) guards the transition from meta- to anaphase, preventing premature segregation of the sister chromatids of the duplicated genome to the spindle poles. A very similar mechanism controls the corresponding transitions during meiosis, but this is not considered here because the focus of this thesis is solely on mitosis. In contrast to SAC, the spindle position checkpoint (SPOC) ensures that during asymmetric cell division in the budding yeast *S. cerevisiae* mitotic exit does not occur until the spindle is properly aligned with the cell polarity axis. Although there are no known homologs, there is indication that functionally similar checkpoints exist also in animal cells.

The first goal of this work was to understand the impact of localization of checkpoint key components to tiny subcellular structures. Therefore I extended a previously existing minimal model of the SAC to enable a detailed analysis of the kinetic consequences of localization and found that binding kinetics and stoichiometry are limiting factors for the overall dynamics of the SAC.

Second, a first detailed model of the SPOC should be developed. SPOC is build on regulation of a small guanosin-triphosphat hydrolayse (GTPase) through a GTPase-activating protein (GAP). GTPases are common intracellular signal transducers, thus I developed a general, physically meaningful and minimal model of the relevant GTPase reactions. This minimal model then served as the basis for the SPOC model. To constrain the model parameters, molecule numbers of the key components were determined by collaborating experimental biologists. The fully parameterized model made it eventually possible to draw important, non-trivial conclusions about the mode of operation of SPOC *in vivo*.

Both analyses provide valuable insights into mitotic transition control on a systems level and demonstrate that mathematical modeling, despite all unavoidable abstraction, constitutes a powerful tool for investigation of the dynamic properties of complex biological systems. The close combination of experimental work with rigorous mathematical models was central to the success of physics in our modern world. Similarly, systems biology joins forces from different disciplines to achieve a wholistic understanding of biological systems. This work aims at contributing to the development of this young multidisciplinary field.

Zusammenfassung

Der eukaryotische Zellzyklus ist eine straff regulierte Folge von Prozessen, die vom Zellwachstum über die DNS-Replikation hin zur physikalischen Teilung einer Mutter- in zwei Tochterzellen mit je einem vollständigen Satz an Chromosomen und Organellen führt. Der Übergang von einem Prozess zum Nächsten wird von einigen wesentlichen Kontrollmechanismen, den sogenannten "Checkpoints", überwacht. Deregulation des Zellzyklus durch Fehlfunktion eines Checkpoints kann zu Entwicklungsstörungen führen und zur Entstehung oder zum Wachstum von Tumoren beitragen. Die Checkpoints des Zellzyklus sind komplexe biochemische Signaltransduktionsnetze, deren ausgefeilte räumlich-zeitliche Dynamik intuitiv nur schwer zu erfassen ist. Mathematische Modellierung und Computersimulationen können dabei helfen, die zugrundeliegenden Prinzipien zu entschlüsseln.

Diese Dissertation behandelt zwei wichtige mitotische Checkpoints mittels mathematischer Modellierung und Simulation. Der stark konservierte "Spindle Assembly Checkpoint" (SAC) reguliert den Übergang von Meta- zur Anaphase und verhindert die vorzeitige Aufteilung der Schwesterchromatiden des replizierten Genoms zwischen den Spindelpolen. Ein sehr ähnlicher Mechanismus kontrolliert die entsprechenden Übergange in der Meiose, was hier allerdings keine Berücksichtigung finden, da der Schwerpunkt dieser Arbeit ausschliesslich auf der Mitose liegt. Im Gegensatz zum SAC stellt der "Spindle Position Checkpoint" sicher, dass während der asymmetrischen Zellteilung in der Bäckerhefe *S. cerevisiae* die Mitose nicht beendet wird, bis die Spindel entlang der Zellpolaritätsachse ausgerichtet ist. Zwar ist kein zum SPOC homologer Mechanismus bekannt, es gibt jedoch Hinweise auf die Existenz funktional ähnlicher Checkpoints in tierischen Zellen.

Das erste Ziel der Arbeit war, die Auswirkung der Lokalisierung zentraler Komponenten der Checkpoints an winzigen subzellulären Strukturen zu verstehen. Dazu habe ich ein bereits bestehendes minimales Modell des SAC erweitert, so dass eine detaillierte Analyse der kinetischen Auswirkungen der Lokalisierung möglich wurde. Es zeigte sich, dass Bindekinetik und Stöchiometrie limitierende Faktoren für die gesamte Dynamik des SAC sind.

Zweitens sollte ein erstes, detailliertes Model des SPOC entwickelt werden. Der SPOC basiert auf der Regelung einer kleinen Guanosintriphosphat-Hydrolase (GTPase) durch ein GTPase-aktivierendes Protein (GAP). GTPasen sind geläufige intrazelluläre Signalüberträger, daher habe ich ein allgemeines, physikalisch aussagefähiges und minimales Modell der relevanten GTPase-Reaktionen entwickelt. Dieses min-

imale Modell diente nachfolgend als Basis für das SPOC-Modell. Um die Modellparameter einzuschränken wurden die Molekülzahlen der Schlüsselkomponenten von mit uns zusammenarbeitenden experimentellen Biologen bestimmt. Das vollparametrisierte Modell hat es schliesslich ermöglicht, nicht triviale Schlüsse über die Arbeitsweise des SPOC *in vivo* zu ziehen.

Beide Analysen liefern wertvolle Erkenntnisse über die Kontrolle der Übergänge zwischen den Phasen der Mitose auf der Systemebene und zeigen, dass mathematische Modellierung trotz aller unvermeidlicher Abstraktion ein mächtiges Werkzeug zur Untersuchung der dynamischen Eigenschaften komplexer biologischer Systeme ist. Die Verbindung experimenteller Arbeit mit rigorosen mathematischen Modellen war wesentlich für den Erfolg der Physik in unserer modernen Welt. In ähnlicher Weise bündelt die Systembiologie Kräfte verschiedener Disziplinen um ein ganzheitliches Verständnis biologischer Systeme zu erreichen. Diese Arbeit soll einen kleinen Beitrag zur Entwicklung dieses jungen, multidisziplinären Feldes leisten.

Contents

List of Figures

List of Tables

1 Introduction

1.1 Overview

The eukaryotic cell cycle is the driving mechanism in development and maintenance of multicellular organisms. It is a tightly regulated sequence of processes culminating in the physical division of the mother into two daughter cells, each containing a complete set of chromosomes and organelles. Transition from one process to the next is guided by a number of crucial surveillance mechanisms coupling progress or proper completion of the preceding process to the activation of the next (Murray, 1992, 1995; Nigg, 2001; Tyson *et al.*, 2003). Dis-regulation of the cell cycle through malfunction of any of these so-called checkpoints can lead to developmental defects and contribute to the development or progression of tumors (Cimini *et al.*, 2005; Gordon *et al.*, 2012; Holland *et al.*, 2009; Kops *et al.*, 2005; Malumbres *et al.*, 2009; Weaver *et al.*, 2008).

The cell cycle checkpoints are signal transduction networks integrating biochemical and biophysical signals from different sources (Malumbres *et al.*, 2005; Morgan, 2007; Murray, 1992, 1995). Generating the appropriate biochemical response to the information provided by their various inputs requires the coordinated interplay of

many heterogeneous biochemical species (Deribe *et al.*, 2010; Jordan *et al.*, 2000). The inherent complexity of such networks limits our ability to intuitively understand their dynamics and how particular perturbations affect them (Kitano, 2002; Rao *et al.*, 2002; Westerhoff *et al.*, 2004). Approaching biological systems with the formal toolbox of mathematics and computer science, with mathematical modeling and computer simulation in particular, helps to overcome this limitation. Formal and *in-silico* models allow for manipulation and analysis of network features which often only with great effort or possibly not at all are accessible experimentally (Di Ventura *et al.*, 2006; T. Ideker *et al.*, 2001, 2003; Kitano, 2002).

This thesis approaches two important mitotic checkpoints with mathematical modeling and simulation. Both checkpoints delay cell cycle progression in response to errors related to the organization of the mitotic spindle apparatus (in the remainder of this text referred to as spindle). The highly conserved spindle assembly checkpoint (SAC) ensures that the sister chromatids of the duplicated genome are not separated and distributed to the spindle poles before all chromosomes have been properly attached to the spindle (Musacchio *et al.*, 2007). In turn, the spindle position checkpoint (SPOC) of the budding yeast *S. cerevisiae* monitors proper positioning of the spindle within the cell and delays exit from mitosis in case of errors (Caydasi, Ibrahim, *et al.*, 2010; Fraschini *et al.*, 2008). Thus, both checkpoints ensure necessary conditions for successful completion of mitosis. Improving our comprehension of how these vital surveillance mechanisms function is the aim of this work.

A common feature of both checkpoints is the localization of key components to small subcellular structures, essentially forming small reactive compartments which are not bounded by membranes. The models feature the localization of the respective key components and make it possible to study how this affects network dynamics.

This work is divided into five chapters. The remaining sections of this first chapter introduce briefly the biological background required for the reading of the other chapters. Furthermore, previous and possible approaches to modeling of the eukaryotic cell cycle are discussed. More detailed information on the biological background is provided in an introductory section in the beginning of each of the chapters two to four.

Chapter two presents a pseudo-spatial simulation of the SAC (Lohel *et al.*, 2009). SAC key components localize to the spindle-attachment sites of chromosomes and generate a cytosolic cell cycle-delaying signal until correct attachment shuts the signal off, chromosome by chromosome. The simulation focuses on the effect of the key components' localization and the stepwise decrease of signaling spindle-attachment

sites during the process of spindle assembly. The analysis of abstract models of the proposed checkpoint mechanism implies that the key components must bind to their chromosomal anchor with high affinity where they need to process the signaling molecule with high catalytic rate constants.

The third chapter shows how a minimal model for a small guanosine-triphosphate hydrolase (GTPase) can be derived such that the effects of two relevant antagonizing cofactors and available kinetic data can easily be incorporated in a physicochemichally meaningful way. GTPases play an important role in many signal transduction networks as slowly self-deactivating switches, considered active only when in complex with guanosine-triphosphate (GTP). GTP-hydrolysis by the catalytic domain leads to the inactive guanosine-diphosphate-bound form of the GTPase. The minimal GTPase-model constitutes the centerpiece of the model presented in the subsequent chapter.

In chapter four, a dynamical model of the SPOC is presented (Caydasi *et al.*, 2012). SPOC couples spindle alignment to exit from mitosis through a complex network regulating activity of a small GTPase. Thus, the GTPase-model from chapter three is incorporated into a compartmental model accounting for the dynamic localization of the GTPase and its SPOC-specific inhibitory cofactor to the spindle poles. Accounting for experimentally determined molecule numbers, the model implies that the GTPase needs to interact with its inhibitory cofactor in the cytoplasm and at the spindle poles as well. Additional analysis of the parameter space supports the existence of another yet unknown regulator of the inhibitory cofactor.

Finally a summary and outlook is given in chapter five.

1.2 Biological background: Cell cycle and Checkpoints

1.2.1 Cell cycle

The eukaryotic cell cycle is a tightly regulated sequence of events cumulating in the physical division of the parent cell into two daughter cells. As shown in Figure 1.1 (cf. Figure 1.2 for details), dividing cells pass through four major phases which consecutively accomplish cell growth (G1), genome and centrosome duplication (S), protein synthesis in preparation for mitosis (G2), and segregation of the duplicated DNA during mitosis (M). At the very end of mitosis cells eventually divide in a process termed cytokinesis. However, The duration of the different phases varies widely in different organisms. A comprehensive introduction into the cell cycle and its regulation is given in the book by Morgan (2007).

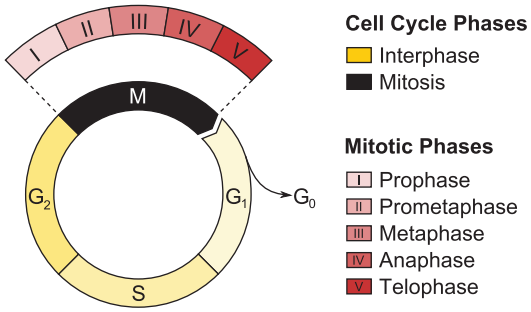

Figure 1.1: Phases of the eukaryotic cell cycle. See main text for details.

The sequence of G1, S, and G2 is termed interphase (yellow facets in Figure 1.1). Mitosis (black facet and enlargement in Figure 1.1) itself consists of five distinguishable stages, namely prophase, prometaphase, metaphase, anaphase and telophase (corresponding to roman numerals I-V in the enlargement in Figure 1.1; for details see Figure 1.2). During prophase, the nuclear DNA condenses into chromosomes (Hirano, 2000), the nuclear envelope disassembles (Georgatos *et al.*, 1997) and the microtubules, highly dynamic cytoskeletal fibers (Desai *et al.*, 1997), start to rearrange into the bipolar spindle apparatus (Gadde *et al.*, 2004; O'Connell *et al.*, 2007; Wittmann *et al.*, 2001). Throughout this rearrangement process, which continues in prometaphase, the microtubules attach to the kinetochores, complex proteinous structures forming at the centromere region of each chromosome already during prophase (Cheeseman *et al.*, 2008; Maiato *et al.*, 2004; McAinsh *et al.*, 2003; Westermann *et al.*, 2007). Mounting the chromosomes onto microtubules during prometaphase is a non-deterministic process (Holy *et al.*, 1994; T. U. Tanaka *et al.*, 2005; Wollman *et al.*, 2005), yet finally it is ensured that the two chromatids of each chromosome are attached to microtubules emanating from opposite spindle poles (Musacchio *et al.*, 2002, 2007). This state, where all chromosomes line up in the equatorial plate of the spindle apparatus, is termed metaphase. Shortly after, the cell progresses into anaphase, during which the two sister-chromatids of each chromosome are separated and rapidly pulled towards opposite spindle poles by the attached microtubules. Thereafter, in telophase the nuclear envelopes reassemble and cytokinesis begins.

A striking difference of mitosis in human and budding yeast cells is that the former undergo open mitosis while the latter undergo closed mitosis, that is, with ('open') or without ('closed') disassembly of the nuclear envelope during prophase.

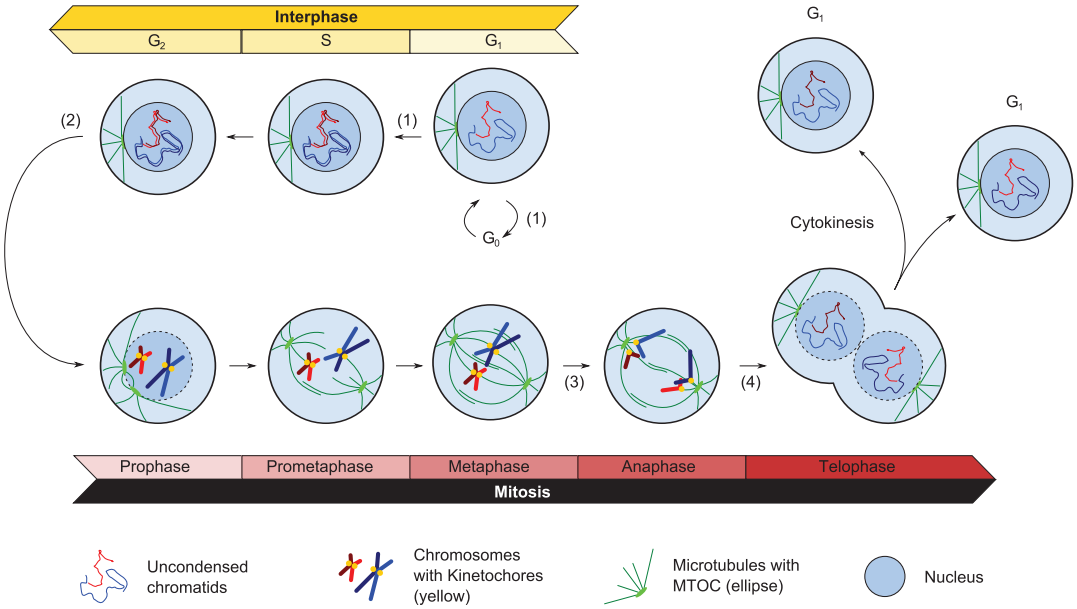

Figure 1.2: The eukaryotic cell cycle in detail. During G1, cells mature until they reach the restriction point (1) where they decide wether to commit to another cell cycle round or enter a resting state (G0). Past the restriction point, cells start replication of DNA and centrosome in S-phase. Before they can enter mitosis, the DNA damage checkpoint (2) ensures that the DNA has been correctly doubled. Upon entry into mitosis, the chromatids condense and the nuclear envelope disassembles. During prometaphase, the microtubules, which are now much more dynamic then during interphase, grow and shrink rapidly to explore the cellular space in order to attach to the kinetochores (yellow dots) at the chromosomes. At metaphase, all chromosomes are mounted on microtubules and line up in the equatorial plate. Transition from metaphase to anaphase, during which actual segregation of the DNA takes place, is guarded by the spindle assembly checkpoint (3). In asymmetrically dividing cells, mitotic exit needs to be coordinated with the spatial arrangement of the spindle aparatus. For instance, the spindle position checkpoint (4) prevents premature exit from mitosis in response to malpositioned spindles in budding yeast. Finally, cells exit mitosis and actual cell division takes place (cytokinesis).

1.2.1.1 The cell cycle is driven by a complex biochemical oscillator

Cell cycle progression is governed by the cyclin-dependent kinases (CDKs) together with their cyclin-cofactors (Enserink *et al.*, 2010; Malumbres *et al.*, 2005; Mendenhall *et al.*, 1998; Murray, 2004). While the level of the CDKs remains largely constant throughout the cell cycle, the cyclins levels differ vastly between the various phases

Phase	Budding yeast	Human
G1	Cln3	Cyclin D1, D2, D3
G1/S	Cln1, Cln2	Cyclin E
S	Clb5, Clb6	Cyclin A1, A2
M	Clb1, Clb2, Clb3, Clb4	Cyclin B1, B2

Table 1.1: Cyclins by cell cycle phase in budding yeast and human cells. Budding yeast and human cells as well feature many cyclins which do not notably contribute to cell cycle signaling and are thus not listed here (Malumbres *et al.*, 2005, 2009).

(Morgan, 2007; Murray, 2004; Sullivan *et al.*, 2007). So every phase features a different set of cyclins (see Table 1.1), which bind to the CDKs and define their specificity. The different cyclin-CDK complexes maintain the cellular machinery in a state appropriate to the tasks to be accomplished during the respective phases (Malumbres *et al.*, 2005; Mendenhall *et al.*, 1998; Murray, 2004). Most notably, cyclin-CDK complexes hallmarking one phase suppress activity of the cyclin-CDK complexes from the preceding phase while at the same time they enhance their own activity and promote expression of the cyclins required for the next phase (Amon *et al.*, 1993; Mendenhall *et al.*, 1998; Murray, 2004; Yeong *et al.*, 2001). Hence, positive and negative feedback loops drive the irreversible transitions from one phase to the next, making the cyclin-CDK system a complex biochemical oscillator (Novak *et al.*, 2008, 2007; Tyson *et al.*, 2003).

Cyclin levels are regulated by balancing transcription and translation with proteolytic degradation. Ubiquitin-ligase-complexes together with specificity-cofactors polyubiquitinate the cyclins and so tag them for recognition by the proteasome. The G1-cyclins (Cln1-3 in yeast and D- and E-type cyclins in human cells) are recognized by an Skp, cullin and F-box protein containing E3 ubiquitin ligase complex (SCF) in a phosphorylation dependent manner (King *et al.*, 1996; Mendenhall *et al.*, 1998; Siu *et al.*, 2012; Willems *et al.*, 1999). In contrast, proteolysis of S-phase and mitotic cyclins (Clb1-6 in yeast and A- and B-type cyclins in human cells) is initiated in mitosis through ubiquitination by another, tightly regulated E3 ubiquitin ligase, the anaphase promoting complex or cyclosome (APC/C; King *et al.* 1995; Sudakin *et al.* 1995).

1.2.1.2 Cell cycle checkpoints

Progression through the cell cycle is controlled by dedicated surveillance mechanisms ensuring that all requirements are met before transition from one phase to the next. The most important decision cells have to make is whether to commit to a new round of the cell cycle or not. To this end the restriction point in human cells (Pardee, 1974; Planas-Silva *et al.*, 1997; Weinberg, 1995) and START in budding yeast (Dirick *et al.*, 1995; Mendenhall *et al.*, 1998) monitor intracellular and extracellular cues in G1-phase and, if appropriate, activate a transcriptional program initiating the G1/S-transition (cf. (1) in Figure 1.2). Fidelity of DNA replication during S-phase is ensured by the G2/M or DNA damage checkpoint, which delays entry into mitosis in response do DNA damage to provide the repair-machinery with the necessary extra time (Branzei *et al.*, 2008; Zhou *et al.*, 2000) (cf. (2) in Figure 1.2). The metaphase-to-anaphase transition is guarded by the highly conserved spindle assembly checkpoint (SAC; Musacchio *et al.*, 2007). The SAC ensures adequate partitioning of the chromosomes between the spindle poles by delaying anaphase onset and sister-chromatid separation until all chromosomes are properly linked to the mitotic spindle (cf. (3) in Figure 1.2).

Budding yeast cells divide always asymmetrically by budding. They start growing the bud in G1, meaning that the mother-to-daughter cell polarity axis and the later site of cytokinesis is defined early in the cell cycle (A. S. Howell *et al.*, 2012; Pruyne *et al.*, 2000). Therefore, budding yeast requires two more checkpoints for reliable cell division. First, the morphogenesis checkpoint ensures maturation of the bud before cells are given permission to enter mitosis (Lew, 2003), thus serving as an additional G2/M-checkpoint. Second, the spindle position checkpoint (SPOC) ensures proper spindle alignment along with the cell polarity axis before exit from mitosis (cf. (4) in Figure 1.2; Caydasi, Ibrahim, *et al.*, 2010; Fraschini *et al.*, 2008). However, a similar checkpoint in asymmetrically dividing human cells has not been proven so far (Pereira *et al.*, 2012).

1.2.2 Spindle assembly checkpoint (SAC)

Before cytokinesis, sister-chromatids must be separated and distributed between the spindle poles such that both emerging daughter cells become genetically equal. To this end, cells make sure that the two kinetochores of every chromosome have been attached to microtubules emanating from opposite spindle poles before entering anaphase where the connections between the sister-chromatids are cut (compare

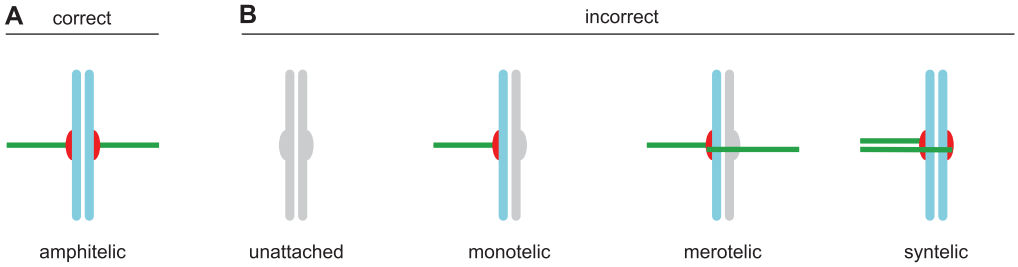

Figure 1.3: Microtubules can be attached to chromosomes in different ways. (**A**) Proper chromosome segregation in anaphase requires all chromosomes to have amphitelic attachment, that is, both kinetochores of every chromosome must be attached to microtubules from opposite poles. (**B**) Before all chromosomes have established amphitelic attachment, chromosomes having no or incorrect attachment are frequent intermediates. Erroneous connections between microtubules and kinetochores spontaneously detach, facilitating proper re-attachment. Chromosomes showing merotelic attachment have a kinetochore which is simultaneously attached to microtubules from opposite poles. In contrast, chromosomes with syntelic attachment have both kinetochores connected to microtubules from the same pole.

Figure 1.3A and 1.3B). If sister-chromatid separation occurs while not all erroneous attachments have been resolved, aneuploidy can result (Cimini *et al.*, 2005).

Consequently, a mechanism must exist which links the biophysical attachment status of the chromosomes to cell cycle progression. This mechanism, the spindle assembly checkpoint (Ciliberto *et al.*, 2009; Musacchio *et al.*, 2002, 2007; Shah *et al.*, 2000), broadcasts a 'wait'-signal from unattached kinetochores as is illustrated in Figure 1.4A. Upon microtubule attachment, the signaling pathway is turned off at the respective kinetochore (see Figure 1.4B). Importantly, the remaining unattached kinetochores are not affected and the cells manage to keep SAC-signaling upright until the last chromosome has been attached to the spindle.

But how do cells discriminate between chromosomes with both kinetochores properly connected to microtubules from opposite spindle poles (bi-polar attachment) from chromosomes which are not? Microtubules immediately start pulling the chromosome towards their spindle pole upon attachment, and tension develops between kinetochores only of correctly attached chromosomes (see Figure 1.4C). Indeed, lack of tension between kinetochores of sister-chromatids activates SAC-signaling, presumably by disconnecting the microtubules from incorrectly attached chromosomes (Maresca *et al.*, 2010; Nezi *et al.*, 2009; Stern *et al.*, 2001). However, whether sensing of tension is suitable and required for proper SAC response is not without debate

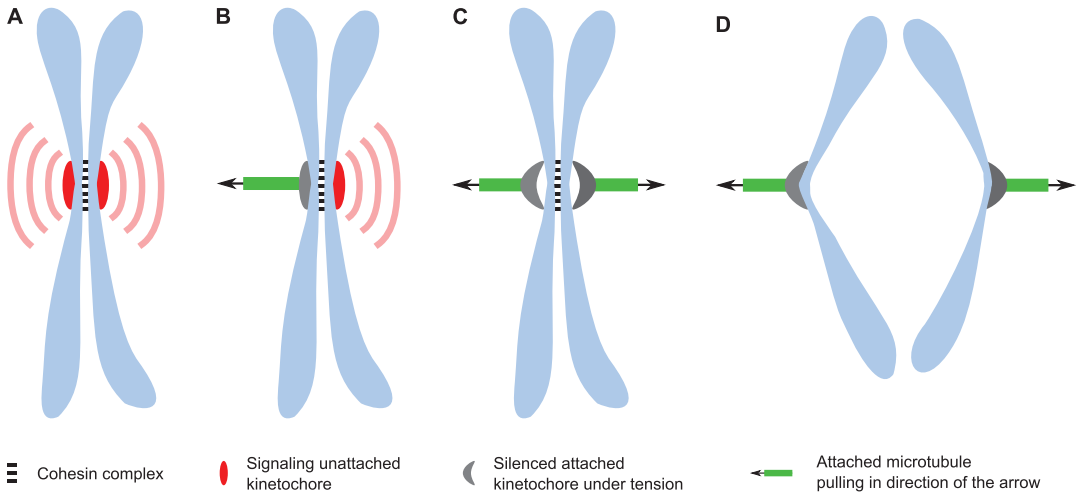

Figure 1.4: Dependency of spindle assembly checkpoint signaling on microtubule attachment and tension. (**A**) The SAC emits a cytosolic 'WAIT'-signal from kinetochores which are not attached to the spindle apparatus. (**B**) Attachment of microtubules to a kinetochore terminates its contribution to SAC-signaling while the connected microtubule-(+)-ends start to disassemble, pulling the chromosome towards the connected pole. However, the connection between the microtubules and the kinetochore remains unstable during monotelic attachment. (**C**) When both kinetochores are attached to microtubules from opposite poles, tension develops between the two kinetochores. This tension appears to stabilize the connection between the microtubules and kinetochores upon amphitelic attachment. (**D**) If the last kinetochore is attached to the mitotic spindle, SAC is turned off and gives way to cohesin cleavage, resulting in chromosome segregation.

(Khodjakov *et al.*, 2010).

Biochemically SAC delays cell cycle progress by preventing activation of APC/C, presumably mainly through sequestering the ACP/C-activator Cdc20 (cf. Figure 1.5A). Furthermore, degradation of Cdc20 might be necessary for maintaining the SAC active (Nilsson *et al.*, 2008). The active APC/C-Cdc20 complex is not only responsible for degradation of mitotic cyclins, additionally it tags securin (budding yeast Pds1) for degradation by the proteasome (Figure 1.5B). Securin binds and thereby inhibits separase (budding yeast Esp1), a protease required to cleave cohesin, which is the 'glue' connecting the two sister-chromatids of every chromosome (cf. Figures Figure 1.5B and 1.3). Thus, activation of APC/C by Cdc20 initiates sister-chromatid separation, which marks the transition to anaphase. The protein Mad2 is present in two stable conformations differing in the spatial arrangement of

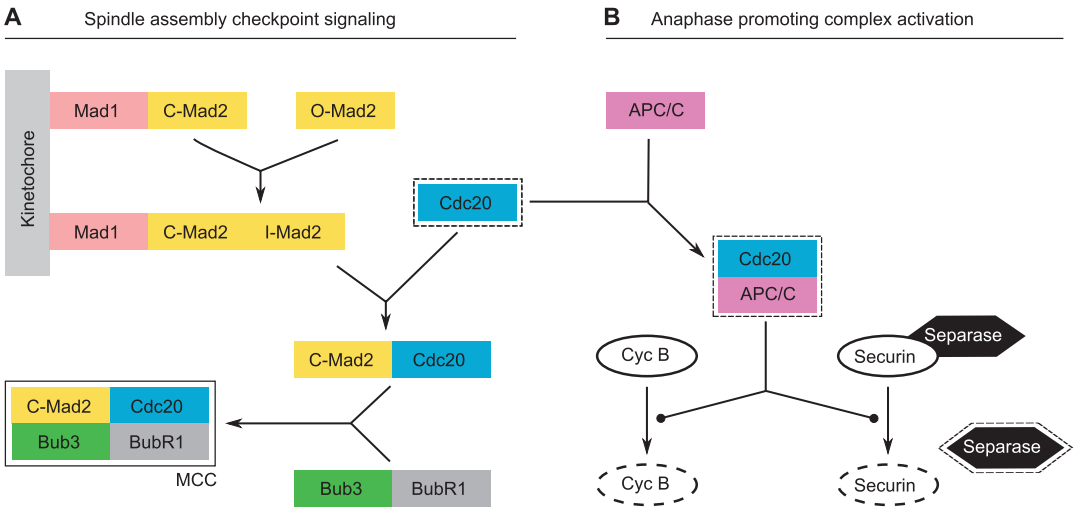

Figure 1.5: The core mechanism of the spindle assembly checkpoint. (**A**) The SAC functions through sequestration of the APC/C-activator Cdc20 by Mad2. Mad2 in closed conformation (C-Mad2) anchored at the kinetochore via Mad1 recruits cytosolic Mad2 in open conformation (O-Mad2). The so recruited Mad2 is stabilized in an intermediate conformation (I-Mad2), which in turn is able to bind Cdc20 efficiently. The resulting C-Mad2-Cdc20 dimers are released from the kinetochore and form the mitotic checkpoint complex (MCC) together with Bub3 and BubR1. The Cdc20-containing complexes are not stable and dissociate with a certain rate, thus Cdc20 becomes available for APC/C-activation soon after the last signaling Kinetochore is silenced by proper microtubule attachment. (**B**) If SAC signaling is turned off, Cdc20 binds to and thereby activates the APC/C. Active APC/C-Cdc20 promotes degradation of securin, which leads to cohesin cleavage by now active separase. The resulting separation of sister-chromatids is the hallmark of anaphase. In parallel, APC/C-Cdc20 promotes degradation of cyclin B, a requirement for mitotic exit.

a 'safety-belt' which is either open (O-Mad2) or closed (C-Mad2) (De Antoni *et al.*, 2005; Luo *et al.*, 2004; Sironi *et al.*, 2002). O-Mad2 is able to bind Cdc20, though the resulting complex is rather transient. C-Mad2 cannot bind to Cdc20, but in contrast, the complex of C-Mad2 and Cdc20 is quite stable. Central to the SAC-network is a kinetochore-bound template complex made up from Mad1 and C-Mad2. This template complex recruits O-Mad2 and stabilizes an intermediate conformation (I-Mad2) which can bind Cdc20 efficiently and switches to closed conformation upon Cdc20-binding, tightening the connection between both with the 'safety-belt' (Figure 1.5A; De Antoni *et al.*, 2005; Luo *et al.*, 2004; Vink *et al.*, 2006). The C-Mad2-Cdc20 complexes formed by this mechanism, which has been given the name 'template-

model' (De Antoni *et al.*, 2005), can further associate with the two proteins BubR1 (homologue of budding yeast Mad3) and Bub3 to form the mitotic checkpoint complex (MCC; see Figure 1.5A; Chao *et al.*, 2012; Díaz-Martínez *et al.*, 2007; Kulukian *et al.*, 2009; Sudakin *et al.*, 2001). The MCC inhibits the APC/C in two ways. First it binds to the APC/C in a way preventing Cdc20 from interacting with mitotic APC/C-targets (Chao *et al.*, 2012). Second it directs APC/C-activity towards ubiquitination of Cdc20 (Díaz-Martínez *et al.*, 2007; Nilsson *et al.*, 2008). Microtubule attachment depletes the template-complexes from the respective kinetochore, thereby silencing SAC-signaling locally (Buffin *et al.*, 2005; B. J. Howell *et al.*, 2001; Sivaram *et al.*, 2009). Thus, after proper attachment of the last chromosome, SAC signaling ceases and passage to anaphase is granted.

1.2.3 Spindle position checkpoint (SPOC)

Budding yeast cells divide always asymmetrically, that is, the division results in distinguishable mother- and daughter cells. This contrasts with the largely equal daughter cells resulting from symmetric cell division of, for instance, human somatic cells. In budding yeast cells, the site of later cell division and thus the mother-daughter-polarity axis is determined early in the cell cycle (A. S. Howell *et al.*, 2012; Pruyne *et al.*, 2000). Therefore, budding yeast cells require to position the mitotic spindle such that the spindle axis is in line with the polarity axis before the spindle elongates upon exit from mitosis (Caydasi, Ibrahim, *et al.*, 2010; Fraschini *et al.*, 2008; Segal *et al.*, 2001). Spindle elongation delivers one set of chromosomes to the bud and fixes the other in the mother-cell. Hence failure to position the spindle appropriately beforehand results in cells with aberrant number of nuclei after cytokinesis (Daum *et al.*, 2000; Pereira *et al.*, 2000). The spindle position checkpoint aims to prevent this fatal scenario by delaying exit from mitosis and cytokinesis to provide extra time for error correction in response to an inappropriately positioned spindle (cf. Figure 1.6).

Exit from mitosis requires complete inactivation of the mitotic kinase complex Cdc28-Clb2, which in turn is mediated through activation of the phosphoprotein phosphatase Cdc14 (Simanis, 2003; Stegmeier *et al.*, 2004; Sullivan *et al.*, 2007). Activation of Cdc14 is the downstream event of the mitotic exit network (MEN; Figure 1.7B; Simanis, 2003, Stegmeier *et al.*, 2004, Sullivan *et al.*, 2007). Before initiation of MEN by the small GTPase Tem1, Cdc14 is kept inactive through sequestration by the nucleolar protein Net1. Active Tem1 activates the protein kinase Cdc15, which in turn activates the protein kinase complex Dbf2-Mob1. Dbf2-Mob1, finally, pro-

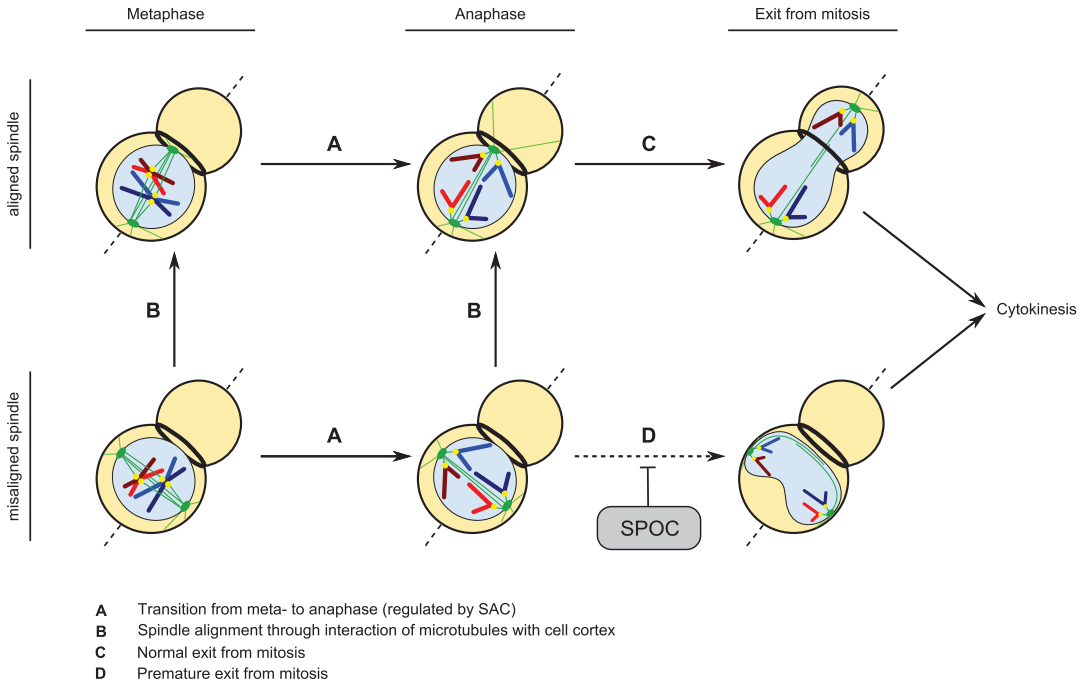

Figure 1.6: Regulation of the transition from anaphase to mitotic exit by the spindle position checkpoint in budding yeast. During unperturbed mitosis, cells progress from meta- to anaphase with a properly aligned spindle which elongates and distributes chromosomes and spindle poles evenly between mother- and daughter cell (upper path via **A** and **C**). Spindle positioning relies on the concerted interaction of astral microtubules with anchors and motors at the cell cortex. This mechanism is usually able to correct spindle misalignment rapidly (arrows labeled with **B**). Though, if the cell progresses into anaphase with a misaligned spindle, SPOC delays mitotic exit to provide the cell with some extra time for the correction (blocked lower path via **D**). Cells with impaired spindle positioning machinery and defective SPOC often end up with aberrant chromosome content after cytokinesis.

motes release of Cdc14 from the nucleolus by impeding Cdc14-sequestration through phosphorylation of Net1 (Simanis, 2003; Stegmeier *et al.*, 2004; Sullivan *et al.*, 2007).

In contrast to other small GTPases, Tem1 can be considered preferably active during unperturbed mitosis because it does not require the aid of a Guanine-nucleotide-exchange factor (GEF) for its activation (Geymonat *et al.*, 2002). Tem1 can, however, be deactivated with the help of the GTPase-activating protein (GAP) complex Bfa1-Bub2 (Geymonat *et al.*, 2002). Regulation of Bfa1-Bub2 activity in response to spindle alignment is subject to SPOC (Figure 1.7A). While Bfa1-Bub2 becomes hyper-phosphorylated by the polo-like kinase Cdc5 during unperturbed mitosis (Gey-

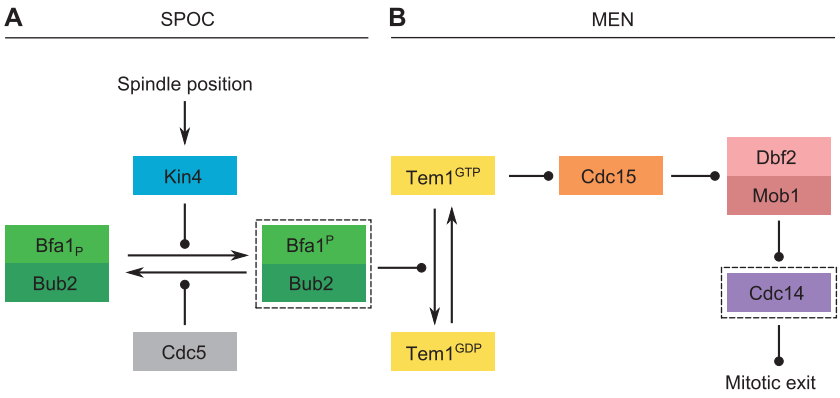

Figure 1.7: Regulatory network of SPOC and MEN. Downstream effectors of both, SPOC and MEN, ares indicated with dashed outline. (**A**) SPOC signaling is centered around the GAP-complex Bfa1-Bub2. During unperturbed mitosis, Polo-like kinase Cdc5 inactivates the GAP through hyperphosphorylation of the Bfa1 subunit (indicated by subscript 'P'). Upon erroneous spindle positioning, phoshporylation of the Bfa1-subunit by Kin4 kinase (indicated by superscript 'P') prevents hyperphosphorylation through Cdc5, ensuring GAP-complex activity. (**B**) The active form of the GAP-complex (drawn with dashed outline) binds to the small GTPase Tem1 and stimulates GTP-hydrolysis, shifting the equilibrium towards the inactive, GDP-bound form of Tem1. Correct spindle positioning leads to inactivation of the GAP-complex, allowing Tem1 to accumulate in its active, GTP-bound state. Active Tem1 initiates the MEN through SPB-recruitment of kinase Cdc15, which in turn activates the kinase-complex Dbf2-Mob1. The latter complex triggers release of the phosphatase Cdc14 from the nucleus into the cytoplasm where it shuts down Cdk1-activity and promotes exit from mitosis.

monat *et al.*, 2003; Hu *et al.*, 2001), this inactivating phosphorylation is prevented through antagonistic phosphorylation of Bfa1 by protein kinase Kin4 in response to spindle misalignment (Caydasi *et al.*, 2009; D'Aquino *et al.*, 2005; Maekawa *et al.*, 2007; Pereira *et al.*, 2005). Thus, SPOC delays exit from mitosis through inhibition of the MEN-activator Tem1 until the spindle is properly aligned.

1.3 Approaching the Eukaryotic Cell Cycle by Mathematical and Computational Modeling

1.3.1 Models of the Cell Cycle Oscillator

Shortly after the molecular basis of the eukaryotic cell cycle oscillator was proposed to be the tightly regulated interaction of cyclin with the cyclin dependent kinase (cdk) about 25 years ago (Evans *et al.*, 1983; Labbé *et al.*, 1989; Murray *et al.*, 1989; Nurse, 1990; Nurse *et al.*, 1976), pioneering mathematical models extrapolated the new findings such that oscillations can arise (Goldbeter, 1991; Norel *et al.*, 1991; Tyson, 1991). Although these early models relied on ordinary differential equations (ODEs) as the modeling formalism, the perspective on the biological mechanism was considerably different. Norel *et al.* followed a population dynamic approach modeling the cell cycle oscillator by a predator (the active cdk-cyclin complex) and its linearly accumulating prey (free cyclin). Goldbeter assumed that cyclin activates cdk, which in turn activates a protease which then degrades cyclin. The resulting two-step signaling cascade exhibits mutual zero-order-ultrasensitivity (Goldbeter *et al.*, 1981) towards the concentrations of cyclin and cdk, which constitutes the driving force of the oscillations. In contrast, Tyson focused on the mechanistic details of the cyclin-cdk interaction and constructed a kinetic model with 6 species and 9 reactions. Interestingly, this very limited model could already capture key features of cdk-cyclin regulation in early frog embryos by progressing through a two-dimensional parameter subspace potentially related to two putative regulators of cdk-cyclin activity. Two years later, in 1993, Novak *et al.* presented a more comprehensive model which incorporated these two regulators and detailed the mechanism of cyclin degradation.

In the following years, the laboratories of J. J. Tyson and B. Novak refined their models of the cell cycle oscillator, culminating in a comprehensive model of the budding yeast cell cycle (K. C. Chen *et al.*, 2004), integrating many important cell cycle control mechanisms at least on a rudimentary level. This model, formulated in terms of ODEs, conforms with a considerable number of mutant phenotypes and served, together with its predecessor (K. C. Chen *et al.*, 2000), as a basis for numerous other modeling studies.

While ordinary differential equations are a well established formalism in chemical kinetics and profit from a broad theoretical foundation, alternative modeling approaches have been applied to study particular aspects modeling of the eukaryotic cell cycle. The non-deterministic nature of chemical reactions can significantly alter system dynamics (Rao *et al.*, 2002) and results in significant intra-population vari-

ance (Bryan *et al.*, 2010; Di Talia *et al.*, 2007). Stochastic models can shed light on the consequences of intrinsic and extrinsic noise on cell cycle dynamics. Barik *et al.* (2010) and Kar *et al.* (2009) employ the "stochastic simulation algorithm" (SSA; D. T. Gillespie, 1976) to simulate the dynamics of individual budding yeast cells. Both split the simulated cells at the end of the cell cycle two generate virtual populations and find that statistics of cycle time, cell size and RNA-levels are comparable to experimental results. Steuer (2004) makes use of stochastic differential equations (SDEs) of the Langevin type to show that intrinsic noise can induce oscillations in a model of the fission yeast cell cycle and leads to realistic population statistics of certain mutant phenotypes.

All previously mentioned models are essentially quantitative, kinetic models of the cell cycle. While academic examples with two or three dimensions can often be exhaustively studied analytically, utilizing phase portraits and bifurcation analysis to grasp the significance of individual parameters, more realistic models exhibit considerable higher complexity. Such models require substantial effort to set up and validate the model parameters, sometimes suffering from complete lack of suitable experimental data. Approaches to parameter estimation and sensitivity analysis in the context of biochemical models were reviewed by Jaqaman *et al.* (2006) and Ashyraliyev *et al.* (2009).

Purely qualitative approaches avoid this complicated matter and make it possible to study high level properties of the modeled systems. F. Li *et al.* (2004) construct a Boolean network of the budding yeast cell cycle. Their model considers 11 species, which is equivalent to 2048 possible states. They find that a super fixed point with a basin of attraction comprising about 86% of all states exists, which is remarkably robust to topological changes of the model. Davidich *et al.* (2008) assembled a comparable model for fission yeast which led to very similar results. Singhania *et al.* (2011) used the state sequence of the budding yeast model by F. Li *et al.* (2004) to control the topology of a piecewise linear ODE model of cyclins A, B, E to successfully predict flow cytometry data. Faure *et al.* (2009) reformulate the comprehensive model by K. C. Chen *et al.* (2004) in terms of multi-valued logic and demonstrate that the general dynamic features can be captured at such a coarse level, albeit the coverage of the mutant phenotypes is reduced.

Broader discussions of general mechanisms relevant to biochemical oscillations in the context of the cell cycle can be found in Novak *et al.* (2008) and Ferrell *et al.* (2011).

1.3.2 Models of Isolated Transition Control Mechanisms

The models discussed in the previous section have in common that they focus on the interplay of the various control mechanisms which shall ensure the ordered sequence of cell cycle events, rather than on their detailed mechanisms. However, the individual mechanisms are highly complex signal transduction networks on their own and conceptual as well as detailed mechanistic models have been developed to investigate how they work internally. In this work, models of the spindle assembly checkpoint (SAC) and of the mitotic exit network (MEN) are of particular interest.

1.3.2.1 Spindle Assembly Checkpoint

The SAC is an intriguingly sensitive checkpoint: improper attachment of even a single kinetochore suffices to delay cell cycle progression (Musacchio *et al.*, 2007). Though, it is still puzzling which molecular mechanisms can achieve reliable cell cycle arrest while remaining highly responsive. To even complicate the matter, SAC must link the biomechanics of the mitotic spindle with a biochemical signal transduction network, thus posing an inherently spatial problem.

In a pioneering paper, Doncic *et al.* (2005) approached the SAC in budding yeast with reaction-diffusion-equations describing simplistic models of potential modes of action and predicted a mechanism which matches well with the widely accepted "template model" proposed by De Antoni *et al.* (2005). Sear *et al.* (2006) build on the model proposed by Doncic *et al.* (2005) and adapt it to animal cells. To cope with the substantially larger animal cell volume, they propose two potentially complementary pathways, featuring a non-autocatalytic amplification step or active transport from the kinetochore towards the spindle pole. In a very recent publication, J. Chen *et al.* (2014) discussed an elaborate reaction-advection-diffusion-model of SAC in animal cells and emphasized the importance of streaming of SAC-components from attached kinetochores towards the centrosomes.

Ibrahim *et al.* (2008) employ a straight-forward ODE-model of the "template model" with realistic parameters and find that neither autocatalytic amplification nor competitive inhibition of the template complexes can improve the model performance with respect to Cdc20-sequestration or -release. The same authors developed comprehensive mechanistic models of the SAC to study the kinetics of MCC formation, and APC/C inhibition or activation (Ibrahim, Diekmann, *et al.*, 2008; Ibrahim *et al.*, 2009). A pivotal role for MCC in APC/C inhibition is predicted from the models.

The robustness of putative SAC signaling mechanisms to intrinsic noise has been studied by Doncic *et al.* (2006) and Ibrahim *et al.* (2007). Doncic *et al.* construct simplistic models which suggest that dimerization of the SAC key players Mad2 and Cdc20 can serve as a low pass filter to reduce noise induced by fluctuations of the rate of Cdc20-degradation. Ibrahim *et al.* employ a significant more elaborate SDE-model considering a discrete compartment for each kinetochore. The compartments are coupled by diffusion-like mass transfer, and it turns out that high diffusion rates can suppress the intrinsic noise of the kinetochore "micro-reactors".

Simonetta *et al.* (2009) perform a thorough kinetic study driven by a detailed model of the SAC core mechanism. Lohel *et al.* (2009; see chapter 2 of this work) build on this kinetic data and challenge the model proposed by Doncic *et al.* (2005), which assumes instantaneous activation and release of the inhibitor upon kinetochore contact. It turns out that this assumption is a critical over-simplification because accounting for realistic kinetochore-binding kinetics does significantly affect model performance.

Mistry *et al.* (2008) combines the conceptual model by Sear *et al.* (2006) with a ODE model of the chromosome attachment state and does so provide a framework for integration with models accounting for the correction mechanism for improper chromosome attachment. Such a model could probably have been discussed by He *et al.* (2011): they assume two antagonistic positive feedback loops linking chromosome tension with checkpoint activation and show that this topology makes cyclin degradation upon SAC silencing irreversible.

Finally, an interesting approach to deduce the kinetochore-related interaction network of the SAC was followed by Doncic *et al.* (2009). They screen randomized network topologies for conformance with a suitably chosen set of *in vivo* deletion mutants and end up with a topology which is in good agreement with many experimental findings.

1.3.2.2 Mitotic Exit Network

Only few models exist which consider the MEN in some detail. The previously discussed comprehensive model by K. C. Chen *et al.* (2004) was probably the first model considering details of FEAR, MEN and SPOC pathways. Of all models discussed here, it contains the most elaborate (though still at best rudimentary) description of the SPOC. Queralt *et al.* (2006) developed a reduced, yet powerful mathematical model of MEN and FEAR to analyze their findings about the regulation of the protein phosphatase 2A (PP2A) from a systems perspective. The model distinguished

between active and inactive Tem1, although Tem1 regulation is simplified to activation by the polo-like kinase Cdc5 and deactivation through the counteracting PP2A. This model was subsequently analyzed in detail by Tóth *et al.* (2007), revealing two bistable switches implemented by positive feedback loops activating Cdc14 and cyclin degradation. Vinod *et al.* (2011) present an extension of the model and works out the regulation of cyclin production and degradation. The model experienced a further extension with focus on the function of Cdc5 (Hancioglu *et al.*, 2012); however, the regulation of Tem1 has not been detailed in any of the models. Caydasi *et al.* (2012; see chapters 3 and 4 of this work) presented the first model of the spindle position checkpoint, focusing on the details of the regulation of Tem1.

1.3.3 Modeling Paradigms and Technologies for Signal Transduction Networks

1.3.3.1 Differential Equations

Differential equations (DE) are a well established branch of mathematics with a wealth of excellent literature available. Differential equations describe the temporal and spatial evolution of continuous quantities by specifying their rate of change. Mass action kinetics (MAK) constitute a quasi-standard in chemical modeling, expressing chemical reaction rates by products of rate coefficients and reactant concentrations. Thus, chemical equations can easily be translated into DEs whenever their reaction rates can be expressed in terms of MAK. Mathematics provides a rich toolbox for analytical and numerical treatment of DEs, and it is generally possible to switch between temporal dynamics and stationary solutions within the same formal framework. Although many analytical tools require the DEs to be linear, they can be used to obtain approximate results for nonlinear DEs by linearization or through numerical methods.

A big advantage and a serious drawback at the same time is the very nature of the rate equations. Every single reaction requires at least one parameter describing its rate of change. Thus there exist many degrees of freedom to fine-tune the kinetics of the model, but on the other hand, all parameters must be assigned a value, even if the true values are unknown. Estimation of unknown parameter values is a complicated problem, and numerous methods have been developed (Ashyraliyev *et al.*, 2009; Jaqaman *et al.*, 2006).

The simplest case are ordinary differential equations (ODE), that is, DEs which are limited to temporal evolution. Due to their formal simplicity and the availability

of efficient numerical methods for their solution, they are by far the most popular approach to modeling of biochemical networks and are frequently employed as instructive examples (Aldridge *et al.*, 2006; W. W. Chen *et al.*, 2010). Many functional motifs occurring in biochemical networks have been identified and illustrated in terms of ODEs (Novak *et al.*, 2008; Tyson *et al.*, 2003, 2010).

Spatial problems are more complicated and their numerical solution can be computationally demanding. Such problems can be described in terms of partial differential equations (PDE). Reaction-diffusion equations (RD) or the more general reaction-advection-diffusion equations suffice to describe most biochemical problems adequately (Kholodenko, 2006). Generally, they are simply sums of terms describing diffusion, directional transport, and the same rate laws one would have specified for an ODE model.

1.3.3.2 Stochastic Simulation

The inherent stochastic and discrete nature of chemical reactions implies that the evolution of the state of every chemical system must conform to a time dependent probability distribution which depends only on the initial state. This probability distribution can be formally defined through an intricate differential equation, the so called chemical master equation (CME; D. T. Gillespie, 1992). Unfortunately, the CME of most systems cannot be solved analytically. Therefore, several algorithmic approaches have been proposed to approximate the probability distribution dictated by the CME. D. T. Gillespie (1976) proposed the exact "stochastic simulation algorithm" (SSA), which samples a random path through the state space with transition probabilities concordant with the CME. Estimates of the sought-after probability distribution can then be obtained by averaging many individual trajectories. Because this procedure samples every single reaction, simulation using the SSA is often prohibitively time consuming, especially for large systems. Numerous techniques have emerged which sample approximate trajectories, but at computationally significantly reduced cost (Cao *et al.*, 2007; D. Gillespie, 2001; Haseltine *et al.*, 2002). The "finite state projection algorithm" developed by Munsky *et al.* (2006) allows approximation of the probability distribution without repetitive simulation, albeit only for comparably small systems.

It is also possible to bestow DEs with random noise, leading to so called stochastic differential equations (SDE) which can be simulated efficiently. A particular SDE, which approximates the intrinsic noise of chemical reactions according to the CME, is the chemical Langevin equation (D. Gillespie, 2000).

1.3.3.3 Rule Based Models

Signal transduction networks rely heavily on complex formation and enzymatically reversible post-translational modifications. Complex networks can arise even from a single molecular species: consider a protein which can be phosphorylated at N sites, then this protein can exists in up to 2^N different states, depending on which sites are phosphorylated. If such a protein is embedded in a complex network, then all reactions have to be considered for every possible state. It is clear that such models suffer from a combinatorial explosion of states and interactions, which are hard to set up and maintain manually. Hlavacek *et al.* (2006) discuss an approach where the individual molecules are structurally defined and interactions are expressed by rules modifying particular structural features of the reactant molecules. From a stringent graph theoretic formulation of the molecules and rules, the full reaction network can be automatically generated (Blinov *et al.*, 2006). Grünert *et al.* (2010) extended this approach to enable spatial simulations with spatially structured molecules.

1.3.3.4 Qualitative Modeling

Whether individual genes are transcribed or not can often be considered a binary decision. Consequently, Boolean networks have proven useful in the context of gene regulatory networks and have been applied to infer network structure from gene expression profiles (T. E. Ideker *et al.*, 2000; Martin *et al.*, 2007) or enabled analysis of statistical network properties (Kauffman *et al.*, 2003). Despite the rather quantitative nature of signal transduction networks, Boolean modeling has been successfully applied to the eukaryotic cell cycle (Davidich *et al.*, 2008; F. Li *et al.*, 2004). Boolean models feature high level properties and are applicable even if knowledge about the network structure is incomplete, making them a good starting point for more detailed models (Bornholdt, 2008).

There is also rich literature on Petri nets, which have been applied to metabolic modeling with success (Chaouiya, 2007; Hardy *et al.*, 2004). Sackmann *et al.* (2006) showed convincingly that Petri nets could also be used to deduce high level properties of signal transduction networks.

1.3.3.5 The Method of Choice

Differential equations are a well established tool in chemical physics. Thus, DEs allow to create physically meaningful models, provided the kinetic properties are carefully integrated with the network topology. Physical meaningfulness is an important re-

quirement for the models presented in chapters 2-4. If it were not met, no conclusions could be drawn based on the consequences of the installed reaction kinetics.

An additional advantage of DE-models is the seamless integration with numerical software like matlab (MathWorks, 2009), which provides various highly efficient solvers in a powerful production environment facilitating data analysis and visualization dramatically.

Rule based modeling seems appealing to deal efficiently with the combinatorial complexity in the SPOC model (see chapter 4). However, the kinetics of many state combinations would need to be treated differently, making the model less generic.

2 Pseudo-spatial simulation of the spindle assembly checkpoint

This work results from a collaboration with Prof. Dr. Stephan Diekmann from the Leibnitz Institute for Age Research in Jena, Germany, and has been described in a publication (Lohel *et al.*, 2009) to which I contributed the modeling work and the theoretical and computational analysis.

2.1 Introduction

All proliferating cells are challenged to properly divide their replicated genome among the two daughter cells during mitosis, a precisely regulated sequence of processes, which first prepares the cell for and finally regulates cell division. To make sure that the chromosomes will be correctly distributed, the cell must guarantee that each chromosome has established a tight bipolar attachment to the spindle apparatus before sister-chromatid separation is initiated in anaphase. The mitotic spindle assembly

checkpoint (SAC) is a surveillance mechanism that arrests mitotic cells in metaphase until the last chromosome has been correctly attached to the spindle (Musacchio *et al.*, 2007). Its failure results in aneuploidy (Cimini *et al.*, 2005) and likely contributes to cancer (Kops *et al.*, 2005).

The connection between the microtubules of the spindle apparatus and the chromosomes is established and maintained at the kinetochores, large protein assemblies forming at centromeric DNA during prophase (Cheeseman *et al.*, 2008; Maiato *et al.*, 2004; Westermann *et al.*, 2007). The SAC works by inhibiting the APC:Cdc20 complex, which will trigger a signalling cascade resulting in sister-chromatid separation upon activation. The SAC delays mitotic progression even if only one kinetochore is not properly attached to the spindle. It is not clear how this last kinetochore can maintain checkpoint function alone. It has been proposed that a diffusible "wait anaphase"-signal is produced at unattached kinetochores (Shah *et al.*, 2000) and the Mad2 protein is a likely candidate (De Antoni *et al.*, 2005).

Most proteins involved in the SAC are localized at least transiently at the kinetochores (Musacchio *et al.*, 2007), some are specifically recruited only to unattached kinetochores or even actively removed after microtubule attachment, like the essential checkpoint proteins Mad1 and Mad2 (Cheeseman *et al.*, 2008; Maiato *et al.*, 2004; Musacchio *et al.*, 2007; Yu, 2002). This has the consequence that reactions involving these species will only take place at unattached kinetochores or have their rates reduced. Therefore checkpoint operation can be thought of as regulated by the attachment state of the kinetochores. In addition, the spatial extend of the cell is likely to influence checkpoint operation because localization of the bulk of checkpoint proteins at the kinetochores will make diffusion and high local concentrations important factors.

To evaluate possible mechanisms for signal generation and propagation, mathematical models have been developed during the past years. Doncic *et al.* (2005) as well as Sear *et al.* (2006) analyzed simple spatial models of potential checkpoint mechanisms with focus on yeast or animals, respectively. They showed theoretically that a diffusible signal-species can generally account for checkpoint operation. Recently we have proposed a more complete model of the SAC including many of the confirmed interactions (Ibrahim, Diekmann, *et al.*, 2008; Ibrahim *et al.*, 2008, 2009). A mathematical model for the checkpoint activation based on the " Mad2 template" model by De Antoni *et al.* (2005) has been supported with *in vitro* experiments by Simonetta *et al.* (2009). However, these models do not take into account localization of checkpoint proteins at, and control of reactions by, a realistic number of kineto-

chores, which change their attachment state over time. A recent work by Mistry *et al.* (2008) develops a detailed model for the time evolution of the distribution of the attachment states of 92 kinetochores considering not only attached and unattached states but also merotelic and syntelic misalignments. In addition they integrate function of Aurora B in correcting misattachments into their model. Nevertheless, they limit the influence of the attachment-mechanism to damping of the reaction rates and do not consider species localization.

Here we propose a simple method for the quasi-spatial simulation of reaction networks considering a realistic number of kinetochores at which species localize and participate in reactions according to the kinetochore attachment status. Differences of the species concentrations in the kinetochore volumes and the bulk solution are handled and diffusion is introduced implictly. This method yields insight into how spatial properties and a realistic number of kinetochores affect the operation of the mitotic spindle assembly checkpoint.

2.2 Methods

This section introduces in a general way the method we developed for the quasi-spatial simulation of the above discussed models. Therefore the term "model" refers to an arbitrary network model rather than to any of the models discussed above. Similarly, the term "species" is a placeholder for an arbitrary species. We use the terms "original model" (or simply "model") and "internal model" to distinguish between the model of the network to simulate and its technical reformulation. Similarly, we use "original species" (or simply "species") and "internal species" to refer to species from the respective model.

In the following, we show how kinetochores and microtubule attachments can be handled, and how the internal model is generated from an original model. The internal model can then be expressed in terms of coupled ordinary differential equations (ODEs) by computing $d\mathbf{S}/dt = \mathbf{N}\mathbf{v}(\mathbf{S})$ with state vector $\mathbf{S}$, flux vector $\mathbf{v}(\mathbf{S})$ and stoichiometric matrix $\mathbf{N}$.

As physical unit all computations involving species amounts use molecule counts instead of molar concentrations. This makes it much simpler to assemble the final ODE-system, as all volume- dependent scaling (which changes with the attachments) can be put into the flux vector while the stoichiometric matrix is constant. A major consequence is that reaction rate coefficients of a reaction R which are given in concentration based units have to be transformed appropriately. For a molar-based rate

coefficient k of a reaction R described with mass action kinetics, this transformation into a molecule-based, volume dependent rate $k'(V)$ is done according to

$$k'(V) = k \cdot (V N_{\mathrm{A}})^{1-order(R)}. \tag{2.2.1}$$

In this equation, V is the volume of interest with respect to the environment of the reaction and $N_{\mathrm{A}}$is Avogadro's number.

2.2.1 Concentration Gradients

Following the argument given by Sear *et al.* (2006), we assume that no noteworthy gradients persist for more than a few seconds if diffusion is not overly slow (i.e. $D \gtrsim 0.1\ \mu\mathrm{m}^2\mathrm{s}^{-1}$). The idea is that (1) the average lifetimes of the checkpoint-relevant species produced at the kinetochores are long compared to the time they need to cross the cell and (2) in addition the expected time until collision with a kinetochore is long compared to the crossing time for the cellular space. In addition, in experiments with large scale spatial stochastic simulations of the SAC we observed perceptible gradients only immediately after kinetochore attachment and those gradients lasted for no more than 15-20 seconds even with diffusion constants of about $D \gtrsim 0.1\ \mu\mathrm{m}^2\mathrm{s}^{-1}$ (unpublished data). We will therefore assume that the bulk solution is in quasi steady state and gradients appear only locally at the encounter volumes.

2.2.2 Kinetochore Representation and Microtubule Attachments

Kinetochores are modeled by spherical regions, which we call " encounter volumes". The naming indicates that these regions are not necessarily equal to the kinetochore volume or shape, but represent the environment wherein molecules encounter a kinetochore. The encounter volumes are similar to ordinary compartments in that they provide a designated area for reactions that should not take place in the remainder of the cellular volume. However, as they are open regions instead of membrane- bound subspaces, only diffusion accounts for influx and outflux. This is sketched in Figure 2.1, derivations of the rate coefficients $\mathrm{k_{in}}$ and $\mathrm{k_{out}}$ are given later. All encounter volumes have the same radius r and thus the same volume $V_{\mathrm{kin}} = 4\pi r^3/3$. The entirety of encounter volumes together with the volume of the bulk solution make up the "system volume" V_{sys}.

The kinetochore contained in an encounter volume can either be unattached or attached to spindle microtubules. Consequently, the set of all n encounter volumes splits into two corresponding subsets with n_{u} and n_{a} elements, respectively. Because

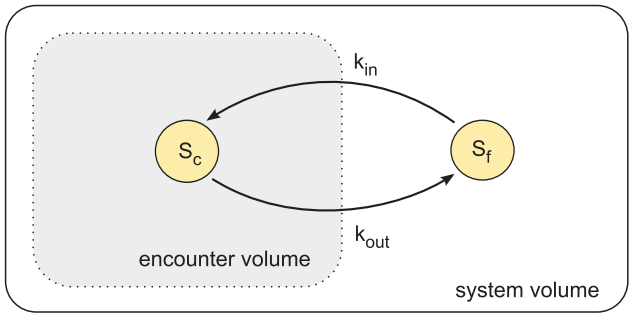

Figure 2.1: Schematic of encounter species and encounter volume. Encounter species can behave differently in the vicinity of kinetochores, for instance by interaction with kinetochore-bound species which do not exist in the bulk solution. Therefore the vicinity of the kinetochore is defined by the respective encounter volume, an open (accessible by diffusion) region within the total system volume. Flux into the encounter volume is proportional to the amount of "far" molecules (S_f) while flux out of the encounter volume is proportional to the amount of "close" molecules (S_c). Only "close" molecules can participate in reactions at the kinetochore.

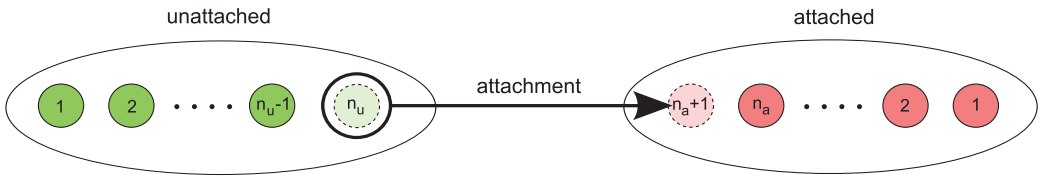

Figure 2.2: Schematic of the two meta-compartments. All molecules in encounter volumes belonging to the n_u unattached or n_a attached kinetochores are grouped in the "unattached" or the "attached" meta-compartment, respectively. Upon microtubule attachment, the fraction of molecules belonging to one unattached kinetochore is transfered from the "unattached" meta-compartment to the "attached" meta-compartment, simultaneously decreasing or increasing the respective size n_u or n_a by one.

there will not be any noteworthy concentration gradients, we can expect the molecule amounts in all encounter volumes of the same subset to evolve equally. We can therefore group the encounter volumes in two meta-compartments.

Upon every kinetochore attachment, it is necessary to move one encounter volume with all associated molecules from the unattached -meta-compartment to the attached-meta-compartment as displayed in Figure 2.2. Let a species S be represented by two state variables S_u and S_a, denoting the amount of molecules in encounter volumes of unattached and attached kinetochores immediately before the attachment.

There are S_u/n_u molecules close to (or at) a single unattached kinetochore. At the moment of the attachment, we must (in this order) recompute the following quantities as given on the right-hand-side:

$$S_a \leftarrow S_a + \frac{S_u}{n_u} \tag{2.2.2}$$

$$S_u \leftarrow S_u \frac{n_u - 1}{n_u} \tag{2.2.3}$$

$$n_u \leftarrow n_u - 1 \tag{2.2.4}$$

$$n_a \leftarrow n_a + 1 \tag{2.2.5}$$

The arrows should avoid confusion with algebraic identity and indicate that this changes have to be introduced manually as events during the integration of the final ODE-system.

The waiting times for the individual attachments can be obtained from the series of compound Poisson-processes as described in Doncic *et al.* (2005).

2.2.3 Transformation of the Original Model Into the Internal Model

We distinguish up to three types of species in a network model, and identifying the appropriate type for each species is important:

- "Localized species" are firmly bound to the kinetochores and can therefore only be found within encounter volumes of attached and unattached kinetochores. They can not participate in reactions in the system volume far from the kinetochores. Each localized species S is internally represented by two subtypes S_u and S_a. They represent the molecules of the species bound to unattached (S_u) and attached (S_a) kinetochores.

  Upon microtubule attachment, S_u-molecules are transformed to S_a-molecules as described above.

- "Encounter species" interact with kinetochores the one or the other way. Therefore we must take into account that they undergo diffusive motion until they finally encounter the vicinity of a kinetochore. Encounter species S are internally represented by three subtypes, S_f, $S_{c,u}$ and $S_{c,a}$. The first subtype, S_f, is considered to be *far* from, or more precisely, *not close* to any kinetochore. In contrast, $S_{c,u}$ and $S_{c,a}$ subtypes are close to either unattached or attached kinetochores, respectively. The latter, "close" subtypes, can react with localized species of the corresponding attachment status. Clearly, either of the three

subtypes can only react with molecules of the same or another encounter species if their subtypes match.

Upon microtubule attachment, $S_{c,u}$-molecules are transformed to $S_{c,a}$-molecules as described above.

Transition from one subtype to another is shown in Figure 2.1. S_f-molecules enter an encounter volume and become either $S_{c,u}$-molecules with rate $n_u k_{in} S_f$ or $S_{c,a}$-molecules with rate $n_a k_{in} S_f$. Conversely, $S_{c,u}$ and $S_{c,a}$ molecules leave an encounter volume and become S_f-molecules again with rates $k_{out} S_{c,u}$ and $k_{out} S_{c,a}$. The derivation of k_{in} and k_{out} is given in later sections.

- "Ubiquitous species" are always uniformly distributed throughout the system volume and must not participate in reactions with the two other types. Nevertheless, their reactions may result in molecules of the encounter type. This type is suited for long living products which are majorly consumed by reactions in the bulk solution; they can serve as I/O-species in the connection with other reaction networks. Ubiquitous species are not affected by kinetochore attachment.

Some reactions can depend on the attachment status of the kinetochores, so all reactions can be classified by whether they —upon microtubule attachment—are unaffected ("uncontrolled"), turned off ("off-controlled") or turned on ("on-controlled"). Only reactions involving localized or encounter species can be controlled. Note that we assume that mass-action-kinetics is used for all reactions. If other kinetics should be used, they have to be transformed to mass action kinetics.

- A reaction of ubiquitous species is taken "as is" if only ubiquitous species are produced. If encounter species are produced, the reaction must appear three times to produce the different subtypes of the encounter species with the right proportions. That is, each appearance of the ubiquitous species S must be multiplied by either $V_{sys} - (n_u + n_a) V_{kin}$ if the "far"-subtypes of the encounter species are produced or by $n_u V_{kin}$ or $n_a V_{kin}$, if the "close"- subtypes are produced. Because the reactions take place in the whole system volume, the molar-based reaction rate coefficient must be scaled with V_{sys} as the volume of interest (cf. equation (2.2.1)).

- For uncontrolled reactions, we must generate the same reaction two or three times (depending on whether or not localized species participate): Once with

only the attached- subtypes, once with only the unattached-subtypes. Here molar reaction rate coefficients have to be scaled with the volume of the respective meta-compartment, either $n_{\mathrm{u}}V_{\mathrm{kin}}$ or $n_{\mathrm{a}}V_{\mathrm{kin}}$ (cf. equation (2.2.1)). If no localized species participates, a third variant must be added where only the "far"-subtypes appear. The molar rate coefficient of this reaction must be scaled with $V_{\mathrm{sys}} - (n_{\mathrm{u}} + n_{\mathrm{a}})\, V_{\mathrm{kin}}$ as the volume of interest (cf. equation (2.2.1)).

- Controlled reactions are unambiguous, so we need only the variant with all species appearing in the unattached-subtype if it is off-controlled, or all species appearing in the attached- subtype if it is on-controlled. The rate coefficient scaling is the same as for uncontrolled reactions with localized species.

2.2.4 Flux Into an Encounter Volume

In this section we derive an expression for the rate coefficient $\mathrm{k_{in}}$ of the influx of molecules of subtype $\mathrm{S_f}$ of an encounter species S into an encounter volume (cf. Figure 2.1). We assume that the bulk solution is a rather homogeneous mixture and only the encounter volumes act locally as sinks. We can then use the maximal association rate for a molecular interaction of two molecules (Berg *et al.*, 1985), $k_{\mathrm{a}} = 4\pi(D_A + D_B)(r_A + r_B) = 4\pi D' r'$, to model the influx rate coefficient: We can think of encounter volumes as large, virtually immobile molecules with radius r. Let the encounter species S be small compared to r, but move much faster with diffusion coefficient D_{S}. Then we have approximations for the effective diffusion coefficient $D' \approx D_{\mathrm{S}}$ and the effective radius $r' \approx r$. We now relate k_{a} to the system volume V_{sys} and obtain an expression for the rate coefficient $\mathrm{k_{in}} = 4\pi D_{\mathrm{S}} r / V_{\mathrm{sys}}$.

2.2.5 Flux Out of an Encounter Volume

We now consider the flux of molecules of subtype $\mathrm{A_c}$ of an encounter species A out of the encounter volume V they are currently in. To obtain an expression for the rate coefficient $\mathrm{k_{out}}$ (see Figure 2.1), we use an approach similar to finite volume methods for the numeric approximation of partial differential equations. We denote the number of molecules with a capital letter and the corresponding molecule density by a capital letter in brackets. According to Fick's first law, the flux of $\mathrm{A_c}$-molecules due to diffusion can be described by (Glaser, 2001):

$$\mathbf{J} = -D\nabla[\mathrm{A_c}], \tag{2.2.6}$$

where D is the constant diffusion coefficient for species A and $[\mathrm{A_c}]$ denotes the molecule density of the $\mathrm{A_c}$- molecules. As the total number of molecules $\mathrm{A_c}$ inside V can only change by flux across its surface S in the direction of the outward pointing unit normal vector $\mathbf{n}$, the total change of the species' amount over time is given by:

$$\begin{aligned}\frac{d\mathrm{A_c}}{dt} &= \oint_S \mathbf{J}\cdot\mathbf{n}\,dS \\ &= -D\oint_S \nabla[\mathrm{A_c}]\cdot\mathbf{n}\,dS.\end{aligned} \tag{2.2.7}$$

Above we defined an encounter volume as a sphere of radius r. We will now extend this definition by declaring a spherical kinetochore region of radius r_{kin} in each encounter volume. Within this inner region, we assume the gradient of the molecule density $\nabla[\mathrm{A_c}]$ to be zero. With r_{kin} we can choose the width $h = 2(r - r_{\mathrm{kin}})$ of the gradient around the encounter volume. By definition, there are no $\mathrm{A_c}$-molecules outside any encounter volume, so we can approximate the $[\mathrm{A_c}]$-gradient at the boundary of the encounter volume by

$$\nabla[\mathrm{A_c}] \approx -\frac{[\mathrm{A_c}]}{h}\cdot\mathbf{n} \tag{2.2.8}$$

where $\mathbf{n}$ is the unit normal. With this, we can rewrite equation (2.2.7):

$$\frac{d\mathrm{A_c}}{dt} = D\,\frac{[\mathrm{A_c}]}{h}\oint_S \mathbf{n}\cdot\mathbf{n}\,dS. \tag{2.2.9}$$

Because of $|\mathbf{n}| = 1$, we have $\mathbf{n}\cdot\mathbf{n} = 1$ and so above integral evaluates to $4\pi r^2$. Substituting this into (2.2.9), we obtain

$$\frac{d\mathrm{A_c}}{dt} = 4\pi D r^2\,\frac{[\mathrm{A_c}]}{h}. \tag{2.2.10}$$

The average density of $\mathrm{A_c}$-molecules within the encounter volume is given by

$$[\mathrm{A_c}] = \frac{\mathrm{A_c}}{\frac{4\pi}{3}r^3}, \tag{2.2.11}$$

so we finally get by substituting (2.2.11) into (2.2.10)

$$\begin{aligned}\frac{d\mathrm{A_c}}{dt} &\approx \frac{3D}{rh}\,\mathrm{A_c} \\ &= \frac{3D}{2r(r - r_{\mathrm{kin}})}\,\mathrm{A_c}.\end{aligned} \tag{2.2.12}$$

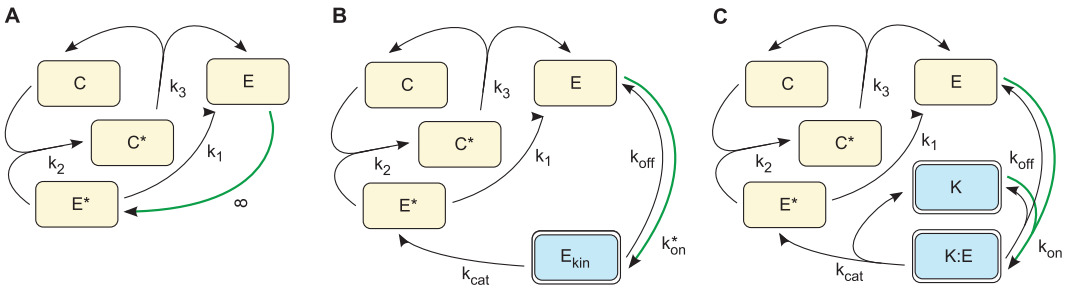

Figure 2.3: Reaction scheme of the "emitted-inhibition" model and variants. Thick green arrows indicate reactions restricted to the vicinity of unattached kinetochores, blue boxes with double outline denote kinetochore-localized species. (**A**) Original "emitted-inhibition" model without binding kinetics. (**B**) "Implicit binding" variant. (**C**) "Explicit binding" variant.

Abbreviation	Full protein name
APC	Anaphase promoting complex/Cyclosome
Cdc20	Cell Division cycle 20 homolog
Mad1	Mitotic arrest deficient 1
O-Mad2	Mitotic arrest deficient 2, "open" conformation
C-Mad2	Mitotic arrest deficient 2, "closed" conformation

Table 2.1: Abbreviations

It is therefore reasonable to choose the rate coefficient for the flux out of an encounter volume according to

$$\mathrm{k_{out}} = D\,\frac{3}{2r(r - r_{\mathrm{kin}})} \tag{2.2.13}$$

For $r_{\mathrm{kin}} \to 0$, we obtain the simpler expression $\mathrm{k_{out}} = 3D/2r^2$. However, this simpler expression bears the problem that with increasing kinetochore size the encounter volumes become more diffuse.

2.3 Results

2.3.1 Modification of the "Emitted Inhibition" Model to Account for Kinetochore Binding Kinetics

In the "Mad2 exchange" model for SAC activation (Luo *et al.*, 2004) , Mad1 at unattached kinetochores converts O-Mad2 to its active form C-Mad2, which can sub-

sequently sequester Cdc20 throughout the cell. The abstract "emitted-inhibition" model (Eq. (2.3.1) and Fig. 2.3A) by Doncic *et al.* (2005) resembles this mechanism closely, yet the authors did not explicitly map their abstract species to known checkpoint proteins.For ease of comparison with other models discussed later, we assume that E, E*, C and C* can be mapped to O-Mad2, C-Mad2, Cdc20 and Cdc20:C-Mad2, respectively. The full names of these abbreviations can be looked up in Table 2.1. The "emitted- inhibition" model is given by the following reaction rules:

$$\mathrm{E} \xrightarrow{\infty} \mathrm{E}^* \tag{2.3.1a}$$

$$\mathrm{E}^* \xrightarrow{\mathrm{k}_2} \mathrm{E} \tag{2.3.1b}$$

$$\mathrm{E}^* + \mathrm{C} \xrightarrow{\mathrm{k}_3} \mathrm{C}^* \tag{2.3.1c}$$

$$\mathrm{C}^* \xrightarrow{k_4} \mathrm{C} + \mathrm{E} \tag{2.3.1d}$$

The mathematical analysis carried out by Doncic *et al.* (2005) shows that the presence of a diffusive inhibitor species E* could indeed account for proper checkpoint function. However, in the "emitted-inhibition" model, E molecules are instantaneously activated upon entering the kinetochore region (indicated by ∞ in Eq. (2.3.1a), see also Fig. 2.3A). This scenario is unrealistic, because kinetochore-dependence implies an interaction of the E molecules with any structure at the kinetochore, which will neccessarily take some time to proceed. The rate of kinetochore binding of E molecules might potentially be limiting for checkpoint activation.

To determine the effect of realistic binding kinetics on checkpoint activation, we studied two slightly different modifications of the original "emitted-inhibition" model: the first variant models kinetochore-recruitment of the inhibitor molecules with implicit binding sites while the second variant introduces the binding sites explicitly. For the "implicit- binding" variant (Fig. 2.3B), we replaced reaction (2.3.1a) by the process

$$\mathrm{E} \xrightarrow{\mathrm{k}^*_{\mathrm{on}}} \mathrm{E}_{\mathrm{kin}} \tag{2.3.2a}$$

$$\mathrm{E}_{\mathrm{kin}} \xrightarrow{\mathrm{k}_{\mathrm{off}}} \mathrm{E} \tag{2.3.2b}$$

$$\mathrm{E}_{\mathrm{kin}} \xrightarrow{\mathrm{k}_{\mathrm{cat}}} \mathrm{E}^* \tag{2.3.2c}$$

where $\mathrm{E}_{\mathrm{kin}}$ denotes the kinetochore-bound (yet still inactive) inhibitor. The binding reaction (2.3.2a) is restricted to E-molecules in the vicinity of unattached kinetochores. Although this process looks similar to Michaelis- Menten kinetics at a first

glance, it is basically different because the binding sites are not explicitly considered and therefore saturation is impossible. In contrast, the "explicit binding" variant (Fig. 2.3C) replaces the kinetochore-dependent reaction (2.3.1a) with the Michaelis-Menten-like reaction rules

$$\mathrm{K} + \mathrm{E} \xrightarrow{\mathrm{k_{on}}} \mathrm{K{:}E} \tag{2.3.3a}$$

$$\mathrm{K{:}E} \xrightarrow{\mathrm{k_{off}}} \mathrm{K} + \mathrm{E} \tag{2.3.3b}$$

$$\mathrm{K{:}E} \xrightarrow{\mathrm{k_{cat}}} \mathrm{K} + \mathrm{E}^* \tag{2.3.3c}$$

The binding sites K and thus the complex K:E are localized at the kinetochores; the binding reaction (2.3.3a) is restricted to unattached kinetochores as in the "implicit binding" variant. In analogy to the molecular identities assumed above, K could be mapped to Mad1. The most significant difference compared to the former variant is the possibility of saturation of the binding sites. A more formal difference lies in the nature of the association rate constants $\mathrm{k}^*_{\mathrm{on}}$ and $\mathrm{k_{on}}$. While $\mathrm{k_{on}}$ is an ordinary second- order rate constant, $\mathrm{k}^*_{\mathrm{on}}$ is an effective first-order rate constant which is roughly equal to $\mathrm{k_{on}} \cdot [\mathrm{K}]_0$, where $[\mathrm{K}]_0$ is the initial concentration of binding sites at a single kinetochore. As a consequence, one will not obtain the $\mathrm{K_D}$ of the actual binding reaction from the quotient $\mathrm{k_{off}}/\mathrm{k}^*_{\mathrm{on}}$. However, one can observe a " phantom" dissociation constant $\mathrm{K}^*_{\mathrm{D}}$ which relates the product of the equilibrium concentrations of the free inhibitor E and the kinetochores to the concentration of the kinetochore-bound inhibitor.

If, for instance, the complex K:E has the dissociation constant $\mathrm{K_D}$ and every kinetochore bears exactly one binding site K, then (excluding the possibility of saturation) one would observe a phantom-dissociation constant $\mathrm{K}^*_{\mathrm{D}} = \mathrm{K_D}$ because the kinetochore and K-molecules are equally concentrated. If the amount of binding sites increases n-fold, one would observe $\mathrm{K}^*_{\mathrm{D}} = n^{-1}\mathrm{K_D}$ whereas the effective association rate constant $\mathrm{k}^*_{\mathrm{on}}$ would increase n-fold since the kinetochore concentration stays constant while the amount of E molecules bound to the kinetochore increases n-fold.

2.3.2 Checkpoint Activation Requires Fast Association Rates

Figure 2.4 shows the influence of implicit and explicit kinetochore-binding on the level of checkpoint activity, i.e., C-inhibition, for various combinations of association rate constant k_{on} (or k^*_{on} respectively) and catalytic activity k_{cat}. All plots show the level of inhibition reached at the time the last kinetochore is attached. The plots

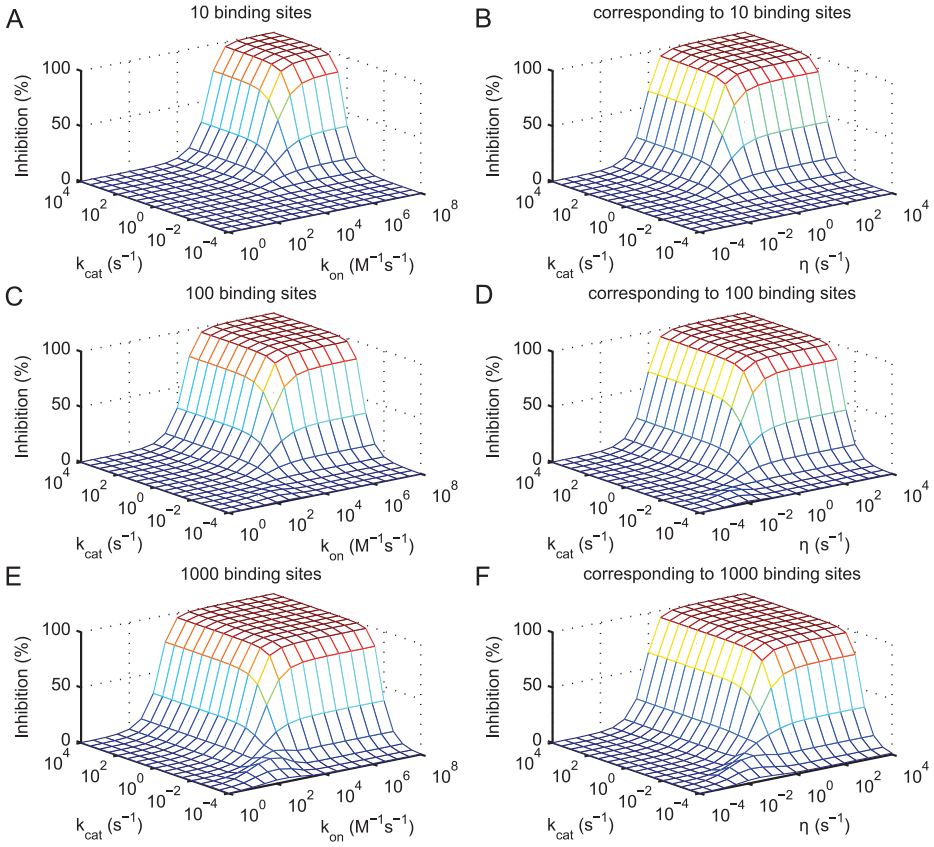

Figure 2.4: Effect of binding kinetics on the "emitted- inhibition" model. Plots show the level of C- inhibition as a function of the rate constant of inhibitor- activation (equations (2.3.2a) and (2.3.3a)) (k_{cat}) and the rate constant of inhibitor- binding to the kinetochores (equations (2.3.2b) and (2.3.3b).) The function value was taken at the time of the attachment of the last kinetochore. (**A**) Explicit binding with 10 binding sites per kinetochore, $K_D = 10^{-6}$ M. (**B**) Implicit binding corrsponding to **A**, $K_D^* = 10^{-7}$ M. (**C**) Explicit binding with 100 binding sites per kinetochore, $K_D = 10^{-6}$ M. (**D**) Implicit binding corrsponding to **B**, $K_D^* = 10^{-8}$ M. (**E**) Explicit binding with 1000 binding sites per kinetochore, $K_D = 10^{-6}$ M. (**F**) Implicit binding corrsponding to **E**, $K_D^* = 10^{-9}$ M. See main text for details.

on the left display the result of the "explicit binding"-variant with 10, 100 and 1000 binding sites. The plots on the right show the result of the "implicit binding"-variant with the phantom dissociation constant K_D^* chosen according to K_D and the same

Parameter	Value[E]	Value[I]	Unit	Remarks
		Rate constants		
k_1	0.1	0.1	s^{-1}	Doncic *et al.* (2005)
k_2	$2.5 \cdot 10^6$	$2.5 \cdot 10^6$	$M^{-1}s^{-1}$	(Doncic *et al.*, 2005)
k_3	0.02	0.02	s^{-1}	Doncic *et al.* (2005)
k_{on}	$10^0 - 10^8$		$M^{-1}s^{-1}$	this study
k^*_{on}		$10^{-4} - 10^4$	s^{-1}	this study
k_{cat}	$10^{-4} - 10^4$	$10^{-4} - 10^4$	s^{-1}	this study
K_D	10^{-6}		M	this study
K^*_D		$10^{-7} - 10^{-9}$	M	this study
		Initial amounts		
C	10^3	10^3	molecules	Doncic *et al.* (2005)
E	10^4	10^4	molecules	Doncic *et al.* (2005)
K	$3.2 \cdot 10^2 - 3.2 \cdot 10^4$		molecules	this study
all other species	0	0	molecules	
		Environment		
kinetochore number	32	32		
kinetochore radius	0.1	0.1	μm	(O'Connell *et al.*, 2007)
radius of the nucleus	1	1	μm	(Doncic *et al.*, 2005)
diffusion rates	1	1	$\mu m^2 s^{-1}$	(Doncic *et al.*, 2005)
		Phase durations		
Before 1st attachment:	15	15	min	
32 attachments during	20	20	min	(Wollman *et al.*, 2005), HeLa cells

[E] Explicit binding variant [I] Implicit binding variant

Table 2.2: Parameters of the "emitted inhibition" model.

number of binding sites. The parameter set used for the simulations was taken from Doncic *et al.* (2005) when appropriate and therefore reflects the situation in budding yeast. A summary is given in Table 2.2.

We find that the "emitted inhibition" model can only maintain checkpoint activity properly if association and catalysis are fast, even if no saturation of binding sites can occur ("implicit binding" variant). With implicit binding, the lower limit for the association rate constant is $k^*_{on} \approx 10\ s^{-1}$. Taking into account the kinetochore volume of about $4.2 \cdot 10^{-18}$ l, 10 to 1000 binding sites/ kinetochore correspond to local concentrations $[K]_0$ of $4 \cdot 10^{-6}$ – $4 \cdot 10^{-4}$ M. Thus we expect lower limit second-order association rate constants ranging from $2.5 \cdot 10^6\ M^{-1}s^{-1}$ down to $2.5 \cdot 10^4\ M^{-1}s^{-1}$ for explicit binding because $k_{on} \approx k^*_{on}/[K]_0$. These rates are indeed in good agreement with the lower limit association rate constants obtained from the simulation of the "explicit binding"-variant (Fig. 2.4).

2.3.3 Microtubule Attachments Can Limit Checkpoint Efficiency

For effective checkpoint function, the lower limit for the catalysis rate constant k_{cat} decreases with increasing number of binding sites (respectively decreasing K^*_D in the case of implicit binding, see Fig. 2.4). This is expected, because low k_{cat} results in accumulation of inhibitor molecules at the kinetochores. The activation of all bound inhibitor molecules takes place simultaneously and can compensate for the low catalysis rate.

The maximum amount of inhibitor molecules that can be bound to the kinetochores simultaneously is limited by the K_D of the binding site-inhibitor complex, and by the number of binding sites if their amount is low. Because microtubule attachment deactivates the binding sites at the respective kinetochore (effectively decreasing their amount), checkpoint function becomes sensitive to the number of remaining unattached kinetochores: To guarantee sufficient throughput for checkpoint activation and maintenance, a minimum amount (depending on k_{cat}) of active binding sites is required. If, by attachment, the number of available binding sites falls below this minimum amount for the first time, overall throughput is reduced. This effect will increase with every further microtubule attachment to the kinetochores.

The difference in the system dynamics with moderate and low k_{cat} is shown in Figure 2.5 (vertical gray lines mark the individual microtubule attachments). It compares the time-course of a simulation of the "explicit binding"-variant under equal conditions but for different k_{cat}. At fast catalysis rate k_{cat} (Fig. 2.5A), no accumulation of the inhibitor E can be observed (compare lines for the binding site-inhibitor complex K:E and unoccupied binding sites K). If k_{cat} is significantly decreased, about 75% of the binding sites are occupied before the attachment (Fig. 2.5B). With every attachment, the number of K:E complexes decreases. Note that the figures dis-

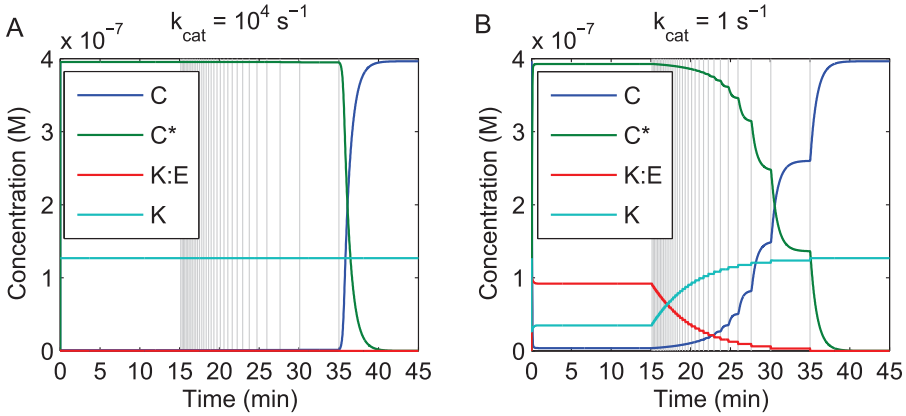

Figure 2.5: Sensitivity of the "explicit binding"- variant to microtubule attachments. Time course of two simulations of the "explicit binding"-variant of the "emitted inhibition" model with binding rate $k_{on} = 10^8$ $M^{-1}s^{-1}$, $K_D = 10^{-6}$ M and 10 binding sites per kinetochore. Vertical gray lines indicate microtubule attachments. (**A**) High catalysis rate $k_{cat} = 10^4$ s^{-1}. (**B**) Low catalysis rate $k_{cat} = 1$ s^{-1}.

play the total concentration of unoccupied binding sites K and do not differentiate between their active and inactive states.

The SAC must not loose efficiency with decreasing numbers of unattached kinetochores, since premature checkpoint deactivation must be prevented. Therefore every kinetochore-localized checkpoint protein with catalytic activity which is negatively regulated by microtubule attachment must have high catalytic activity or appear in high copy numbers per single kinetochore. Conversely, a protein with low catalytic activity existing only in low copy numbers can most likely not keep up checkpoint activity.

2.3.4 Kinetochore-Localization of the Catalyst Alone Does not Acclelerate Checkpoint Activation in the "Mad2 Template" Model

Because the above results showed that binding kinetics can indeed be limiting for checkpoint activation, we guessed that similar effects could be found for the "Mad2 template" model proposed by De Antoni *et al.* (2005) (see also Ibrahim *et al.*,2008, and Simonetta *et al.*, 2009). This model is governed by the following reaction rules (cf. Fig. 2.6):

$$\text{Cdc20} + \text{O-Mad2} \underset{k_{bind,off}}{\overset{k_{bind,on}}{\rightleftharpoons}} \text{Cdc20:C-Mad2} \tag{2.3.4a}$$

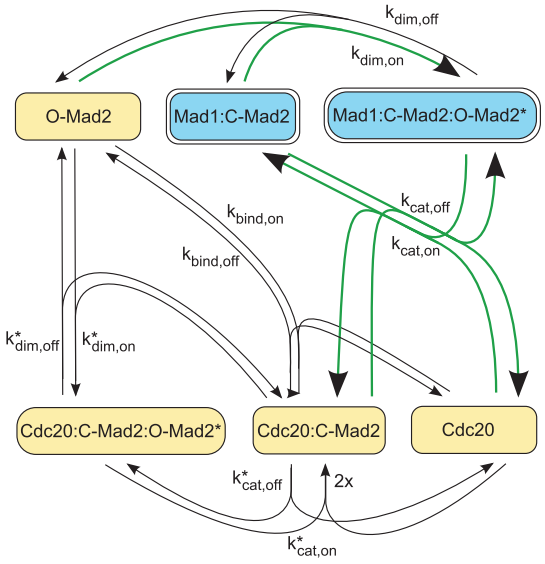

Figure 2.6: Reaction scheme of the "Mad2 template" model. Thick green arrows indicate reactions restricted to the vicinity of unattached kinetochores, blue boxes with double outline denote kinetochore-localized species.

$$\text{Mad1:C-Mad2} + \text{O-Mad2} \underset{k_{dim,off}}{\overset{k_{dim,on}}{\rightleftharpoons}} \text{Mad1:C-Mad2:O-Mad2*} \tag{2.3.4b}$$

$$\text{Mad1:C-Mad2:O-Mad2*} + \text{O-Mad2} \underset{k_{cat,off}}{\overset{k_{cat,on}}{\rightleftharpoons}} \text{Cdc20:C-Mad2} + \text{Mad1:C-Mad2} \tag{2.3.4c}$$

$$\text{Cdc20:C-Mad2} + \text{O-Mad2} \underset{k^*_{dim,off}}{\overset{k^*_{dim,on}}{\rightleftharpoons}} \text{Cdc20:C-Mad2:O-Mad2*} \tag{2.3.4d}$$

$$\text{Cdc20:C-Mad2:O-Mad2*} + \text{O-Mad2} \underset{k^*_{cat,off}}{\overset{k^*_{cat,on}}{\rightleftharpoons}} 2\text{Cdc20:C-Mad2} \tag{2.3.4e}$$

Due to the localization of the Mad1:C-Mad2 complex (Musacchio *et al.*, 2007), reactions (2.3.4b) and (2.3.4c) take place only at unattached kinetochores, while the other reactions proceed everywhere. All kinetic parameters of this model were determined *in vitro* by Simonetta *et al.* (2009) and are used here for the simulations of this model. A summary of all simulation parameters is given in Table 2.3. The authors of (Simonetta *et al.*, 2009) point out the importance of fast checkpoint activation, giving a time constraint of about 10 minutes for reaching maximal Cdc20-inhibition. However, with their kinetic data the checkpoint activation would be too slow. They

suggest that localization of the Mad1:C-Mad2 complex to the kinetochores increases the checkpoint activation rate, because locally the concentration of this complex is much higher. We wanted to find out whether there are combinations of the rate constants for the kinetochore dependent reactions (2.3.4b) and (2.3.4c), that lead to maximal inhibition in at most 10 minutes. Therefore we scanned the parameters $k_{dim,on}$ and $k_{cat,on}$ in a range from 10^2 $M^{-1}s^{-1}$ to 10^8 $M^{-1}s^{-1}$ while keeping the respective K_Ds constant. We measured the level of Cdc20- inhibition after 5, 10, 15, 20, 30 and 60 minutes, the result is shown in Figure 2.7. The critical values for checkpoint activation decrease if the checkpoint is given more time to become fully activated (Fig. 2.7A to 2.7F). Yet even for the much weaker time constraint of 60 minutes, full checkpoint activity needs still dimerization rate constants of $> 10^4$ $M^{-1}s^{-1}$at a catalysis rate constant of $\geq 10^6$ $M^{-1}s^{-1}$.

The parameters measured *in vitro* by Simonetta *et al.* (2009) are significantly lower than the parameter combinations needed for full checkpoint activation in less than 10 minutes (see Fig. 2.7A and 2.7B, "M"- labeled arrows indicate measured parameter values). Because we explicitly considered localization and thus have high local concentrations of the kinetochore-localized complex Mad1:C-Mad2 (blue in Fig. 2.6), this result contradicts the argument given in (Simonetta *et al.*, 2009) that high local concentrations of Mad1:C-Mad2 due to kinetochore-localization could make checkpoint activation sufficiently fast.

According to Simonetta *et al.* (2009), an increase in the catalysis rate constant by a factor of 300 (while maintaining the K_D) should be sufficient to establish full checkpoint activity in 10 minutes. We find instead that full activation is not reached during the first 60 minutes (cf. "$\times$ 300"-labeld arrows in Fig. 2.7A to 2.7F). However, full checkpoint activity might be reached even within 5 minutes with dimerization rate constants above 10^6 $M^{-1}s^{-1}$at a catalysis rate constant $> 10^8$ $M^{-1}s^{-1}$. For full activation within 10 minutes, the *in vitro* measured dimerization rate is barely sufficient if the catalysis rate is increased greatly. If the checkpoint must reach full activity in less time, the dimerization rate constant becomes limiting, too.

2.4 Discussion

We have described a simple method for the quasi-spatial simulation of network models for the spindle assembly checkpoint considering realistic numbers of kinetochores. The internal model has only about three times the number of species and interactions as the original model, so integration of the resulting ODE-system is not much slower.

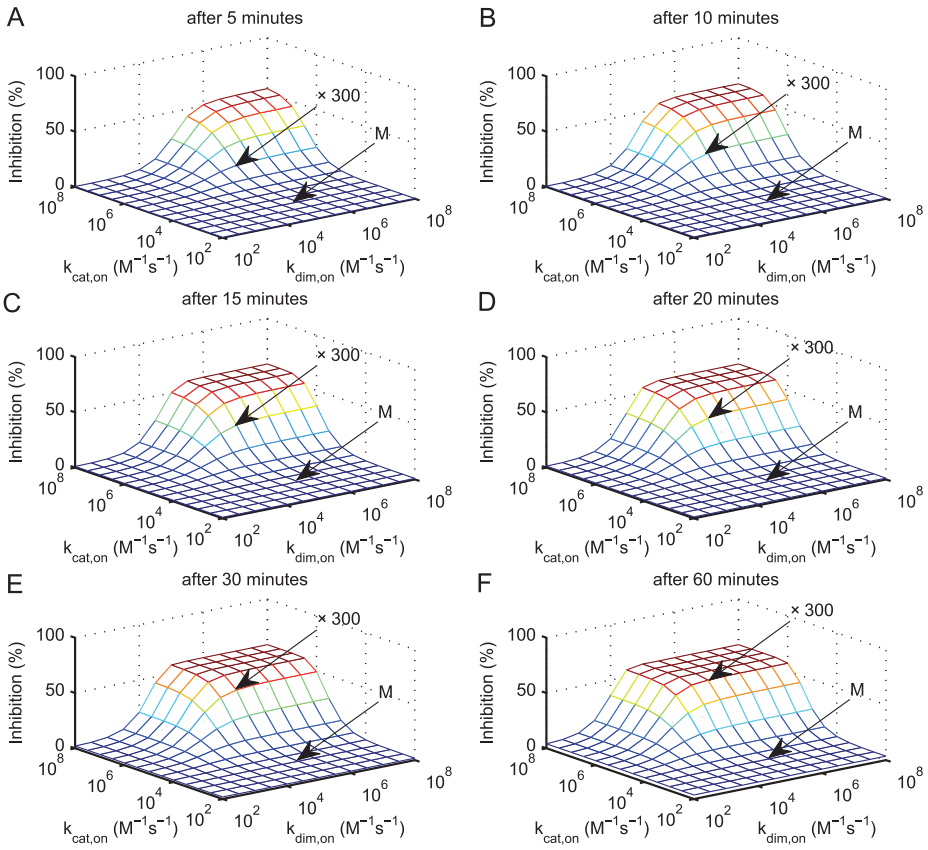

Figure 2.7: Effect of binding kinetics and catalysis on the "Mad2 template" model. Plots show the level of Cdc20- inhibition as a function of the rate constants of the kinetochore dependent dimerization and catalysis reactions with constant K_D. All other parameters were chosen according to Simonetta *et al.* (2009). All kinetochores were kept unattached to allow for maximal checkpoint activation rate. Arrows labeled with "M" mark the experimentally observed parameter values as reported in Simonetta *et al.* (2009). Arrows labeled with "× 300" mark the same dimerization rate, but a 300-fold increased catalysis rate (cf. Simonetta *et al.* (2009)). (**A**) After 5 minutes. (**B**) After 10 minutes. (**C**) After 15 minutes. (**D**) After 20 minutes. (**E**) After 30 minutes. (**F**) After 60 minutes.

However, handling microtubule attachments requires the integration of the ODE-system to be halted and continued after introducing the necessary changes in the species amounts. This introduces additional stiff periods into the integration process

Parameter	Value	Unit	Remarks
		Rate constants	
$k_{bind,on}$	48.3	$M^{-1}s^{-1}$	(Simonetta *et al.*, 2009)
$k_{bind,off}$	$4.83 \cdot 10^{-6}$	s^{-1}	(Simonetta *et al.*, 2009)
$k^*_{dim,on}$	$3 \cdot 10^5$	$M^{-1}s^{-1}$	(Simonetta *et al.*, 2009)
$k^*_{dim,off}$	0.45	s^{-1}	(Simonetta *et al.*, 2009)
$k^*_{cat,on}$	$3 \cdot 10^3$	$M^{-1}s^{-1}$	(Simonetta *et al.*, 2009)
$k^*_{cat,off}$	$2 \cdot 10^2$	s^{-1}	(Simonetta *et al.*, 2009)
$k_{dim,on}$	10^2 – 10^8	$M^{-1}s^{-1}$	this study
$k_{dim,off}$	$1.5 \cdot 10^{-8}$ – $1.5 \cdot 10^{-14}$	s^{-1}	corresponding to $K_D = 1.5\ \mu M$, (Simonetta *et al.*, 2009)
$k_{cat,on}$	10^2 – 10^8	$M^{-1}s^{-1}$	this study
$k_{cat,off}$	$7 \cdot 10^{-4}$ – $7 \cdot 10^{-10}$	$M^{-1}s^{-1}$	corresponding to $K_D = 0.07$, (Simonetta *et al.*, 2009)
		Initial concentrations	
Cdc20	0.1	μM	(Simonetta *et al.*, 2009)
O-Mad2	0.2	μM	(Simonetta *et al.*, 2009)
Mad1:C-Mad2	6.16	nM	(Simonetta *et al.*, 2009)
all other species	0		
		Environment	
kinetochore number	22		
kinetochore radius	0.2	μm	(Simonetta *et al.*, 2009)
radius of the cell	11.25	μm	~ 6 pl, (Simonetta *et al.*, 2009)
diffusion rates	1	$\mu m^2 s^{-1}$	
		Phase durations	
Before 1st attachment:	5 – 60	min	

Table 2.3: Parameters and initial conditions of the "Mad2 template" model.

which slow down integration much more than the larger internal network model. Though, a typical simulation takes much less than 1 second on a recent workstation. It is therefore fast enough for use with parameter fitting algorithms, which require many evaluations of the system dynamics.

The continuous approach for the simulation of microtubule attachment taken by Mistry *et al.* (2008) could make integration faster. Yet this hides the rather instantaneous character of the microtubule attachments especially if there are only few

unattached kinetochores left and the times between subsequent attachments are in the range of several minutes, which might not be desirable.

We extended the "emitted inhibition" model by Doncic *et al.* (2005) by realistic kinetochore binding kinetics and found that checkpoint activation and maintenance is only sufficient if the association rate constant k_{on} is not below a critical value. This critical value is sensitive to the number of binding sites at the kinetochore and lies in a range between 10^4 – 10^6 $M^{-1}s^{-1}$ (assuming $K_D = 10^{-6}$ M for the complex of inhibitor and binding site), which is in the range of typical protein-protein association rate constants (Schlosshauer *et al.*, 2004; Schreiber, 2002). The reactions of the " emitted inhibition" model with explicit binding are similar to those of the "Mad2 exchange" model, assuming the mapping given above. For the association of O-Mad2 and Mad1 (cf. Eq. (2.3.3a)) and the dissociation of Mad1:C-Mad2 complex (cf. Eq. (2.3.3b)), rate constants of $4 \cdot 10^3$ $M^{-1}s^{-1}$ and $1.5 \cdot 10^{-2}$ s^{-1}, respectively (corresponding to $K_D = 3.75 \cdot 10^{-6}$ M) have been measured *in vitro*(Luo *et al.*, 2004). In addition, Luo *et al.* (2004) reported the rate constant for the Mad1-catalyzed conversion from O-Mad2 to C-Mad2 (cf. Eq. (2.3.3c)) to be $2.8 \cdot 10^4$ s^{-1}. These rate constants are clearly below the critical value even for high binding site numbers and make this model unlikely to explain checkpoint function. This is in agreement with our former results (Ibrahim *et al.*, 2008).

The "Mad2 template" model (De Antoni *et al.*, 2005; Ibrahim *et al.*, 2008; Simonetta *et al.*, 2009) is similar to the "Mad2 exchange" model (Ibrahim *et al.*, 2008; Luo *et al.*, 2004) in that both are based on catalysis of the conformational change from O-Mad2 to C-Mad2 at the kinetochores and subsequent sequestration of Cdc20 by C-Mad2. The "Mad2 template" model mainly differs from the "Mad2 exchange" model by splitting Cdc20-sequestration between the kinetochores (Eqs. (2.3.4b) and (2.3.4c)) and a kinetochore independent autocatalytic loop (Eqs. (2.3.4d) and (2.3.4e)). The kinetic parameters for the template model were determined *in vitro* by Simonetta *et al.* (2009).

We showed that localization of the catalyst Mad1:C-Mad2 at the kinetochores does not accelerate checkpoint activation *in silico*. This is expected, because only the catalyst is localized but its "substrate" is not. If for example the catalyst is restricted to only 10% of the total volume, its concentration increases 10-fold. Therefore – assuming that the law of mass action holds – the reaction rate increases also 10- fold. But due to the spatial restriction of the catalyst to 10% of the volume, only 10% of the diffusible substrate participates in these reactions. Therefore the overall rate of change in the concentrations of substrate and product remains unaffected. However,

if both, the catalyst and its substrate, would localize to the kinetochores, the overall catalysis rate would increase. Simonetta *et al.* (2009) hypothesized that unknown molecular mechanisms facilitate catalysis of Cdc20-sequestration at the kinetochores. We see from Figure 2.7A that binding of O-Mad2 to Mad1:C-Mad2 would also have to be increased, if the checkpoint would have to be activated much faster.

Due to our recent finding that the amplification by the autocatalytic loop of the "Mad2 template" model is vanishing if the reaction rate constants are low (Ibrahim *et al.*, 2008), we removed reactions (2.3.4d) and (2.3.4e) from the model. The changes were not perceptible when compared to Figure 2.7 (data not shown). This is because direct binding (Eq. (2.3.4a)) dominates Cdc20 sequestering in the low parameter ranges of Figure 2.7, while kinetochore dependent catalysis ((2.3.4b) and (2.3.4c)) becomes increasingly important in the higher parameter ranges in Figure 2.7. Because accelerated catalysis at the kinetochores seems to be required for fast checkpoint activation, autocatalytic amplification seems to have rather small influence on checkpoint activation.

Our simulations show that the deactivation of molecular species from the kinetochore upon microtubule attachment (e.g., by removal) can negatively affect the efficiency of checkpoint maintenance. If the deactivated species act as catalysts at the kinetochores, the effect is comparable to the reduction of the maximal velocity of Michaelis-Menten kinetics, as the amount of active "enzyme" is reduced. If, on the other hand, a molecular species binds another species (like the Cdc20-binding Bub3:BubR1 complex for example), and its binding ability is reduced by microtubule attachment, then this species cannot serve as a stoichiometric inhibitor. Therefore, it is not sufficient to introduce microtubule attachments by simple linear scaling of the reaction rates.

3 A Minimal Model of the Intrinsic GTPase-cycle of Tem1

This work results from a collaboration with Dr. Gislene Pereira at the German Cancer Research Center and has been described in a publication (Caydasi *et al.*, 2012) to which I contributed the modeling work and the theoretical and computational analysis.

3.1 Introduction

Small GTPases are essential building blocks of many intracellular signal transduction chains. These enzymes constitute a diverse family of proteins sharing important structural features, which provide the ability to bind and hydrolyze guanosine triphosphate (GTP) to guanosine diphosphate (GDP) (Bourne *et al.*, 1991). Binding to GTP or GDP induces a nucleotide-dependent conformational switch, such that their GTP-bound form does generally interact more strongly with their downstream-effectors than thir GDP-bound form (Vetter *et al.*, 2001). Thus, GTP-bound GTPases are considered to be in their active state. Consequently, GTP-hydrolysis impedes interaction with the effectors, rendering the GTPase inactive. The key steps in regulation of

GTPase-activity are summarized in the so called GTPase-cycle (see Figure 3.1). The nucleotide-free GTPase binds reversibly to GTP or GDP, switching activity accordingly. Active, GTP-bound GTPase is transformed into the inactive GDP-bound form through its intrinsic hydrolytic activity (Bourne *et al.*, 1991). GTPases' affinities for GDP and GTP are high (Bourne *et al.*, 1991) while the intrinsic hydrolytic activity of many GTPases is very low (Bourne *et al.*, 1991; Sprang, 1997), so state transitions from active to inactive or vice versa would be very rare events. Two kinds of regulatory co-factors evolved together with the GTPases to turn the GTPase-cycle into a precisely regulated and highly dynamic system. Guanine-nucleotide exchange factors (GEFs) bind to GTPases and reduce the affinity for GTP/GDP, whereas GTPase-activating-proteins (GAPs) bind to make hydrolysis considerably faster (Bos *et al.*, 2007; Bourne *et al.*, 1991; Scheffzek *et al.*, 1998; Sprang, 1997). Generally, the intracellular concentration of GTP is several times higher than that of GDP (Bos *et al.*, 2007; Rudoni *et al.*, 2001). Affinities of the GTPases are similar for GTP and GDP, so GEF-enhanced nucleotide exchange is more likely to result in the GTP-bound active form (Bos *et al.*, 2007). This makes GEFs antagonistic to GAPs, which promote rapid GTPase inactivation.

In the course of this chapter, a model of the intrinsic GTPase-cycle of the small Ras-like GTPase Tem1 of *S. cerevisiae* shall be developed, analyzed and eventually reduced to the smallest possible dynamic model without sacrificing accuracy and interpretability.

3.1.1 The Small Ras-like GTPase Tem1

Tem1 has been identified as a GTP-binding protein in a study seeking for an mitotic interaction partner of the GEF-like protein Lte1, which is a homolog of GEFs of Ras-GTPases (Shirayama, Matsui, and Toh-E, 1994). Because Tem1 has significant sequence identity with GTPases of the Ras-family, it was presumed that Lte1 could act as a positive regulator of Tem1 (i.e., its GEF) (Shirayama, Matsui, and Toh-E, 1994). However, Tem1 turned out to be a somewhat particular GTPase. An *in vitro* study showed that at room temperature Tem1 readily releases bound nucleotides and consequently does not require a GEF for efficient nucleotide exchange (Geymonat *et al.*, 2002). In line with that, Lte1 has been shown to not increase nucleotide turnover of Tem1 (Geymonat *et al.*, 2009). Instead, Lte1 inhibits Kin4-kinase, a negative-regulator of Tem1 activity (Bertazzi *et al.*, 2011). While the active form of Tem1 activates the mitotic exit network (MEN) during unperturbed mitosis, Tem1 must be inactivated in response to spindle misalignment to prevent premature exit from

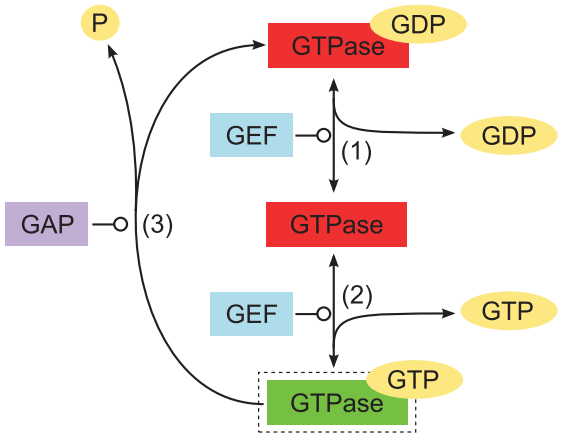

Figure 3.1: The GTPase-cycle. The transition between active (green, with dashed outline) and inactive (red) states of the GTPase is dependent on three reactions. The nucleotide-free GTPase binds cytoplasmic GDP (1) or GTP (2) reversibly, albeit with a very high affinity caused by low dissociation rates. Thus, a once bound nucleotide is rarely released spontaneously. Interaction of the GTPase with a guanine-nucleotide exchange factor (GEF) facilitates dissociation of the bound nucleotide, allowing to rapidly equilibrate with the cytoplasmic ratio of GTP and GDP. Because the cytoplasmic concentration of GTP is in general several times higher than that of GDP, GTP-bound active GTPase becomes the prevalent form in the presence of GEF. The GTPase is inactivated by hydrolysis of the bound GTP (3). Because many GTPases have only low intrinsic hydrolytic activity, they require interaction with a GTPase-activating protein (GAP) for efficient catalysis. See main text for more details.

mitosis. Inactivation of Tem1, however, requires interaction with the two-component GAP Bfa1:Bub2. Tem1, Bfa1 and Bub2 have homologs Spg1, Byr4 and Cdc16 in *S. pombe* (Alexandru *et al.*, 1999; Furge *et al.*, 1998), which participate in an analogous pathway, the septation-initiation network (SIN) (Bardin *et al.*, 2001). The kinetics of these analogous GTPase-cycles have been studied *in vitro* and so sufficient data is available to narrow the parameter space of the mathematical model presented in the next section.

3.2 Results

3.2.1 A Detailed Model of the Intrinsic GTPase-Cycle

The intrinsic GTPase-cycle of Tem1 conforms to the scheme depicted in Figure 3.1 and can be formally written by the detailed reaction scheme below:

$$\mathrm{GTP} + \mathrm{Tem1} \underset{k_{\mathrm{off}}^{\mathrm{T}}}{\overset{\kappa_{\mathrm{T}}}{\rightleftharpoons}} \mathrm{Tem1}^{\mathrm{GTP}} \xrightarrow{k_{\mathrm{cat}}} \mathrm{Tem1}^{\mathrm{GDP}} \underset{\kappa_{\mathrm{D}}}{\overset{k_{\mathrm{off}}^{\mathrm{D}}}{\rightleftharpoons}} \mathrm{Tem1} + \mathrm{GDP}\,. \tag{3.2.1}$$

Note that within chemical reaction equations, Tem1, $\mathrm{Tem1}^{\mathrm{GTP}}$, and $\mathrm{Tem1}^{\mathrm{GDP}}$ represent the molecular species, whereas the same symbols in reaction rate equations are used to denote their respective concentrations.

Considering a cellular volume of about 100 fL and an average number of 3450 Tem1 molecules (see chapter 4), the total cellular concentration of Tem1 is about 0.06 μM. In contrast, intracellular concentrations of GTP and GDP in budding yeast in cultures during mid-exponential growth are about 200 μM and 50 μM, respectively (Rudoni *et al.*, 2001). Thus, concentrations of GTP and GDP exceed the intracellular concentration of Tem1 vastly. Furthermore are the total levels of GTP and GDP metabolically controlled and presumably not substantially altered by the above reactions. Therefore GTP and GDP can be treated as constant external metabolites and the reaction scheme (3.2.1) simplifies to

$$\mathrm{Tem1} \underset{k_{\mathrm{off}}^{\mathrm{T}}}{\overset{k_{\mathrm{on}}^{\mathrm{T}}}{\rightleftharpoons}} \mathrm{Tem1}^{\mathrm{GTP}} \xrightarrow{k_{\mathrm{cat}}} \mathrm{Tem1}^{\mathrm{GDP}} \underset{k_{\mathrm{on}}^{\mathrm{D}}}{\overset{k_{\mathrm{off}}^{\mathrm{D}}}{\rightleftharpoons}} \mathrm{Tem1}\,, \tag{3.2.2}$$

with pseudo first-order rate-constants $k_{\mathrm{on}}^{\mathrm{T}} = \kappa_{\mathrm{T}} \cdot 200\ \mu\mathrm{M}$ and $k_{\mathrm{on}}^{\mathrm{D}} = \kappa_{\mathrm{D}} \cdot 50\ \mu\mathrm{M}$. The simplified reaction scheme is comfortable because it involves only first-order reactions, and so the corresponding reaction rate equations are linear.

3.2.2 Kinetic Parameters

Ras-like GTPases have very high affinities for GTP and GDP, with dissociation constants ranging from 10^{-7} M to 10^{-11} M (Bourne *et al.*, 1991). Hattori *et al.* (1985) and Tucker *et al.* (1986) reported dissociation constants of about $K_{\mathrm{D}} = 10^{-8}$ M for $\mathrm{Ras}^{\mathrm{GDP}}$ and slightly higher values for $\mathrm{Ras}^{\mathrm{GTP}}$. At a temperature of 30° C, $\mathrm{Tem1}^{\mathrm{GTP}}$ releases GTP with a rate $k_{\mathrm{off}}^{\mathrm{T}} = 0.0012\ \mathrm{s}^{-1}$ (Geymonat *et al.*, 2002). GDP-release from $\mathrm{Tem1}^{\mathrm{GDP}}$ was to fast to be measured at 30° C, yet measurements at 13° C resulted in a rate of about 0.0033 s^{-1} (Geymonat *et al.*, 2002). However, the GDP-dissociation

k_{on}^{T}	$k_{\text{off}}^{\text{T}}$	k_{on}^{D}	$k_{\text{off}}^{\text{D}}$	k_{cat}
340 s^{-1}	0.0012 s^{-1}	85 s^{-1}	0.017 s^{-1}	0.002 s^{-1}

Table 3.1: Kinetic parameters of the reaction scheme (3.2.2).

rate of Tem1 homolog Spg1 could be measured at 30° C and was reported to be about 0.012 s^{-1}, 3.5 times faster than the GDP-dissociation rate of Tem1 at 13° C. Because GDP-release from Tem1 appeared to be faster than from Spg1 at 30° C, i choose $k_{\text{off}}^{\text{D}} = 0.017\ \text{s}^{-1}$, the 5-fold of the GDP-dissociation rate at 13° C. The association rate coefficients α_{D} and α_{T} can now be computed from the affinities and the dissociation rates. For simplicity, i assume that the higher affinity for GTP is only due to the lower dissociation rate, i.e., $\kappa_{\text{D}} = \kappa_{\text{T}} = k_{\text{off}}^{\text{D}}/K_{\text{D}} = 1.7 \cdot 10^6\ \text{M}^{-1}\text{s}^{-1}$. The pseudo-first-order association rates follow immediately: $k_{\text{on}}^{\text{D}} = 85\ \text{s}^{-1}$ and $k_{\text{on}}^{\text{T}} = 340\ \text{s}^{-1}$. Notably, these association rates are several orders of magnitude higher than the respective dissociation rate constants, indicating that Tem1 operates at saturation with respect to nucleotide binding.

The rate of GTP-hydrolysis by Tem1 at 30° C is around $k_{\text{cat}} = 0.002\ \text{s}^{-1}$ (Geymonat *et al.*, 2002) and comprises cleavage and subsequent release of the γ-phosphate of GTP. Binding of free phosphate to a ternary GAP:Ras^{GDP} complex has been reported to occur with a low rate of only about 108 $\text{M}^{-1}\text{s}^{-1}$ (Phillips *et al.*, 2003). In turn, the cleaved γ-phosphate is released from the quaternary GAP:$\text{Ras}^{\text{GDP}+\gamma\text{-P}}$ complex with a high rate of 7.8 s^{-1}. This results in a very low affinity of the GAP:Ras^{GDP} complex for free phosphate with a dissociation constant of 72 mM. It is reasonable to assume that that (GAP:)Tem1^{GDP} has a similarly low affinity for free phosphate, thus the GTP-hydrolysis step can be regarded as practically irreversible.

The kinetic parameters are summarized in table 3.1.

3.2.3 Steady State Concentrations of Tem1^{GTP} and Tem1^{GDP}

Equation (3.2.2) can be transformed into a system of linear ordinary differential equations:

$$\begin{aligned}
\frac{\mathrm{d}}{\mathrm{d}t}\text{Tem1}^{\text{GTP}} &= k_{\text{on}}^{\text{T}}\,\text{Tem1} - \left(k_{\text{off}}^{\text{T}} + k_{\text{cat}}\right)\text{Tem1}^{\text{GTP}} \\
\frac{\mathrm{d}}{\mathrm{d}t}\text{Tem1}^{\text{GDP}} &= k_{\text{on}}^{\text{D}}\,\text{Tem1} - k_{\text{off}}^{\text{D}}\,\text{Tem1}^{\text{GDP}} + k_{\text{cat}}\,\text{Tem1}^{\text{GTP}} \\
\frac{\mathrm{d}}{\mathrm{d}t}\text{Tem1} &= k_{\text{off}}^{\text{T}}\,\text{Tem1}^{\text{GTP}} + k_{\text{off}}^{\text{D}}\,\text{Tem1}^{\text{GDP}} - \left(k_{\text{on}}^{\text{T}} + k_{\text{on}}^{\text{D}}\right)\text{Tem1}\,.
\end{aligned} \tag{3.2.3}$$

Note that the stoichiometry of the system implies the conservation law $\mathrm{Tem1} + \mathrm{Tem1}^{\mathrm{GTP}} + \mathrm{Tem1}^{\mathrm{GDP}} = \mathrm{Tem1}_{\mathrm{T}} = const.$ Consequently, the third equation is linearly dependent and can be omitted. Solving the system for the steady state results in the concentrations

$$\begin{aligned} \mathrm{Tem1}_*^{\mathrm{GTP}} &= \frac{\mathrm{Tem1}_{\mathrm{T}}}{a+b}\, k_{\mathrm{off}}^{\mathrm{D}}\, k_{\mathrm{on}}^{\mathrm{T}} \\ \mathrm{Tem1}_*^{\mathrm{GDP}} &= \frac{\mathrm{Tem1}_{\mathrm{T}}}{a+b}\, b \\ \mathrm{Tem1}_* &= \frac{\mathrm{Tem1}_{\mathrm{T}}}{a+b}\left(k_{\mathrm{off}}^{\mathrm{D}}\, k_{\mathrm{off}}^{\mathrm{T}} + k_{\mathrm{off}}^{\mathrm{D}}\, k_{\mathrm{cat}}\right), \end{aligned} \tag{3.2.4}$$

where

$$\begin{aligned} a &= k_{\mathrm{off}}^{\mathrm{D}}\, k_{\mathrm{on}}^{\mathrm{T}} + k_{\mathrm{off}}^{\mathrm{D}}\, k_{\mathrm{off}}^{\mathrm{T}} + k_{\mathrm{off}}^{\mathrm{D}}\, k_{\mathrm{cat}} \\ b &= k_{\mathrm{on}}^{\mathrm{T}}\, k_{\mathrm{cat}} + k_{\mathrm{on}}^{\mathrm{D}}\, k_{\mathrm{off}}^{\mathrm{T}} + k_{\mathrm{on}}^{\mathrm{D}}\, k_{\mathrm{cat}}\,. \end{aligned} \tag{3.2.5}$$

The steady state concentration of Tem1 is significantly smaller than the steady state concentrations of $\mathrm{Tem1}^{\mathrm{GTP}}$ and $\mathrm{Tem1}^{\mathrm{GDP}}$ if, as is the case here, the association rate constants $k_{\mathrm{on}}^{\mathrm{T}}$ and $k_{\mathrm{on}}^{\mathrm{D}}$ are large compared to the dissociation rate constants $k_{\mathrm{off}}^{\mathrm{T}}$, $k_{\mathrm{off}}^{\mathrm{D}}$, and the hydrolysis rate constant k_{cat}. The numerical values of the steady state concentrations, using the kinetic parameters from the previous section and a total Tem1 concentration of 0.06 μM, are listed in Table 3.2. The concentration of nucleotide-free Tem1 is negligible, supporting that Tem1 operates at saturation w.r.t. nucleotide-binding. On the contrary, the active form $\mathrm{Tem1}^{\mathrm{GTP}}$ accounts for 86% of the total Tem1 population.

	$\mathrm{Tem1}^{\mathrm{GTP}}{}_{\mathrm{ss}}$	$\mathrm{Tem1}^{\mathrm{GDP}}{}_{\mathrm{ss}}$	$\mathrm{Tem1}_{\mathrm{ss}}$
Conentration [M]	5.15×10^{-8}	0.85×10^{-8}	5×10^{-13}

Table 3.2: Approximate concentrations of the three forms of Tem1 in steady state according to Eq. (3.2.4) using the parameters listed in Table 3.1.

3.2.4 Sensitivity Analysis of the Steady State Concentrations

While some kinetic parameters have been determined through biochemical experiments involving highly purified Tem1 (Geymonat *et al.*, 2002, 2003, 2009), others need to be transferred from biochemical essays conducted with other Ras-like GTPases. Furthermore, parameters which work for *in vitro* systems might be different in an intracellular environment. To understand how strongly variations of the nominal parameters influence model dynamics, an analysis of the dependency of the steady state concentrations $\mathrm{Tem1}_*^{\mathrm{GDP}}$ and $\mathrm{Tem1}_*^{\mathrm{GTP}}$ with respect to variation of the kinetic

parameters was performed. The corresponding nominal values are listed in Table 3.2.2.

The normalized local sensitivities are defined as

$$\mathcal{S}(X,p) := \frac{p}{X} \cdot \frac{\partial X}{\partial p}$$

where X is a model variable of interest and p is a model parameter. Such sensitivities give information about the relative change of the model variable upon an infinitesimal change of the selected parameter while all other parameters remain at their nominal values. Thus sensitivities are only conclusive if the nominal values of all model parameters are determined with low variation. If this is not the case, then the uncertainties of the respective nominal values must be considered appropriately.

From the steady state defined by Eq. (3.2.4), using the definitions of a and$b$ from Eq. 3.2.5, the following sensitivities result for $\mathrm{Tem1}_*^{\mathrm{GDP}}$:

$$\begin{aligned}
\mathcal{S}\big(\mathrm{Tem1}_*^{\mathrm{GDP}}, k_{\mathrm{on}}^{\mathrm{T}}\big) &= \frac{1}{a\,b+b^2}\, k_{\mathrm{off}}^{\mathrm{D}}\, k_{\mathrm{on}}^{\mathrm{T}}\, \big(k_{\mathrm{off}}^{\mathrm{T}} + k_{\mathrm{cat}}\big)\, \big(k_{\mathrm{cat}} - k_{\mathrm{on}}^{\mathrm{D}}\big) \\
\mathcal{S}\big(\mathrm{Tem1}_*^{\mathrm{GDP}}, k_{\mathrm{off}}^{\mathrm{T}}\big) &= -\frac{1}{a\,b+b^2}\, k_{\mathrm{off}}^{\mathrm{D}}\, k_{\mathrm{on}}^{\mathrm{T}}\, k_{\mathrm{off}}^{\mathrm{T}}\, \big(k_{\mathrm{cat}} - k_{\mathrm{on}}^{\mathrm{D}}\big) \\
\mathcal{S}\big(\mathrm{Tem1}_*^{\mathrm{GDP}}, k_{\mathrm{on}}^{\mathrm{D}}\big) &= \frac{1}{a\,b+b^2}\, k_{\mathrm{on}}^{\mathrm{D}}\, k_{\mathrm{off}}^{\mathrm{D}}\, \big(k_{\mathrm{off}}^{\mathrm{T}} + k_{\mathrm{cat}}\big)\, \big(k_{\mathrm{on}}^{\mathrm{T}} + k_{\mathrm{off}}^{\mathrm{T}} + k_{\mathrm{cat}}\big) \\
\mathcal{S}\big(\mathrm{Tem1}_*^{\mathrm{GDP}}, k_{\mathrm{off}}^{\mathrm{D}}\big) &= -\frac{1}{a\,b+b^2}\, k_{\mathrm{off}}^{\mathrm{D}}\, \big(k_{\mathrm{on}}^{\mathrm{T}} + k_{\mathrm{off}}^{\mathrm{T}} + k_{\mathrm{cat}}\big) \\
\mathcal{S}\big(\mathrm{Tem1}_*^{\mathrm{GDP}}, k_{\mathrm{cat}}\big) &= \frac{1}{a\,b+b^2}\, k_{\mathrm{off}}^{\mathrm{D}}\, k_{\mathrm{on}}^{\mathrm{T}}\, k_{\mathrm{cat}}\, \big(k_{\mathrm{on}}^{\mathrm{T}} + k_{\mathrm{off}}^{\mathrm{T}} + k_{\mathrm{on}}^{\mathrm{D}}\big)\ .
\end{aligned}$$

Similarly, the sensitivities for $\mathrm{Tem1}_*^{\mathrm{GTP}}$ are given by

$$\begin{aligned}
\mathcal{S}\big(\mathrm{Tem1}_*^{\mathrm{GTP}}, k_{\mathrm{on}}^{\mathrm{T}}\big) &= \frac{1}{a+b}\ \big(k_{\mathrm{on}}^{\mathrm{D}} + k_{\mathrm{off}}^{\mathrm{D}}\big)\, \big(k_{\mathrm{off}}^{\mathrm{T}} + k_{\mathrm{cat}}\big) \\
\mathcal{S}\big(\mathrm{Tem1}_*^{\mathrm{GTP}}, k_{\mathrm{off}}^{\mathrm{T}}\big) &= -\frac{1}{a+b}\ \big(k_{\mathrm{on}}^{\mathrm{D}} + k_{\mathrm{off}}^{\mathrm{D}}\big)\, k_{\mathrm{off}}^{\mathrm{T}} \\
\mathcal{S}\big(\mathrm{Tem1}_*^{\mathrm{GTP}}, k_{\mathrm{on}}^{\mathrm{D}}\big) &= -\frac{1}{a+b}\ \big(k_{\mathrm{off}}^{\mathrm{T}} + k_{\mathrm{cat}}\big)\, k_{\mathrm{on}}^{\mathrm{D}} \\
\mathcal{S}\big(\mathrm{Tem1}_*^{\mathrm{GTP}}, k_{\mathrm{off}}^{\mathrm{D}}\big) &= \frac{b}{a+b} \\
\mathcal{S}\big(\mathrm{Tem1}_*^{\mathrm{GTP}}, k_{\mathrm{cat}}\big) &= -\frac{1}{a+b}\ \big(k_{\mathrm{on}}^{\mathrm{D}} + k_{\mathrm{on}}^{\mathrm{T}} + k_{\mathrm{off}}^{\mathrm{D}}\big)\, k_{\mathrm{cat}}\,.
\end{aligned}$$

Table 3.3 lists the numerical sensitivities with respect to the nominal parameter values from Table 3.1. Apparently the steady state concentrations are most sensitive to hydrolysis rate k_{cat} and GDP-dissociation rate $k_{\mathrm{off}}^{\mathrm{D}}$, whereas their dependence on

the rate of GTP-release is only weak.

The absolute values of the sensitivities of $\mathrm{Tem1}_*^{\mathrm{GDP}}$ are larger then those of $\mathrm{Tem1}_*^{\mathrm{GTP}}$. This is the case because the conservation law from the previous section together with the vanishingly small concentration of $\mathrm{Tem1}_*$ (cf. Table 3.2) dictates $\mathrm{Tem1}_*^{\mathrm{GDP}} \approx \mathrm{Tem1}_{\mathrm{T}} - \mathrm{Tem1}_*^{\mathrm{GTP}}$. So every change in $\mathrm{Tem1}_*^{\mathrm{GTP}}$ causes a stoichiometric change in $\mathrm{Tem1}_*^{\mathrm{GDP}}$, yet the relative change in $\mathrm{Tem1}_*^{\mathrm{GDP}}$ is larger by a factor of approximately 6 due to the steady state ratio of $\mathrm{Tem1}_*^{\mathrm{GTP}}$ and $\mathrm{Tem1}_*^{\mathrm{GDP}}$.

Affinities of Tem1 for GTP and GDP have not been reported so far, so they have been transferred from other Ras-like GTPases. Furthermore, pseudo first order association rate coefficients $k_{\mathrm{on}}^{\mathrm{T}}$ and $k_{\mathrm{on}}^{\mathrm{D}}$ are defined as products of the true second order association rate coefficients and the intracellular nucleotide concentrations. Thus they combine two sources of uncertainty, namely inaccurately measured affinities or association rates, and variations of the intracellular nucleotide concentrations. Coefficients $k_{\mathrm{on}}^{\mathrm{T}}$ and $k_{\mathrm{on}}^{\mathrm{D}}$ are therefore parameters with a potentially large deviation of the nominal from the true value. Because the respective sensitivities indicate moderate influence on the steady state (see Table 3.3), it is imperative to further investigate how much these parameters influence the steady state ratio of active and inactive Tem1. Similarly, the impact of their variation on the sensitivities must be evaluated. Both problems are tackled by computing the quantities in question as functions of products $\alpha_{\mathrm{T}} k_{\mathrm{on}}^{\mathrm{T}}$ and $\alpha_{\mathrm{D}} k_{\mathrm{on}}^{\mathrm{D}}$ with the fold-change variables α_{T} and α_{D} varying in a range from 10^{-1} to 10^{1}.

The dependency of the steady state $\mathrm{Tem1}^{\mathrm{GTP}}$-percentage on the nucleotide-association coefficients $k_{\mathrm{on}}^{\mathrm{T}}$ and $k_{\mathrm{on}}^{\mathrm{D}}$ is shown in Figure 3.2. The nominal values for $k_{\mathrm{on}}^{\mathrm{T}}$ and $k_{\mathrm{on}}^{\mathrm{D}}$ lie in a region where the steady state percentage of $\mathrm{Tem1}_*^{\mathrm{GTP}}$ is high and no significant increase is possible without changing the parameters significantly. Furthermore, the steady state is insensitive to a proportional change of both rate constants. Significant decrease of the $\mathrm{Tem1}_*^{\mathrm{GTP}}$ percentage can only be observed in the small part of the parameter space with small $k_{\mathrm{on}}^{\mathrm{T}}$ and large $k_{\mathrm{on}}^{\mathrm{D}}$. Considering the experimentally supported nominal values of the nucleotide-dissociation rate coefficients, these particular parameter combinations can only occur in the unlikely case that the affinity of Tem1 for GDP exceeds its affinity for GTP largely. Hence, at least with respect to all likely scenarios, the steady state concentrations remain basically unchanged by moderate changes of the association rate coefficients.

The results for the dependency of the sensitivities upon changes in the nucleotide-association coefficients are reported in Figure 3.3. The size of the region of approximately equal sensitivities surrounding the nominal values of $k_{\mathrm{on}}^{\mathrm{D}}$ and $k_{\mathrm{on}}^{\mathrm{T}}$ indicates

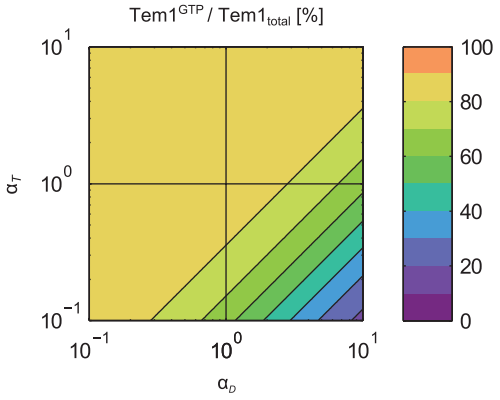

Figure 3.2: Steady state percentage of $\mathbf{Tem1^{GTP}}$. *Figure adapted from Caydasi et al. (2012).* Percentages are plotted as a function of the fold-change variables α_{D} and α_{T} varying GDP and GTP association rate coefficients $k_{\mathrm{on}}^{\mathrm{D}}(\alpha_{\mathrm{D}})$ and $k_{\mathrm{on}}^{\mathrm{T}}(\alpha_{\mathrm{T}})$ in a range from 10^{-1} to 10^{1} times their respective nominal value (crossing of vertical and horizontal lines at $\alpha_{\mathrm{D}} = \alpha_{\mathrm{T}} = 10^{0}$). For the nominal values, the steady state percentage of $\mathrm{Tem1}^{\mathrm{GTP}}$ is near-maximal. Within the scanned parameter range, the percentage depends only on the ratio of $k_{\mathrm{on}}^{\mathrm{D}}$ and $k_{\mathrm{on}}^{\mathrm{T}}$ rather than on their absolute values. Higher percentages of $\mathrm{Tem1}^{\mathrm{GTP}}$ can hardly be reached for any combination of the parameters. However, $\mathrm{Tem1}^{\mathrm{GDP}}$ becomes the prevalent form if the GDP-association rate $k_{\mathrm{on}}^{\mathrm{D}}$ is increased while the GTP-association rate $k_{\mathrm{on}}^{\mathrm{T}}$ is decreased significantly, i.e, if the affinity of Tem1 for GDP becomes significantly higher than its affinity for GTP.

how much their nominal values can deviate from their true values until the sensitivity is not conclusive anymore. As was the case for the steady state percentage of $\mathrm{Tem1}_{*}^{\mathrm{GTP}}$, proportional changes of $k_{\mathrm{on}}^{\mathrm{D}}$ and $k_{\mathrm{on}}^{\mathrm{T}}$ do not change the sensitivities of $\mathrm{Tem1}_{*}^{\mathrm{GTP}}$ or $\mathrm{Tem1}_{*}^{\mathrm{GDP}}$ with respect to any parameter. As discussed previously, the magnitude of the sensitivities of $\mathrm{Tem1}_{*}^{\mathrm{GDP}}$ are generally larger than those of $\mathrm{Tem1}_{*}^{\mathrm{GTP}}$. Both forms of Tem1 are tightly coupled and so are their sensitivities. As the steady state concentration of $\mathrm{Tem1}^{\mathrm{GTP}}$ is the most important quantity with respect to the biological interpretation, the corresponding sensitivities can be regarded as representative for the robustness of the model against inappropriate parameter choices. The sensitivities of $\mathrm{Tem1}_{*}^{\mathrm{GDP}}$ merely complement them. The sensitivities of $\mathrm{Tem1}_{*}^{\mathrm{GTP}}$ are largely unaffected by changes of the nucleotide-association rate coefficients, with the notable exception of the region combining small $k_{\mathrm{on}}^{\mathrm{T}}$ with large $k_{\mathrm{on}}^{\mathrm{D}}$. Following the same argument as for the steady state concentrations, moderate changes of the association rate coefficients do barely alter the sensitivities of $\mathrm{Tem1}_{*}^{\mathrm{GTP}}$. So the numerical

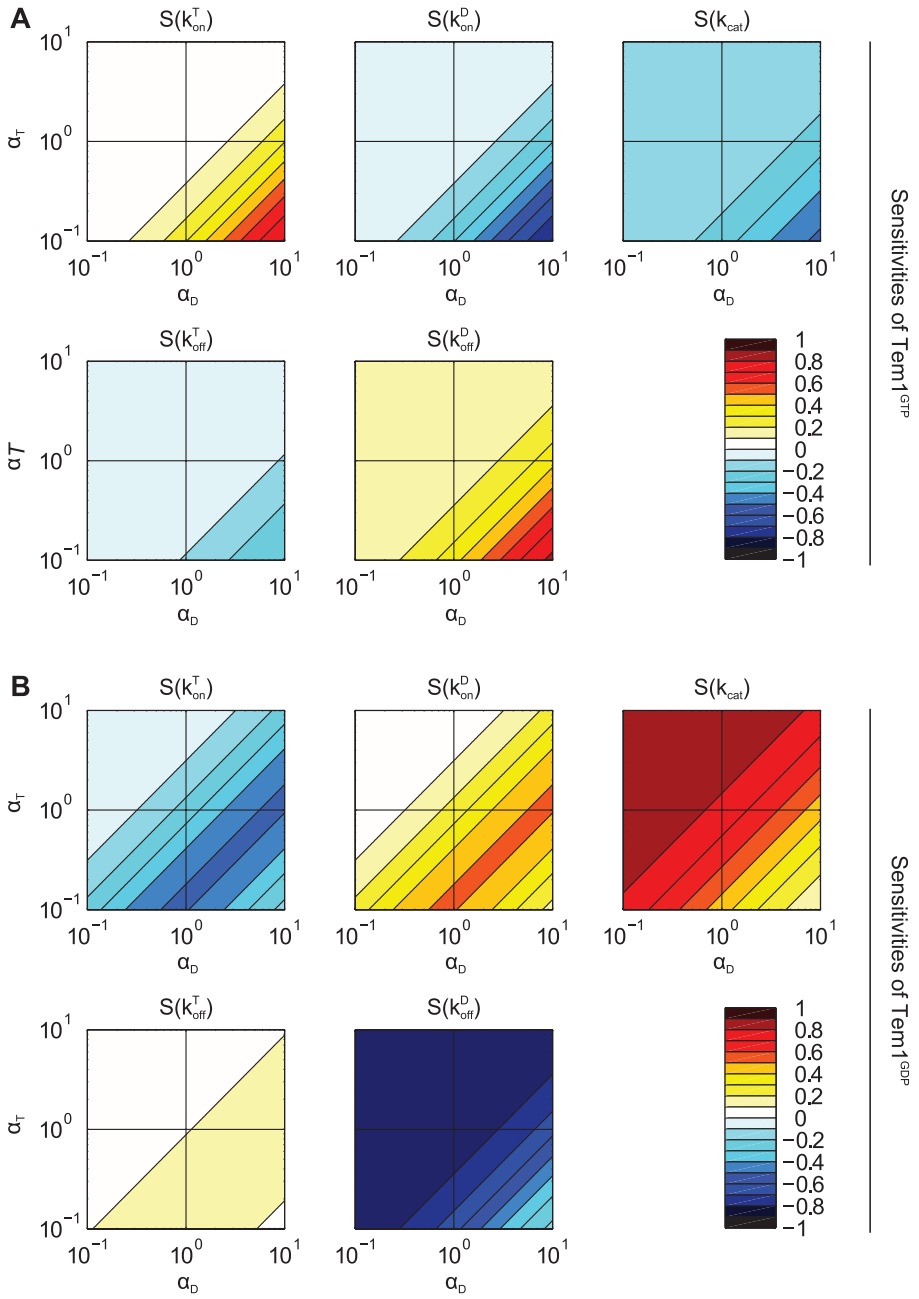

Figure 3.3: Sensitivity analysis. *Figure adapted from Caydasi et al. (2012).* Local sensitivities of the steady state concentrations of nucleotide-bound Tem1 are plotted as a function of the fold-change variables α_{D} and α_{T} varying GDP and GTP association rate coefficients $k_{\mathrm{on}}^{\mathrm{D}}(\alpha_{\mathrm{D}})$ and $k_{\mathrm{on}}^{\mathrm{T}}(\alpha_{\mathrm{T}})$ in a range from 10^{-1} to 10^{1} times their respective nominal value (crossing of vertical and horizontal lines at $\alpha_{\mathrm{D}} = \alpha_{\mathrm{T}} = 10^{0}$). Similar to the percentage of $\mathrm{Tem1}^{\mathrm{GTP}}$ in steady state, sensitivities depend on the ratio of $k_{\mathrm{on}}^{\mathrm{D}}$ and $k_{\mathrm{on}}^{\mathrm{T}}$ and not on their absolute values within the scanned parameter range. (**A**) Sensitivities of the steady state concentration of $\mathrm{Tem1}^{\mathrm{GTP}}$. (**B**) Sensitivities of the steady state concentration of $\mathrm{Tem1}^{\mathrm{GDP}}$.

sensitivities reported in Table 3.3 can be regarded as conclusive.

Table 3.3: Sensitivities of the steady state concentrations $\mathrm{Tem1}_*^{\mathrm{GDP}}$ and $\mathrm{Tem1}_*^{\mathrm{GTP}}$

	$k_{\mathrm{on}}^{\mathrm{T}}$	$k_{\mathrm{off}}^{\mathrm{T}}$	$k_{\mathrm{on}}^{\mathrm{D}}$	$k_{\mathrm{off}}^{\mathrm{D}}$	k_{cat}
$\mathrm{Tem1}_*^{\mathrm{GDP}}$	-0.2453	0.0920	0.2453	-0.8586	0.7666
$\mathrm{Tem1}_*^{\mathrm{GTP}}$	0.0404	-0.0152	-0.0404	0.1414	-0.1263

3.2.5 Derivation of a Minimal Model for the Tem1-GTPase-Cycle

The previous discussion of the kinetic parameters and the sensitivity analysis of the steady state concentrations with respect to them provide two key insights for the reduction of the detailed model. First, the concentration of nucleotide-free Tem1 is vanishingly small in steady state (see Table 3.2). Second, association of GDP and GTP with Tem1 is very fast while dissociation is several orders of magnitude slower. Hence the time-scale of Tem1-depletion must be very small, such that the steady state is approached rapidly from all initial conditions (cf. dynamics of the detailed model in Figure 3.5). It is therefore possible to make use of the quasi steady state assumption and consequently eliminate Tem1 from the model. From

$$\frac{\mathrm{d}}{\mathrm{d}t}\mathrm{Tem1}^{\mathrm{GDP}} \approx 0$$

follows

$$\mathrm{Tem1} \approx \frac{k_{\mathrm{off}}^{\mathrm{T}}\,\mathrm{Tem1}^{\mathrm{GTP}} + k_{\mathrm{off}}^{\mathrm{D}}\,\mathrm{Tem1}^{\mathrm{GDP}}}{k_{\mathrm{on}}^{\mathrm{T}} + k_{\mathrm{on}}^{\mathrm{D}}} \tag{3.2.6}$$

and substitution of (3.2.6) into equation (3.2.3) yields

$$\begin{aligned}
\frac{\mathrm{d}}{\mathrm{d}t}\mathrm{Tem1}^{\mathrm{GTP}} &= -\left(k_{\mathrm{off}}^{\mathrm{T}} + k_{\mathrm{cat}}\right)\mathrm{Tem1}^{\mathrm{GTP}} + \frac{k_{\mathrm{on}}^{\mathrm{T}}}{k_{\mathrm{on}}^{\mathrm{T}} + k_{\mathrm{on}}^{\mathrm{D}}}\left(k_{\mathrm{off}}^{\mathrm{T}}\,\mathrm{Tem1}^{\mathrm{GTP}} + k_{\mathrm{off}}^{\mathrm{D}}\,\mathrm{Tem1}^{\mathrm{GDP}}\right)\\
\frac{\mathrm{d}}{\mathrm{d}t}\mathrm{Tem1}^{\mathrm{GDP}} &= -k_{\mathrm{off}}^{\mathrm{D}}\,\mathrm{Tem1}^{\mathrm{GDP}} + k_{\mathrm{cat}}\,\mathrm{Tem1}^{\mathrm{GTP}} + \frac{k_{\mathrm{on}}^{\mathrm{D}}}{k_{\mathrm{on}}^{\mathrm{T}} + k_{\mathrm{on}}^{\mathrm{D}}}\left(k_{\mathrm{off}}^{\mathrm{T}}\,\mathrm{Tem1}^{\mathrm{GTP}} + k_{\mathrm{off}}^{\mathrm{D}}\,\mathrm{Tem1}^{\mathrm{GDP}}\right).
\end{aligned}$$

For brevity, let

$$p_{\mathrm{GTP}} = \frac{k_{\mathrm{on}}^{\mathrm{T}}}{k_{\mathrm{on}}^{\mathrm{T}} + k_{\mathrm{on}}^{\mathrm{D}}} \qquad \text{and} \qquad p_{\mathrm{GDP}} = \frac{k_{\mathrm{on}}^{\mathrm{D}}}{k_{\mathrm{on}}^{\mathrm{T}} + k_{\mathrm{on}}^{\mathrm{D}}}\,. \tag{3.2.7}$$

These two quotients have a manifest physical interpretation: they can be considered probabilities of the nucleotide-free GTPase to bind either GTP or GDP. Using the

identity $p_{\mathrm{GTP}} = 1 - p_{\mathrm{GDP}}$, the first differential equation can be rearranged to show that this system is fully determined with only one linear differential equation and the conservation law $\mathrm{Tem1}^{\mathrm{GTP}} + \mathrm{Tem1}^{\mathrm{GDP}} = \mathrm{Tem1}_{\mathrm{T}} = const$:

$$\begin{aligned}\frac{\mathrm{d}}{\mathrm{d}t}\mathrm{Tem1}^{\mathrm{GTP}} &= -\left(k_{\mathrm{off}}^{\mathrm{T}} + k_{\mathrm{cat}}\right)\mathrm{Tem1}^{\mathrm{GTP}} + p_{\mathrm{GTP}}\left(k_{\mathrm{off}}^{\mathrm{T}}\,\mathrm{Tem1}^{\mathrm{GTP}} + k_{\mathrm{off}}^{\mathrm{D}}\,\mathrm{Tem1}^{\mathrm{GDP}}\right)\\ &= k_{\mathrm{off}}^{\mathrm{D}}\,\mathrm{Tem1}^{\mathrm{GDP}} - k_{\mathrm{cat}}\,\mathrm{Tem1}^{\mathrm{GTP}} - p_{\mathrm{GDP}}\left(k_{\mathrm{off}}^{\mathrm{T}}\,\mathrm{Tem1}^{\mathrm{GTP}} + k_{\mathrm{off}}^{\mathrm{D}}\,\mathrm{Tem1}^{\mathrm{GDP}}\right)\\ &= -\frac{\mathrm{d}}{\mathrm{d}t}\mathrm{Tem1}^{\mathrm{GDP}}\,.\end{aligned}$$

The number of kinetic parameters can be reduced as well. Collecting the terms in $\mathrm{Tem1}^{\mathrm{GTP}}$ yields

$$\frac{\mathrm{d}}{\mathrm{d}t}\mathrm{Tem1}^{\mathrm{GTP}} = \underbrace{\left(p_{\mathrm{GDP}}\,k_{\mathrm{off}}^{\mathrm{T}} + k_{\mathrm{cat}}\right)}_{k_{\mathrm{hyd}}}\mathrm{Tem1}^{\mathrm{GTP}} + \underbrace{p_{\mathrm{GTP}}\,k_{\mathrm{off}}^{\mathrm{D}}}_{k_{\mathrm{nex}}}\mathrm{Tem1}^{\mathrm{GDP}} \tag{3.2.8}$$

and reveals the effective hydrolysis and nucelotide-exchange rate coefficients

$$\begin{aligned}k_{\mathrm{hyd}} &= p_{\mathrm{GDP}}\,k_{\mathrm{off}}^{\mathrm{T}} + k_{\mathrm{cat}}\\ k_{\mathrm{nex}} &= p_{\mathrm{GTP}}\,k_{\mathrm{off}}^{\mathrm{D}}\,.\end{aligned} \tag{3.2.9}$$

Importantly, each effective rate coefficient incorporates one of the two most regulatory kinetic parameters, k_{cat} and $k_{\mathrm{off}}^{\mathrm{D}}$ (cf. sensitivities in Table 3.3). The effective rate coefficients make it possible to reduce the chemical reaction equation (3.2.2) to

$$\mathrm{Tem1}^{\mathrm{GTP}} \underset{k_{\mathrm{nex}}}{\overset{k_{\mathrm{hyd}}}{\rightleftharpoons}} \mathrm{Tem1}^{\mathrm{GDP}}\,. \tag{3.2.10}$$

It is obvious that every model of any cyclic reaction system requires at least two states and two state transitions, hence this model is minimal.

3.2.6 Validation of Minimal Model Steady State and Dynamics

To qualify as an replacement for the detailed model, the minimal model must meet the following requirements:

1. Approximation of the same steady state as the detailed model with a reasonably small relative error, particularly with respect to $\mathrm{Tem1}^{\mathrm{GTP}}$, for a wide range of nucleotide-association rates.

2. Model dynamics should match those of the detailed model with a reason-

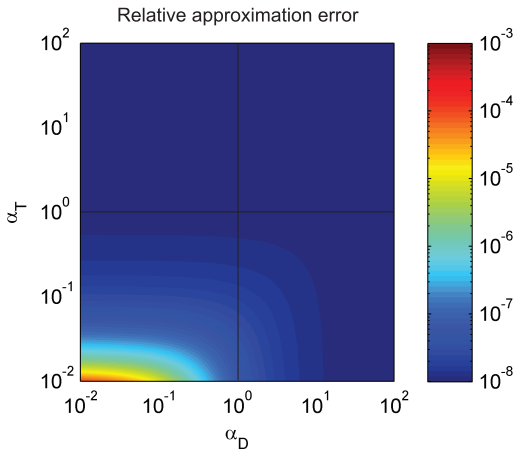

Figure 3.4: Relative error of the approximation of the steady state. Relative errors η are plotted as a function of the fold-change variables α_{D} and α_{T} varying GDP and GTP association rate coefficients $k_{\mathrm{on}}^{\mathrm{D}}(\alpha_{\mathrm{D}})$ and $k_{\mathrm{on}}^{\mathrm{T}}(\alpha_{\mathrm{T}})$ in a range from 10^{-2} to 10^{2} times their respective nominal value (crossing of vertical and horizontal lines at $\alpha_{\mathrm{D}} = \alpha_{\mathrm{T}} = 10^{0}$). See main text for details.

ably small relative error for all initial conditions involving only $\mathrm{Tem1}^{\mathrm{GDP}}$ and $\mathrm{Tem1}^{\mathrm{GTP}}$ (i.e., without nucleotide-free Tem1)..

An analytical expression for the relative approximation error which compares the steady state concentrations of the minimal model with that of the detailed model can be derived easily. With b from Eq. (3.2.5), the steady state solution of Eq. (3.2.8) reads

$$\begin{aligned} \mathrm{Tem1}_*^{\mathrm{GTP}} &= \frac{\mathrm{Tem1_T}}{b + k_{\mathrm{off}}^{\mathrm{D}}\, k_{\mathrm{on}}^{\mathrm{T}}}\, k_{\mathrm{off}}^{\mathrm{D}}\, k_{\mathrm{on}}^{\mathrm{T}} \\ \mathrm{Tem1}_*^{\mathrm{GDP}} &= \mathrm{Tem1_T} - \mathrm{Tem1}_*^{\mathrm{GTP}}\,. \end{aligned} \tag{3.2.11}$$

The relative approximation error for $\mathrm{Tem1}^{\mathrm{GTP}}$, using the respective steady state concentration according to Eq. (3.2.4) as reference value R, is then given by

$$\eta = \left| 1 - \frac{\mathrm{Tem1}_*^{\mathrm{GTP}}}{R} \right| = \left| \frac{k_{\mathrm{off}}^{\mathrm{D}}\, k_{\mathrm{on}}^{\mathrm{T}} - a}{b + k_{\mathrm{off}}^{\mathrm{D}}\, k_{\mathrm{on}}^{\mathrm{T}}} \right|,$$

where a and b are taken from Eq. (3.2.5). Note that the corresponding result obtained by comparing $\mathrm{Tem1}_*^{\mathrm{GDP}}$ to the steady state concentration of $\mathrm{Tem1}^{\mathrm{GDP}}$ according to Eq. (3.2.4) turns out to be identical to η.

With the nominal values of the kinetic parameters from Table 3.1, the relative error of $\mathrm{Tem1}^{\mathrm{GTP}}$ is less than 10^{-5}, hence the steady state can be considered equivalent to that of the detailed model. Figure 3.4 shows that the relative error of $\mathrm{Tem1}^{\mathrm{GTP}}$ remains below 10^{-3} even if both, $k_{\mathrm{on}}^{\mathrm{D}}$ and $k_{\mathrm{on}}^{\mathrm{T}}$, are varied in a range from 10^{-2} to 10^{2} around their nominal values.

Figure 3.5 shows that simulations of the two models using the nominal values of the kinetic parameters exhibit virtually identical dynamics for initial conditions involving only $\mathrm{Tem1}^{\mathrm{GTP}}$ or $\mathrm{Tem1}^{\mathrm{GDP}}$, except for significant, yet rapidly vanishing deviations due to transiently accumulating Tem1 in the detailed model.

Taken together, the minimal model meets above requirements and qualifies as the sought-after replacement for the more detailed model.

3.2.7 Incorporation of the Kinetic Effects of GAPs and GEFs

Careful modification of the effective rate parameters enables the minimal model to account for the kinetic effects of co-factors like GEFs and GAPs with minimal effort.

Binding of an active GAP to a GTPase increases the rate of GTP-hydrolysis significantly. The GAP might additionally hinder dissociation of the nucleotide from the GTPase. In contrast, binding of a GEF to a GTPase facilitates nucleotide exchange by increasing the respective dissociation rates, and additionally it could prevent GTP-hydrolysis. Thus, both kinds of co-factors can be considered to modify the rates of hydrolysis and nucleotide dissociation simultaneously. A general modification of the effective rate coefficients will multiply hydrolysis and nucleotide dissociation rates with separate characterizing factors λ and ρ. For instance, $\lambda = 10^2$ and $\rho = 0$ would characterize a GAP which accelerates hydrolysis by a factor of 100 and prevents nucleotide dissociation, whereas $\lambda = 1$ and $\rho = 10$ describe a GEF which does not affect hydrolysis.

To this end it might be helpful to understand the anatomy of the effective rate coefficients from Eq. (3.2.9). The effective hydrolysis rate coefficient $k_{\mathrm{hyd}} = k_{\mathrm{cat}} + p_{\mathrm{GDP}}\, k_{\mathrm{off}}^{\mathrm{T}}$ defines the rate of the transition from GTP-bound to GDP-bound state. For obvious reasons k_{hyd} contains a coefficient accounting for the hydrolysis step, k_{cat}. The other term, $p_{\mathrm{GDP}}\, k_{\mathrm{off}}^{\mathrm{T}}$, results from the necessity to include the exchange of GTP for GDP as a parallel mechanism for the state transition. The effective nucleotide exchange rate $k_{\mathrm{nex}} = p_{\mathrm{GTP}}\, k_{\mathrm{off}}^{\mathrm{D}}$ models the converse transition from GDP-bound to GTP-bound state. Its single term complements the term for nucleotide exchange included in k_{hyd}.

The aforementioned general modification of the effective rate coefficients to account

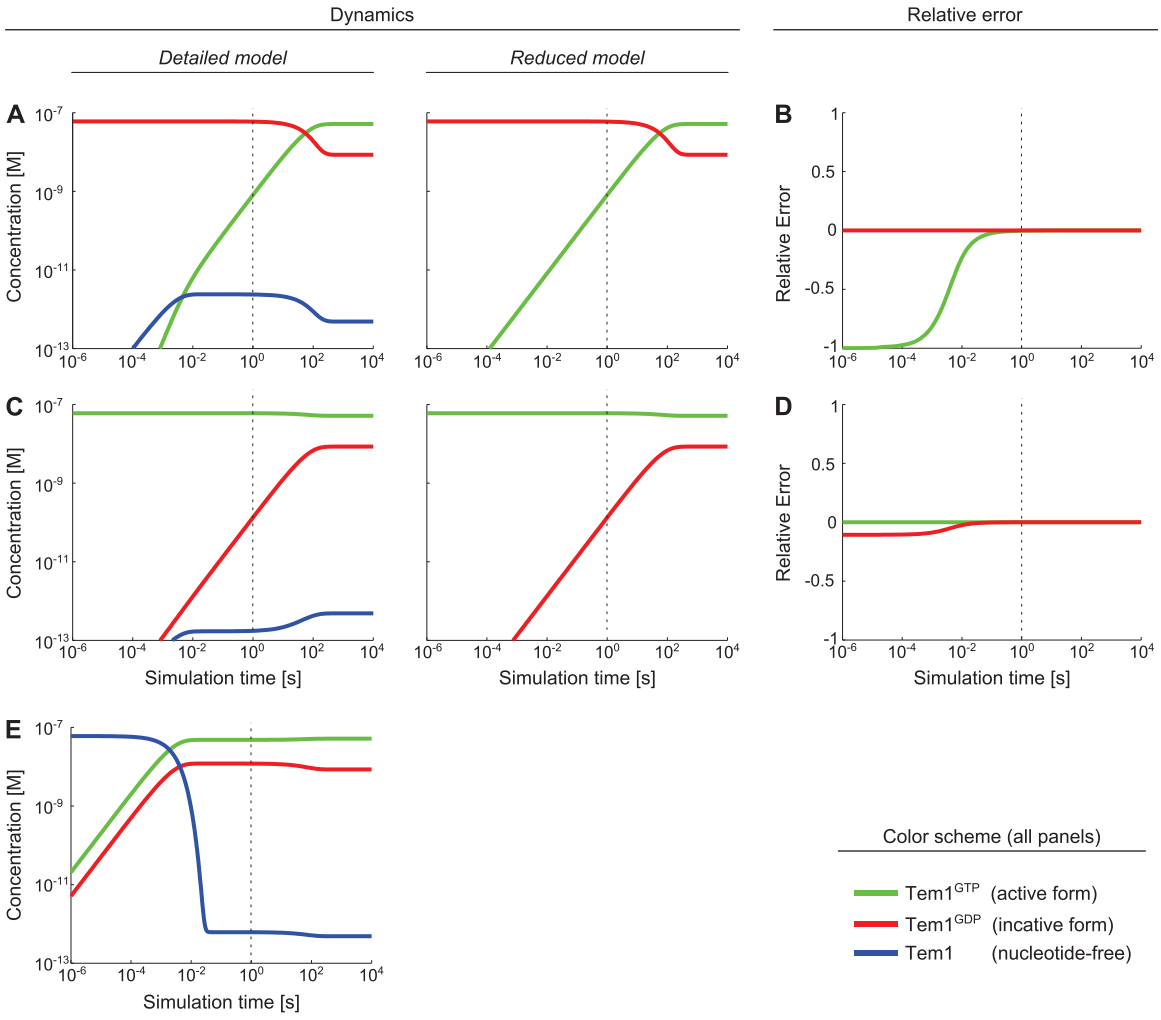

Figure 3.5: Comparison of the dynamics of detailed and reduced model of the intrinsic Tem1-GTPase-cycle. Dynamics and relative error are shown starting from the 3 extreme initial conditions where exactly one state is assigned 100% of total Tem1. The relative error is defined here to be $(C_{\mathrm{detailed}}(t) - C_{\mathrm{reduced}}(t))\,/C_{\mathrm{detailed}}(t)$. (**A**) Initially 100% of total Tem1 are in GDP-bound form ($\mathrm{Tem1}^{\mathrm{GDP}}$). (**B**) Relative error of the reduced model. Although the relative error of $\mathrm{Tem1}^{\mathrm{GTP}}$ is extreme in the very beginning of the simulation, it virtually vanishes within the first second of simulation time. (**C**) Initially 100% of total Tem1 are active, i.e., in GTP-bound form ($\mathrm{Tem1}^{\mathrm{GTP}}$). (**D**) Relative error of the reduced model. Similar to the error of $\mathrm{Tem1}^{\mathrm{GTP}}$ shown in panel B, the initially large error of $\mathrm{Tem1}^{\mathrm{GDP}}$ virtually vanishes within the first second of simulation time. (**E**) Initially 100% of total Tem1 are in nucleotide-free form ($\mathrm{Tem1}$). Note that this initial condition cannot be simulated with the reduced model. $\mathrm{Tem1}$ virtually vanishes within the first second of simulation time and reaches a concentration close to the steady state.

for a co-factor i with characterizing factors λ_i and ρ_i leads to the following definitions:

$$\begin{aligned} k^i_{\mathrm{hyd}} &= p_{\mathrm{GDP}}\,\rho_i\,k^{\mathrm{T}}_{\mathrm{off}} + \lambda_i k_{\mathrm{cat}} \\ k^i_{\mathrm{nex}} &= p_{\mathrm{GTP}}\,\rho_i\,k^{\mathrm{D}}_{\mathrm{off}} \end{aligned} \tag{3.2.12}$$

In the remainder of the text, the characterizing factors are also referred to as fold-acceleration of GTP-hydrolysis or nucleotide dissociation, respectively.

3.3 Discussion

Starting from a generally accepted, moderately detailed model of the intrinsic GTPase-cycle of small Ras-like GTPases, a set of kinetic parameters specific to the Tem1-GTPase of *S. cerevisiae* was derived. Analysis of local sensitivities combined with parameter scans showed that the chosen parameter set does not lie in a critical region of the parameter space, hence the model is robust against modest parameter variation. Furthermore, sensitivity analysis reveals that the rates of GTP-hydrolysis and GDP-dissociation are the main regulatory factors for model dynamics and the ratio of $\mathrm{Tem1}^{\mathrm{GTP}}$ and $\mathrm{Tem1}^{\mathrm{GDP}}$. Subsequently, this model was reduced to a truly minimal model containing only two molecular species and two reactions. The two resulting rate coefficients have a clear physical interpretation and were extended by factors to include the kinetic alterations through bound co-factors like GAPs and GEFs.

Such a minimal model is indispensable for the dynamical SPOC model discussed in the next chapter, because localization and reversible binding of the GAP to the Tem1 must be considered explicitly. Incorporation of a detailed model of the GTPase-cycle would result in a combinatorial explosion of states and transitions. Besides the technical difficulties in adjusting, maintaining and analyzing such huge combinatorial models, they are also hard to understand. This problem is reduced vastly with the minimal model developed here. Together with the meaningful effective rate coefficients, this model enables *in silico* analysis of Tem1-activity within the complex context of the dynamical SPOC model.

Besides the immediate use for modeling the SPOC, the presented minimal model can easily be adapted to other small GTPases by an appropriate choice of parameter values.

4 A Dynamical Model of the Spindle Position Checkpoint

This work results from a collaboration with Dr. Gislene Pereira at the German Cancer Research Center and has been described in a publication (Caydasi *et al.*, 2012) to which I contributed the modeling work and the theoretical and computational analysis.

4.1 Introduction

In contrast to many eukaryotic cell types which define the site of cell division relative to the equatorial plate of the mitotic spindle (Straight *et al.*, 2000), budding yeast determines the later site of cytokinesis (the so called bud neck) and thereby the cell polarity axis early in the cell cycle via a dedicated pathway (Casamayor *et al.*,

2002; Pruyne *et al.*, 2000). To make sure that the replicated genome is segregated evenly between mother and daughter cells, budding yeast must arrange the mitotic spindle such that it is aligned with the cell polarity axis (Caydasi, Ibrahim, *et al.*, 2010; Fraschini *et al.*, 2008; Segal *et al.*, 2001). Spindle elongation can then push one spindle pole together with its associated chromosomes through the bud neck into the daughter cell compartment (the bud). Spindle orientation is achieved by two redundant pathways which link or move the astral microtubules towards the cell poles. The Kar9-dependent pathway links the tips of astral microtubules to Myosin-V motor molecules moving along poleward directed actin cables, whereas microtubules are pulled along the cell cortex in the Dynein-dependent pathway (Fraschini *et al.*, 2008; Moore *et al.*, 2010; Siller *et al.*, 2009). To recover from improper spindle alignment, the spindle position checkpoint (SPOC; Figure 1.7A) delays exit from mitosis until correct spindle orientation is established (Figure 1.6; Caydasi, Kurtulmus, *et al.*, 2010).

The mitotic exit network (MEN; Figure 1.7B), a complex signal transduction cascade, coordinates mitotic exit in budding yeast (Jaspersen *et al.*, 1998). The small Ras-like GTPase Tem1 is the most upstream effector of MEN (Lee *et al.*, 2001); the regulation of Tem1 activation is poorly understood, though. For many years, Lte1 was considered a putative guanine nucleotide exchange factor (GEF) for Tem1 because it is a positive regulator of mitotic exit and its sequence is homologous to CDC25, a GEF for Ras (Shirayama, Matsui, K. Tanaka, *et al.*, 1994; Shirayama, Matsui, and Toh-E, 1994). Despite these indications, it turned out that Lte1 lacks any GEF-activity with respect to Tem1 and promotes mitotic exit differently (Bertazzi *et al.*, 2011; Falk *et al.*, 2011; Geymonat *et al.*, 2009, 2010; Yoshida *et al.*, 2003). No other GEF for Tem1 has been identified so far and the unusually high intrinsic nucleotide-exchange rate of Tem1 question the need for a GEF (Geymonat *et al.*, 2002, 2009). Turning off active, GTP-bound Tem1 requires GTP-hydrolysis, which is accelerated by the Bfa1-Bub2 GTPase activating protein (GAP) complex (Geymonat *et al.*, 2002). Bfa1 and Bub2 are integral parts of the SPOC and constitute its most downstream effector for inhibition of MEN (Fesquet *et al.*, 1999; Fraschini *et al.*, 1999; R. Li, 1999; Pereira *et al.*, 2000; Wang *et al.*, 2000).

Regulation of Bfa1-Bub2 GAP-complex activity must be coupled to the physical orientation of the spindle. While the nature of this interface is still elusive, the kinases Cdc5 and Kin4 appear to be spindle-dependent key regulators of Bfa1-Bub2 activity (Figure 1.7A). In cells with correctly aligned spindles, the Cdc5 inactivates the GAP complex by phosphorylating Bfa1 (Geymonat *et al.*, 2003; Gruneberg *et al.*, 2000;

Hu *et al.*, 2001; Park *et al.*, 2004). However, upon spindle misalignment, the kinase Kin4 phosphorylates Bfa1, preventing its inhibitory phosphorylation by Cdc5. Kin4 is therefore crucial for maintaining the GAP complex active (Caydasi *et al.*, 2009; D'Aquino *et al.*, 2005; Maekawa *et al.*, 2007; Pereira *et al.*, 2005).

The yeast centrosomes (termed spindle pole bodies, SPBs) have a critical role in the regulation of mitotic exit. Association of Tem1 with SPBs is indispensable for MEN activation (Gruneberg *et al.*, 2000; Valerio-Santiago *et al.*, 2011). Active Tem1 at the SPBs promotes SPB binding of its effector kinase Cdc15, which in turn is required for activation and SPB localization of the downstream kinase Dbf2 in complex with its regulatory subunit Mob1 (Figure 1.7B) (Asakawa *et al.*, 2001; Cenamor *et al.*, 1999; Visintin *et al.*, 2001). The SPB also plays a key role in SPOC regulation. Inhibition of the GAP complex by Cdc5 occurs exclusively at the SPBs (Maekawa *et al.*, 2007). During an unperturbed mitosis, Bfa1-Bub2 and Tem1 preferentially bind to the SPB that moves into the daughter cell (dSPB, daughter SPB), whereas during spindle misalignment they associate equally with both SPBs albeit at reduced levels compared to cells with correctly aligned spindles (Caydasi *et al.*, 2009; Molk *et al.*, 2004; Pereira *et al.*, 2000) (Figure 4.1). This localization change, which appears to be crucial for checkpoint activity, is a consequence of the phosphorylation of Bfa1 by Kin4, which promotes binding of Bfa1 to Bmh1, which in turn destabilizes the association of the Bfa1-Bub2 GAP complex with the SPBs (Caydasi *et al.*, 2014a, 2009; Pereira *et al.*, 2005), and seems to be crucial for the checkpoint activity (). Although Tem1 SPB binding is highly dynamic irrespective of the spindle orientation status, Tem1 levels at the SPBs also decrease during spindle misalignment because Tem1 SPB association mainly occurs via its interaction with the GAP complex (Caydasi *et al.*, 2009; Molk *et al.*, 2004; Valerio-Santiago *et al.*, 2011). However, a small pool of Tem1 can bind more stably to the SPBs in a GAP-independent manner (Caydasi *et al.*, 2009; Pereira *et al.*, 2000; Valerio-Santiago *et al.*, 2011). However, the physiological significance and regulation of this pool is not yet understood.

It is clear that inhibition of the MEN in response to spindle misalignment involves an intricate regulatory network that controls Tem1 localization and GTP hydrolysis by the Bfa1-Bub2 GAP-complex, and additionally Bfa1 localization and phosphorylation by Kin4 and Cdc5 kinases. Quantitative analysis and mathematical modeling are important tools that help to elucidate how such elaborate systems might work. So far, mathematical models have helped to enlighten some mitotic control mechanisms, however, no modeling has been done for SPOC (K. C. Chen *et al.*, 2004; Doncic *et al.*,

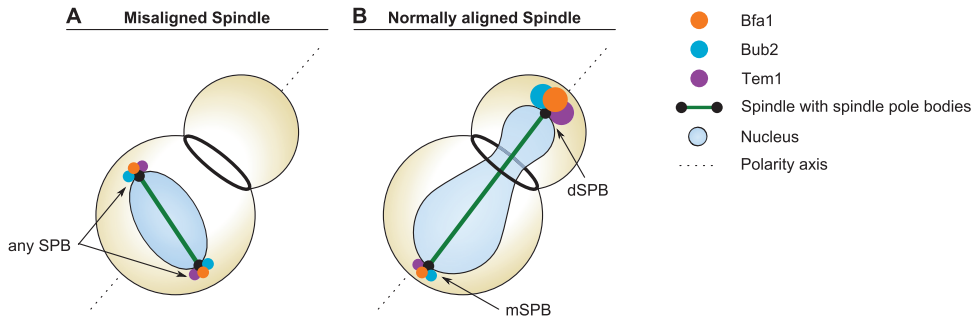

Figure 4.1: Localization pattern of Bfa1, Bub2 and Tem1 at SPBs. *Figure adapted from Caydasi et al. (2012).* (**A**) In cells with a spindle which is not aligned with the polarity axis, equally low amounts of Bfa1, Bub2 and Tem1 localize to both SPBs. (**B**) In cells with a normally aligned anaphase spindle, Bfa1, Bub2, and Tem1 accumulate at the SPB directed towards the daughter cell (dSPB), whereas amounts at the SPB in the mother cell (mSPB) remain at a level comparable to that in cells with a misaligned spindle.

2005; Lohel *et al.*, 2009; López-Avilés *et al.*, 2009; Simonetta *et al.*, 2009; Tóth *et al.*, 2007). One of the reasons for this is the lack of quantitative data on SPOC, which is restricted to *in vitro* assays of Tem1 (nucleotide binding properties and GTPase activity) in addition to microscopy studies of Bfa1-Bub2 and Tem1 (SPB binding dynamics and localization) (Caydasi *et al.*, 2009; Geymonat *et al.*, 2002, 2003; Molk *et al.*, 2004; Monje-Casas *et al.*, 2009; Valerio-Santiago *et al.*, 2011).

A fluorescence microscopy based strategy was employed to quantify the number of Bfa1, Bub2 and Tem1 molecules associated with the SPBs and diffusing in the cytosol (Caydasi *et al.*, 2012). The resulting data served as a basis to construct a compartmentalized dynamical model of the SPOC. The model highlights the importance of cytoplasmic Bfa1-Tem1 interactions for robust inhibition of Tem1 in response to spindle misalignment and implies that Cdc5-independent mechanisms for inhibition of Bfa1-Bub2 are required for timely deactivation of SPOC upon spindle re-alignment.

4.2 Methods

4.2.1 Estimation of the Tem1, Bfa1 and Bub2 Number of Molecules at the SPBs

Molecule numbers at the SPBs were computed by comparing the fluorescence signal of GFP-tagged variants of the proteins of interest (POI; i.e., Bfa1, Bub2, and Tem1)

with a reference fluorescence signal of GFP-tagged kinetochore protein Nuf2. Nuf2 was chosen as a reference, because it occurs with a known stoichiometry of $N \approx 352$ copies at each kinetochore cluster, which are in immediate vicinity of the SPBs during anaphase. The experimental setup is described in detail by Caydasi *et al.* (2012).

A naive estimate of the POI-molecule numbers could be obtained by multiplying the signal ratio of POI and reference by N. However, the measured fluorescence signals of all POIs and the reference protein Nuf2 are distributed over a wide range compared to the absolute signal intensities. Furthermore, the data points are sparse and distributions appear skewed. Hence, the naive estimate will neither result in a reliable estimate of the expected value of the distribution of POI molecule numbers, nor reveal how broad their distribution is.

A more reliable estimate can be obtained from the joint distribution of the normalized fluorescence signals of the POI (X) and the reference protein Nuf2 (Y). To this end, the normalized fluorescence signals are considered samples of independent random variables $X \sim SN(\xi_X, \omega_X, \alpha_X)$ and $Y \sim SN(\xi_Y, \omega_Y, \alpha_Y)$, where $SN(\xi, \omega, \alpha)$ denotes the skewed normal distribution with location ξ, scale ω, and shape α. The corresponding probability density functions p_X and p_Y were determined by fitting the cumulative density function (CDF) to the empirical CDF obtained from the respective data set. The number of molecules is given by the ratio of POI and reference protein fluorescence, thus forming a new random variable $Z = N \cdot X/Y$. The probability that there are exactly k molecules of the POI is then given by

$$\begin{aligned} \Pr(Z = k) &= \sum_{(x,y)\,:\,x/y=k/N} \Pr(X = x) \cdot \Pr(Y = y) \\ &= \int_0^\infty p_X(uk/N)\, p_Y(u)\, du. \end{aligned} \tag{4.2.1}$$

This distribution was approximated numerically by computing large random samples $S_Z = (z_1, z_2, \ldots, z_M)$ where $z_i = N \cdot x_i/y_i$ with x_i and y_i generated according to the fitted distributions given by p_X and p_Y. Finally, moments and order statistics of the POI molecule number distributions were computed from S_Z.

Proteins				*Complexes*			
B	T	Bfa1	Tem1	Bfa1:Tem1	B:Bfa1	T:Tem1	B:Bfa1:Tem1
1	1	3	2	6	3	2	6

Table 4.1: Proteins and protein complexes considered in the model with their respective number of states. Together, a total of 24 states must be considered in the model.

4.2.2 Mathematical Model of the SPOC

4.2.2.1 Scope of the Model

The main objective of this study is to understand how the regulation of activity and localization of Bfa1[1] in response to changes in spindle alignment translate to regulation of Tem1-activity at the dSPB. An important requirement is that the particular patterns of Bfa1- and Tem1-binding to the dSPB must emerge from the model to allow for comparison with experimental findings from fluorescence microscopy. Thus, the model must account for the direct interaction of Bfa1 and Tem1 and their dynamic associaton with the SPBs. Tem1 associates with the SPBs directly or mediated by Bfa1, so distinct binding-sites for Tem1 and Bfa1 must be considered.

Importantly, it is not necessary to model both SPBs: In case of spindle misalignment, both SPBs behave identically and bind only low amounts of Tem1 and Bfa1. Upon spindle alignment, Bfa1 and Tem1 accumulate significantly only at the dSPB, but remain low at the mSPB. Together with low turn-over rates, this implies that the impact of the mSPB on system dynamics is negligible.

Eventually only four proteins and four relevant complexes thereof need to be included in the model. However, Tem1 and Bfa1 occur in two and three states, respectively. Counting all possible combinations of states, a total of 24 quantities is required to model the relevant part of SPOC with sufficient detail (cf. Table 4.1). The notation defined in Table 4.2 is used in the remainder of this chapter to refer formally to the various states of the four proteins. Three model variants, namely the "ubiquitous association", "hot-spot association" and "ubiquitous inactive" models, were implemented to investigate (1) the effects of cytosolic interaction of Tem1 and Bfa1, and (2) the activity of Bfa1 which was not phosphorylated by either of its regulators Kin4 and Cdc5. The differences of these variantsare described along with the corresponding reaction equations in the following sections.

[1] For simplicity, Bfa1 is assumed to exist in a stable complex with Bub2 at all times, so Bub2 is not considered explicitly in the model. Because Bfa1 is the regulatory subunit of the GAP-complex, Bfa1 is used shorthand for Bfa1:Bub2.

Species	Description
Bfa1	'unphosphorylated' Bfa1, that is, Bfa1 which is neither phosphorylated by Kin4 nor hyperphosphorylated by Cdc5
Bfa1^{P4}	Bfa1 phosphorylated by Kin4
Bfa1^{P5}	Bfa1 hyperphosphorylated by Cdc5
Tem1^{GTP}	Tem1 in GTP-bound state
Tem1^{GDP}	Tem1 in GDP-bound state
B	The binding site for Bfa1 at the dSPB (not yet identified)
T	The Bfa1-independent binding site for Tem1 at the dSPB (not yet identified)

Table 4.2: Notation used to refer formally to the various states of the four proteins considered. Complexes are referred to by a colon-separated list of subunits, e.g., B:Bfa1.

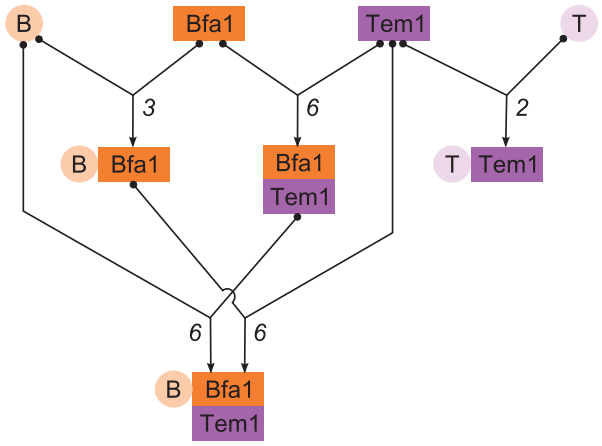

Figure 4.2: Complexes of Bfa1, Tem1 and their binding sites at the SPB. SPB-binding sites for Bfa1 (B) and for Tem1 (T) are shown as circles. The five reversible association reactions apply to all combinations of states of Bfa1 and Tem1 and are annotated with their resulting multiplicity.

4.2.2.2 Association Reactions

The four proteins associate in prototypic five binding reactions (see Figure 4.2) to form four complexes. However, formally these reaction occur with certain multiplicities (cf. Figure 4.2), because the various states of Bfa1 and Tem1 have to be considered.

All binding reactions were described by using reversible mass-action kinetics. Each reaction introduces two kinetic parameters, a first-order dissociation rate coefficient, and a second-order association rate coefficient. Coefficients of equivalent binding reactions were lumped together. For instance, it was assumed that binding of Bfa1 to the SPB occurs with the same kinetics regardless of whether Bfa1 is bound to Tem1 or not, whereas binding kinetics was considered different for Bfa1 that was phosphorylated by Kin4. Reactions considered kinetically equivalent are listed in Table 4.4 with every rate coefficient.

The rate coefficients for Bfa1 and Tem1 dissociation from the SPB were calculated according to the formula $k_{\text{off}} = (ln2)/t_{1/2}$, where the mean residency times $t_{1/2}$ were taken from (Caydasi *et al.*, 2009). Association rates and number of binding sites at the SPB were then adjusted manually such that (1) the respective steady-state amount at the SPB matched the experimentally determined molecule numbers and (2) this state was reached reasonably fast.

While Bfa1 appeared to bind stably to the dSPB of cells with normally aligned spindles ($t_{1/2} \geq 200$ s), binding was considerably more dynamic in cells with misaligned spindles ($t_{1/2} \approx 19$ s). There is no indication that these dynamics are different for Bfa1 in complex with Tem1. Turnover of Tem1 at the SPB is generally much faster than Bfa1 ($t_{1/2}$ between 2.5 and 3.8 s). Because Bfa1 constitutes a large fraction of the Tem1-binding sites at the SPB, the rate coefficient for Tem1 dissociation from the SPB is considered to be a good approximation of the rate coefficient of dissociation of the Bfa1Tem1 complex. Binding to the GAP-independent binding site was slower, with $t_{1/2} \approx 23$ s. The following reactions describe association of Bfa1 and the Bfa1:Tem1-complex with the Bfa1-binding site at the SPB:

$$\mathrm{B} + \mathrm{Bfa1} \underset{k^{\mathrm{B}}_{\mathrm{off}}}{\overset{k^{\mathrm{B}}_{\mathrm{on}}}{\rightleftharpoons}} \mathrm{B:Bfa1} \tag{4.2.2}$$

$$\mathrm{B} + \mathrm{Bfa1}^{\mathrm{P4}} \underset{k^{\mathrm{B4}}_{\mathrm{off}}}{\overset{k^{\mathrm{B4}}_{\mathrm{on}}}{\rightleftharpoons}} \mathrm{B:Bfa1}^{\mathrm{P4}} \tag{4.2.3}$$

$$\mathrm{B} + \mathrm{Bfa1}^{\mathrm{P5}} \underset{k^{\mathrm{B}}_{\mathrm{off}}}{\overset{k^{\mathrm{B}}_{\mathrm{on}}}{\rightleftharpoons}} \mathrm{B:Bfa1}^{\mathrm{P5}} \tag{4.2.4}$$

$$\mathrm{B} + \mathrm{Bfa1:Tem1}^{\mathrm{GTP}} \underset{k^{\mathrm{B}}_{\mathrm{off}}}{\overset{k^{\mathrm{B}}_{\mathrm{on}}}{\rightleftharpoons}} \mathrm{B:Bfa1:Tem1}^{\mathrm{GTP}} \tag{4.2.5}$$

$$\mathrm{B} + \mathrm{Bfa1}^{\mathrm{P4}}\mathrm{:Tem1}^{\mathrm{GTP}} \underset{k^{\mathrm{B4}}_{\mathrm{off}}}{\overset{k^{\mathrm{B4}}_{\mathrm{on}}}{\rightleftharpoons}} \mathrm{B:Bfa1}^{\mathrm{P4}}\mathrm{:Tem1}^{\mathrm{GTP}} \tag{4.2.6}$$

$$\mathrm{B} + \mathrm{Bfa1}^{\mathrm{P5}} : \mathrm{Tem1}^{\mathrm{GTP}} \underset{k^{\mathrm{B}}_{\mathrm{off}}}{\overset{k^{\mathrm{B}}_{\mathrm{on}}}{\rightleftharpoons}} \mathrm{B} : \mathrm{Bfa1}^{\mathrm{P5}} : \mathrm{Tem1}^{\mathrm{GTP}} \tag{4.2.7}$$

$$\mathrm{B} + \mathrm{Bfa1} : \mathrm{Tem1}^{\mathrm{GDP}} \underset{k^{\mathrm{B}}_{\mathrm{off}}}{\overset{k^{\mathrm{B}}_{\mathrm{on}}}{\rightleftharpoons}} \mathrm{B} : \mathrm{Bfa1} : \mathrm{Tem1}^{\mathrm{GDP}} \tag{4.2.8}$$

$$\mathrm{B} + \mathrm{Bfa1}^{\mathrm{P4}} : \mathrm{Tem1}^{\mathrm{GDP}} \underset{k^{\mathrm{B4}}_{\mathrm{off}}}{\overset{k^{\mathrm{B4}}_{\mathrm{on}}}{\rightleftharpoons}} \mathrm{B} : \mathrm{Bfa1}^{\mathrm{P4}} : \mathrm{Tem1}^{\mathrm{GDP}} \tag{4.2.9}$$

$$\mathrm{B} + \mathrm{Bfa1}^{\mathrm{P5}} : \mathrm{Tem1}^{\mathrm{GDP}} \underset{k^{\mathrm{B}}_{\mathrm{off}}}{\overset{k^{\mathrm{B}}_{\mathrm{on}}}{\rightleftharpoons}} \mathrm{B} : \mathrm{Bfa1}^{\mathrm{P5}} : \mathrm{Tem1}^{\mathrm{GDP}} . \tag{4.2.10}$$

In above reactions, binding kinetics of Kin4-phosphorylated Bfa1 are considered different from unphosphorylated and Cdc5-phosphorylated Bfa1. SPB-bound Bfa1 recruits Tem1 to the SPB via the reactions

$$\mathrm{B} : \mathrm{Bfa1} + \mathrm{Tem1}^{\mathrm{GTP}} \underset{k^{\mathrm{BT}}_{\mathrm{off}}}{\overset{k^{\mathrm{BT}}_{\mathrm{on}}}{\rightleftharpoons}} \mathrm{B} : \mathrm{Bfa1} : \mathrm{Tem1}^{\mathrm{GTP}} \tag{4.2.11}$$

$$\mathrm{B} : \mathrm{Bfa1}^{\mathrm{P4}} + \mathrm{Tem1}^{\mathrm{GTP}} \underset{k^{\mathrm{BT}}_{\mathrm{off}}}{\overset{k^{\mathrm{B4T}}_{\mathrm{on}}}{\rightleftharpoons}} \mathrm{B} : \mathrm{Bfa1}^{\mathrm{P4}} : \mathrm{Tem1}^{\mathrm{GTP}} \tag{4.2.12}$$

$$\mathrm{B} : \mathrm{Bfa1}^{\mathrm{P5}} + \mathrm{Tem1}^{\mathrm{GTP}} \underset{k^{\mathrm{BT}}_{\mathrm{off}}}{\overset{k^{\mathrm{B5T}}_{\mathrm{on}}}{\rightleftharpoons}} \mathrm{B} : \mathrm{Bfa1}^{\mathrm{P5}} : \mathrm{Tem1}^{\mathrm{GTP}} \tag{4.2.13}$$

$$\mathrm{B} : \mathrm{Bfa1} + \mathrm{Tem1}^{\mathrm{GDP}} \underset{k^{\mathrm{BT}}_{\mathrm{off}}}{\overset{k^{\mathrm{BT}}_{\mathrm{on}}}{\rightleftharpoons}} \mathrm{B} : \mathrm{Bfa1} : \mathrm{Tem1}^{\mathrm{GDP}} \tag{4.2.14}$$

$$\mathrm{B} : \mathrm{Bfa1}^{\mathrm{P4}} + \mathrm{Tem1}^{\mathrm{GDP}} \underset{k^{\mathrm{BT}}_{\mathrm{off}}}{\overset{k^{\mathrm{B4T}}_{\mathrm{on}}}{\rightleftharpoons}} \mathrm{B} : \mathrm{Bfa1}^{\mathrm{P4}} : \mathrm{Tem1}^{\mathrm{GDP}} \tag{4.2.15}$$

$$\mathrm{B} : \mathrm{Bfa1}^{\mathrm{P5}} + \mathrm{Tem1}^{\mathrm{GDP}} \underset{k^{\mathrm{BT}}_{\mathrm{off}}}{\overset{k^{\mathrm{B5T}}_{\mathrm{on}}}{\rightleftharpoons}} \mathrm{B} : \mathrm{Bfa1}^{\mathrm{P5}} : \mathrm{Tem1}^{\mathrm{GDP}} , \tag{4.2.16}$$

where the affinity of Bfa1 for Tem1 can differ depending on the phosphorylation-state of Bfa1 (cf. Geymonat *et al.*, 2003). In contrast, no difference of Bfa1-affinity for $\mathrm{Tem1}^{\mathrm{GTP}}$ and $\mathrm{Tem1}^{\mathrm{GDP}}$ is made. To allow for testing whether Bfa1 and Tem1 associate in the cytosol as well, the following reactions are part of the "ubiquitous association" and "ubiquitous inactive" models, but excluded to form the "hot-spot association" model:

$$\mathrm{Bfa1} + \mathrm{Tem1}^{\mathrm{GTP}} \underset{k^{\mathrm{BT}}_{\mathrm{off}}}{\overset{k^{\mathrm{BT}}_{\mathrm{on}}}{\rightleftharpoons}} \mathrm{Bfa1} : \mathrm{Tem1}^{\mathrm{GTP}} \tag{4.2.17}$$

$$\mathrm{Bfa1}^{\mathrm{P4}} + \mathrm{Tem1}^{\mathrm{GTP}} \underset{k^{\mathrm{BT}}_{\mathrm{off}}}{\overset{k^{\mathrm{B4T}}_{\mathrm{on}}}{\rightleftharpoons}} \mathrm{Bfa1}^{\mathrm{P4}} : \mathrm{Tem1}^{\mathrm{GTP}} \tag{4.2.18}$$

$$\mathrm{Bfa1^{P5}} + \mathrm{Tem1^{GTP}} \underset{k_{\mathrm{off}}^{\mathrm{BT}}}{\overset{k_{\mathrm{on}}^{\mathrm{B5T}}}{\rightleftharpoons}} \mathrm{Bfa1^{P5}:Tem1^{GTP}} \tag{4.2.19}$$

$$\mathrm{Bfa1} + \mathrm{Tem1^{GDP}} \underset{k_{\mathrm{off}}^{\mathrm{BT}}}{\overset{k_{\mathrm{on}}^{\mathrm{BT}}}{\rightleftharpoons}} \mathrm{Bfa1:Tem1^{GDP}} \tag{4.2.20}$$

$$\mathrm{Bfa1^{P4}} + \mathrm{Tem1^{GDP}} \underset{k_{\mathrm{off}}^{\mathrm{BT}}}{\overset{k_{\mathrm{on}}^{\mathrm{B4T}}}{\rightleftharpoons}} \mathrm{Bfa1^{P4}:Tem1^{GDP}} \tag{4.2.21}$$

$$\mathrm{Bfa1^{P5}} + \mathrm{Tem1^{GDP}} \underset{k_{\mathrm{off}}^{\mathrm{BT}}}{\overset{k_{\mathrm{on}}^{\mathrm{B5T}}}{\rightleftharpoons}} \mathrm{Bfa1^{P5}:Tem1^{GDP}}\,. \tag{4.2.22}$$

Lastly, two reactions incorporate Bfa1-independent association of Tem1 with the SPB:

$$\mathrm{T} + \mathrm{Tem1^{GTP}} \underset{k_{\mathrm{off}}^{\mathrm{T}}}{\overset{k_{\mathrm{on}}^{\mathrm{T}}}{\rightleftharpoons}} \mathrm{T:Tem1^{GTP}} \tag{4.2.23}$$

$$\mathrm{T} + \mathrm{Tem1^{GDP}} \underset{k_{\mathrm{off}}^{\mathrm{T}}}{\overset{k_{\mathrm{on}}^{\mathrm{T}}}{\rightleftharpoons}} \mathrm{T:Tem1^{GDP}}\,. \tag{4.2.24}$$

4.2.2.3 Phosphorylation and Dephosphorylation of Bfa1

Activity of Bfa1 is regulated by mutually exclusive phosphorylation through kinases Kin4 and Cdc5 at the SPB(Hu *et al.*, 2001; Maekawa *et al.*, 2007; Pereira *et al.*, 2001). While it cannot be excluded that freely diffusing Kin4 in the cytosol can phosphorylate Bfa1, hyperphosphorylation of Bfa1 by Cdc5 does not take place in the cytosol (Maekawa *et al.*, 2007). Hyperphosphorylation of Bfa1 by Cdc5 has been shown to reduce its ability to inhibit Tem1 (Geymonat *et al.*, 2003; Hu *et al.*, 2001). Kin4 prevents hyperphosphorylation of Bfa1 by Cdc5, thus Kin4-phosphorylated Bfa1 can be considered an active form. Whether "unphosphorylated" Bfa1 *in vivo* is active or incative is unknown. The "ubiquitous inactive" model differs from "ubiquitous association" and "hot-spot association" models in that unphosphorylated Bfa1 is considered inactive only in the former. This is reflected by the choice of reaction rates (cf. Table 4.4).

Given that no kinetic data are available for phosphorylation of Bfa1 by Kin4 and Cdc5, we modeled these reactions by pseudo first-order processes to introduce the least amount of complexity. The characterizing rate coefficients for the phosphorylation reactions at the SPB (Figure 4A) were manually adjusted, considering that (1) phosphorylation by Cdc5 is fast enough such that not the phosphorylation rate per se, but the turnover rate of Bfa1 at the SPB limits the amount of Bfa1 which

can be phosphorylated by Cdc5 per unit time and (2) phosphorylation by Kin4 is significantly faster than Cdc5 to allow for suppression of further phosphorylation of Bfa1 by Cdc5.

Phosphatases opposing Kin4 and Cdc5 have not been identified so far, although $PP2A^{Cdc55}$ has been suggested as an antagonist of Bfa1-phosphorylation by Cdc5 (Queralt *et al.*, 2006). While $PP2A^{Rts1}$ has been shown to downregulate Kin4-activity, it was excluded that it reverts phosphorylation of Bfa1 by Kin4 (Chan *et al.*, 2009). Like for the kinases, neither kinetic data nor quantitative estimates of the intracellular concentrations are available, so dephosphorylation was modeled by first-order reactions, implying rate coefficients with unit s^{-1}. These rate coefficients can be interpreted as the inverse of the expected lifetime of the respective phosphorylated state. The lifetime of the Kin4-phosphorylated state was chosen such that the steady state is approached within the first 30 min after SPOC deactivation. The lifetime of the Cdc5-phosphorylated state was set to a similar value if the SPOC is active; however, in checkpoint active state, the model is insensitive to this parameter because in this case phosphorylation through Kin4 prevents phosphorylation by Cdc5. In contrast, dephosphorylation of Cdc5 is turned off upon SPOC deactivation to allow for accumulation of this phosphoform during anaphase.

To reflect that spindle misalignment leads to activation of Kin4 (Maekawa *et al.*, 2007; Pereira *et al.*, 2005), phosphorylation of Bfa1 by Kin4 is made dependent on a switching parameter u modeling the spindle alignment status (cf. Table 4.4).

The following reaction equations account for phosphorylation of Bfa1 by Kin4 and Cdc5 at the SPB:

$$\mathrm{B:Bfa1} \xrightarrow{k_+^{\mathrm{Kin4}}} \mathrm{B:Bfa1^{P4}} \tag{4.2.25}$$

$$\mathrm{B:Bfa1:Tem1^{GTP}} \xrightarrow{k_+^{\mathrm{Kin4}}} \mathrm{B:Bfa1^{P4}:Tem1^{GTP}} \tag{4.2.26}$$

$$\mathrm{B:Bfa1:Tem1^{GDP}} \xrightarrow{k_+^{\mathrm{Kin4}}} \mathrm{B:Bfa1^{P4}:Tem1^{GDP}} \tag{4.2.27}$$

$$\mathrm{B:Bfa1} \xrightarrow{k_+^{\mathrm{Cdc5}}} \mathrm{B:Bfa1^{P5}} \tag{4.2.28}$$

$$\mathrm{B:Bfa1:Tem1^{GTP}} \xrightarrow{k_+^{\mathrm{Cdc5}}} \mathrm{B:Bfa1^{P5}:Tem1^{GTP}} \tag{4.2.29}$$

$$\mathrm{B:Bfa1:Tem1^{GDP}} \xrightarrow{k_+^{\mathrm{Cdc5}}} \mathrm{B:Bfa1^{P5}:Tem1^{GDP}}\,. \tag{4.2.30}$$

Similarly putative cytosolic phosphorylation of Bfa1 by Kin4 is described by

$$\mathrm{Bfa1} \xrightarrow{k_{+,\mathrm{cyto}}^{\mathrm{Kin4}}} \mathrm{Bfa1^{P4}} \tag{4.2.31}$$

$$\mathrm{Bfa1:Tem1^{GTP}} \xrightarrow{k_{+,\mathrm{cyto}}^{\mathrm{Kin4}}} \mathrm{Bfa1^{P4}:Tem1^{GTP}} \tag{4.2.32}$$

$$\mathrm{Bfa1:Tem1^{GDP}} \xrightarrow{k_{+,\mathrm{cyto}}^{\mathrm{Kin4}}} \mathrm{Bfa1^{P4}:Tem1^{GDP}}\,. \tag{4.2.33}$$

The putative Cdc5-antagonist $\mathrm{PP2A^{Cdc55}}$ does not localize to the SPBs (Gentry *et al.*, 2002), and no indication for a SPB-bound phosphatase opposing Kin4 exists. Therefore, dephosphorylation of Bfa1 is assumed to take place exclusively in the cytosol:

$$\mathrm{Bfa1^{P4}} \xrightarrow{k_{-}^{\mathrm{Kin4}}} \mathrm{Bfa1} \tag{4.2.34}$$

$$\mathrm{Bfa1^{P4}:Tem1^{GTP}} \xrightarrow{k_{-}^{\mathrm{Kin4}}} \mathrm{Bfa1:Tem1^{GTP}} \tag{4.2.35}$$

$$\mathrm{Bfa1^{P4}:Tem1^{GDP}} \xrightarrow{k_{-}^{\mathrm{Kin4}}} \mathrm{Bfa1:Tem1^{GDP}} \tag{4.2.36}$$

$$\mathrm{Bfa1^{P5}} \xrightarrow{k_{-}^{\mathrm{Cdc5}}} \mathrm{Bfa1} \tag{4.2.37}$$

$$\mathrm{Bfa1^{P5}:Tem1^{GTP}} \xrightarrow{k_{-}^{\mathrm{Cdc5}}} \mathrm{Bfa1:Tem1^{GTP}} \tag{4.2.38}$$

$$\mathrm{Bfa1^{P5}:Tem1^{GDP}} \xrightarrow{k_{-}^{\mathrm{Cdc5}}} \mathrm{Bfa1:Tem1^{GDP}}\,. \tag{4.2.39}$$

4.2.2.4 GTPase-Cycle

The Tem1 GTPase-cycle is integrated in terms of the minimal model discussed in section 3.2.5 on page 54. The corresponding effective kinetic rate parameters are defined in table 4.4 and were derived from Equation (3.2.12) with respect to the parameters given in Table 3.1, using fold-acceleration parameters $\rho = 0$ and $\lambda = 10^3$ to characterize active Bfa1:Bub2. GDP-release is the most sensitive parameter in the model of the GTPase-cycle with respect to the steady-state level of $\mathrm{Tem1^{GTP}}$, and similarly the fold-acceleration of hydrolysis, λ, is highly important for the inactivation of Tem1 in the model. Therefore, the models were simulated with GDP-release rate coefficients and fold accelerations in a range spanning five orders of magnitude (Figure 4.3; for details on the recorded measures see section "Parameter Scans" on page 4.2.5). From these scans, the fold-acceleration was chosen to be $\lambda = 10^3$, such that further increase of the fold-acceleration has only subtle influence on the dependency of all model variants on the GDP-release rate coefficient (cf. region to the right of the vertical lines in Figures 4.3A-C). This fold-acceleration and the resulting effective rate coefficient for GAP-accelerated GTP hydrolysis $k_{\mathrm{hyd}}^{\mathrm{GAP}} = 2\mathrm{s}^{-1}$ are well within the reported limits of GTP hydrolysis by Ras in the presence of RasGAP (Gideon *et al.*, 1992). Consequently, robustness of the model variants with respect to GDP-release

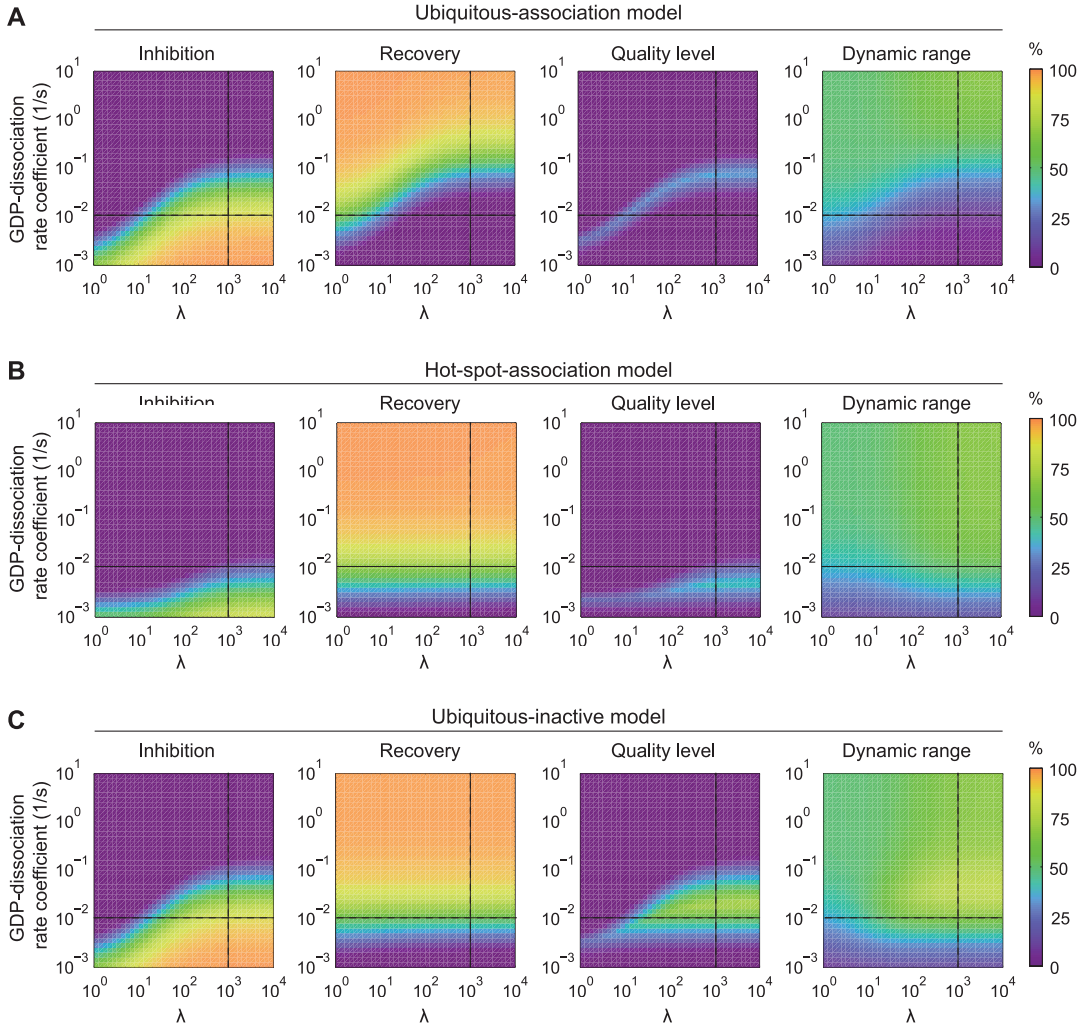

Figure 4.3: Simultaneous parameter scan of GDP-dissociation rate coefficient and fold-acceleration λ of hydrolysis by the GAP complex. *Figure adapted from (Caydasi et al., 2012).* (**A**-**C**) Columns from left to right show relative inhibition of Tem1 when SPOC is active ($t = 30$ min), relative recovery of active Tem1 10 minutes after SPOC deactivation ($t = 40$ min), and the corresponding quality level and dynamic range. Fold-acceleration of hydrolysis (λ) is explained in section 3.2.7 on page 57. The recorded measures are defined in section 4.2.5. Vertical and horizontal lines indicate the selected nominal values of both parameters. **(A)** Ubiquitous association model. **(B)** Hot-spot association model. **(C)** Ubiquitous-inactive model.

can be evaluated by considering the scan of the GDP-release rate coefficient alone, i.e., with the projection of the scans in Figure 4.3 along aforementioned vertical lines

(cf. Figure 4.9).

The intrinsic GTPase-cycle of Tem1 is modeled with reactions

$$\mathrm{Tem1}^{\mathrm{GTP}} \xrightarrow{k_{\mathrm{hyd}}} \mathrm{Tem1}^{\mathrm{GDP}} \tag{4.2.40}$$

$$\mathrm{Tem1}^{\mathrm{GDP}} \xrightarrow{k_{\mathrm{nex}}} \mathrm{Tem1}^{\mathrm{GTP}} \tag{4.2.41}$$

$$\mathrm{T}:\mathrm{Tem1}^{\mathrm{GTP}} \xrightarrow{k_{\mathrm{hyd}}} \mathrm{T}:\mathrm{Tem1}^{\mathrm{GDP}} \tag{4.2.42}$$

$$\mathrm{T}:\mathrm{Tem1}^{\mathrm{GDP}} \xrightarrow{k_{\mathrm{nex}}} \mathrm{T}:\mathrm{Tem1}^{\mathrm{GTP}}\,, \tag{4.2.43}$$

whereas the GTPase-cycle of GAP-associated Tem1 comprises the following reactions:

$$\mathrm{Bfa1}:\mathrm{Tem1}^{\mathrm{GTP}} \xrightarrow{k_{\mathrm{hyd}}^{\mathrm{BT}}} \mathrm{Bfa1}:\mathrm{Tem1}^{\mathrm{GDP}} \tag{4.2.44}$$

$$\mathrm{Bfa1}^{\mathrm{P4}}:\mathrm{Tem1}^{\mathrm{GTP}} \xrightarrow{k_{\mathrm{hyd}}^{\mathrm{B4T}}} \mathrm{Bfa1}^{\mathrm{P4}}:\mathrm{Tem1}^{\mathrm{GDP}} \tag{4.2.45}$$

$$\mathrm{Bfa1}^{\mathrm{P5}}:\mathrm{Tem1}^{\mathrm{GTP}} \xrightarrow{k_{\mathrm{hyd}}} \mathrm{Bfa1}^{\mathrm{P5}}:\mathrm{Tem1}^{\mathrm{GDP}} \tag{4.2.46}$$

$$\mathrm{B}:\mathrm{Bfa1}:\mathrm{Tem1}^{\mathrm{GTP}} \xrightarrow{k_{\mathrm{hyd}}^{\mathrm{BT}}} \mathrm{B}:\mathrm{Bfa1}:\mathrm{Tem1}^{\mathrm{GDP}} \tag{4.2.47}$$

$$\mathrm{B}:\mathrm{Bfa1}^{\mathrm{P4}}:\mathrm{Tem1}^{\mathrm{GTP}} \xrightarrow{k_{\mathrm{hyd}}^{\mathrm{B4T}}} \mathrm{B}:\mathrm{Bfa1}^{\mathrm{P4}}:\mathrm{Tem1}^{\mathrm{GDP}} \tag{4.2.48}$$

$$\mathrm{B}:\mathrm{Bfa1}^{\mathrm{P5}}:\mathrm{Tem1}^{\mathrm{GTP}} \xrightarrow{k_{\mathrm{hyd}}} \mathrm{B}:\mathrm{Bfa1}^{\mathrm{P5}}:\mathrm{Tem1}^{\mathrm{GDP}}\,. \tag{4.2.49}$$

4.2.2.5 Ordinary Differential Equations of the Dynamical Model

The reaction equations (4.2.2)–(4.2.49) were translated into the set of 23 coupled nonlinear ordinary differential equations given below. Conventionally, the species names as they appear in the reaction equations are enclosed in brackets to refer to their respective molar concentrations. Association of cytosolic Bfa1 and Tem1 with their respective binding sites at the SPB involves a transition from a large (cytosol, V_{C}) to a small (SPB, V_{S}) reference volume. The fluxes of reactions (4.2.2)–(4.2.16), (4.2.23), and (4.2.24) must therefore be scaled with $V_{\mathrm{S}}/V_{\mathrm{C}}$ when they contribute to the differential equations of the respective cytosolic species. The fluxes v_1 to v_{48} correspond to reactions (4.2.2)–(4.2.49) defined in the previous sections. The initial conditions of the ODE-system are defined in Table 4.3 on page 77, whereas the kinetic parameters are listed in Table 4.4.

The resulting system of ordinary differential equations is given by the equations

$$\mathrm{d}[\mathrm{T}]/\mathrm{d}t = -v_{22} - v_{23}$$

$$
\begin{aligned}
\mathrm{d}[\mathrm{B}]/\mathrm{d}t &= -\textstyle\sum_{i=1}^{9} v_i \\
\mathrm{d}[\mathrm{Bfa1}]/\mathrm{d}t &= -\left(V_\mathrm{S}/V_\mathrm{C}\right) v_1 - v_{16} - v_{19} - v_{30} + v_{33} + v_{36} \\
\mathrm{d}[\mathrm{Bfa1}^{\mathrm{P4}}]/\mathrm{d}t &= -\left(V_\mathrm{S}/V_\mathrm{C}\right) v_2 - v_{17} - v_{20} + v_{30} - v_{33} \\
\mathrm{d}[\mathrm{Bfa1}^{\mathrm{P5}}]/\mathrm{d}t &= -\left(V_\mathrm{S}/V_\mathrm{C}\right) v_3 - v_{18} - v_{21} - v_{36} \\
\mathrm{d}[\mathrm{Bfa1}:\mathrm{Tem1}^{\mathrm{GTP}}]/\mathrm{d}t &= -\left(V_\mathrm{S}/V_\mathrm{C}\right) v_4 + v_{16} - v_{31} + v_{34} + v_{37} - v_{43} \\
\mathrm{d}[\mathrm{Bfa1}^{\mathrm{P4}}:\mathrm{Tem1}^{\mathrm{GTP}}]/\mathrm{d}t &= -\left(V_\mathrm{S}/V_\mathrm{C}\right) v_5 + v_{17} + v_{31} - v_{34} - v_{44} \\
\mathrm{d}[\mathrm{Bfa1}^{\mathrm{P5}}:\mathrm{Tem1}^{\mathrm{GTP}}]/\mathrm{d}t &= -\left(V_\mathrm{S}/V_\mathrm{C}\right) v_6 + v_{18} - v_{37} - v_{45} \\
\mathrm{d}[\mathrm{Bfa1}:\mathrm{Tem1}^{\mathrm{GDP}}]/\mathrm{d}t &= -\left(V_\mathrm{S}/V_\mathrm{C}\right) v_7 + v_{19} - v_{32} + v_{35} + v_{38} + v_{43} \\
\mathrm{d}[\mathrm{Bfa1}^{\mathrm{P4}}:\mathrm{Tem1}^{\mathrm{GDP}}]/\mathrm{d}t &= -\left(V_\mathrm{S}/V_\mathrm{C}\right) v_8 + v_{20} + v_{32} - v_{35} + v_{44} \\
\mathrm{d}[\mathrm{Bfa1}^{\mathrm{P5}}:\mathrm{Tem1}^{\mathrm{GDP}}]/\mathrm{d}t &= -\left(V_\mathrm{S}/V_\mathrm{C}\right) v_9 + v_{21} - v_{38} + v_{45} \\
\mathrm{d}[\mathrm{B}:\mathrm{Bfa1}]/\mathrm{d}t &= v_1 - v_{10} - v_{13} - v_{24} - v_{27} \\
\mathrm{d}[\mathrm{B}:\mathrm{Bfa1}^{\mathrm{P4}}]/\mathrm{d}t &= v_2 - v_{11} - v_{14} + v_{24} \\
\mathrm{d}[\mathrm{B}:\mathrm{Bfa1}^{\mathrm{P5}}]/\mathrm{d}t &= v_3 - v_{12} - v_{15} + v_{27} \\
\mathrm{d}[\mathrm{B}:\mathrm{Bfa1}:\mathrm{Tem1}^{\mathrm{GTP}}]/\mathrm{d}t &= v_4 + v_{10} - v_{25} - v_{28} - v_{46} \\
\mathrm{d}[\mathrm{B}:\mathrm{Bfa1}^{\mathrm{P4}}:\mathrm{Tem1}^{\mathrm{GTP}}]/\mathrm{d}t &= v_5 + v_{11} + v_{25} - v_{47} \\
\mathrm{d}[\mathrm{B}:\mathrm{Bfa1}^{\mathrm{P5}}:\mathrm{Tem1}^{\mathrm{GTP}}]/\mathrm{d}t &= v_6 + v_{12} + v_{28} - v_{48} \\
\mathrm{d}[\mathrm{B}:\mathrm{Bfa1}:\mathrm{Tem1}^{\mathrm{GDP}}]/\mathrm{d}t &= v_7 + v_{13} - v_{26} - v_{29} + v_{46} \\
\mathrm{d}[\mathrm{B}:\mathrm{Bfa1}^{\mathrm{P4}}:\mathrm{Tem1}^{\mathrm{GDP}}]/\mathrm{d}t &= v_8 + v_{14} + v_{26} + v_{47} \\
\mathrm{d}[\mathrm{B}:\mathrm{Bfa1}^{\mathrm{P5}}:\mathrm{Tem1}^{\mathrm{GDP}}]/\mathrm{d}t &= v_9 + v_{15} + v_{29} + v_{48} \\
\mathrm{d}[\mathrm{Tem1}^{\mathrm{GTP}}]/\mathrm{d}t &= -\left(V_\mathrm{S}/V_\mathrm{C}\right)\left(\textstyle\sum_{i=10}^{12} v_i + v_{22}\right) - \textstyle\sum_{i=16}^{18} v_i - v_{39} + v_{40} \\
\mathrm{d}[\mathrm{Tem1}^{\mathrm{GDP}}]/\mathrm{d}t &= -\left(V_\mathrm{S}/V_\mathrm{C}\right)\left(\textstyle\sum_{i=13}^{15} v_i + v_{23}\right) - \textstyle\sum_{i=19}^{21} v_i + v_{39} - v_{40} \\
\mathrm{d}[\mathrm{T}:\mathrm{Tem1}^{\mathrm{GTP}}]/\mathrm{d}t &= v_{22} - v_{41} + v_{42} \\
\mathrm{d}[\mathrm{T}:\mathrm{Tem1}^{\mathrm{GDP}}]/\mathrm{d}t &= v_{23} + v_{41} - v_{42}
\end{aligned}
$$

where the reaction fluxes v_i are defined by

$$
\begin{aligned}
v_1 &= k_{\mathrm{on}}^{\mathrm{B}}\,[\mathrm{B}]\,[\mathrm{Bfa1}] - k_{\mathrm{off}}^{\mathrm{B}}\,[\mathrm{B}:\mathrm{Bfa1}] \\
v_2 &= k_{\mathrm{on}}^{\mathrm{B4}}\,[\mathrm{B}]\,[\mathrm{Bfa1}^{\mathrm{P4}}] - k_{\mathrm{off}}^{\mathrm{B4}}\,[\mathrm{B}:\mathrm{Bfa1}^{\mathrm{P4}}] \\
v_3 &= k_{\mathrm{on}}^{\mathrm{B}}\,[\mathrm{B}]\,[\mathrm{Bfa1}] - k_{\mathrm{off}}^{\mathrm{B}}\,[\mathrm{B}:\mathrm{Bfa1}^{\mathrm{P5}}] \\
v_4 &= k_{\mathrm{on}}^{\mathrm{B}}\,[\mathrm{B}]\,[\mathrm{Bfa1}:\mathrm{Tem1}^{\mathrm{GTP}}] - k_{\mathrm{off}}^{\mathrm{B}}\,[\mathrm{B}:\mathrm{Bfa1}:\mathrm{Tem1}^{\mathrm{GTP}}] \\
v_5 &= k_{\mathrm{on}}^{\mathrm{B4}}\,[\mathrm{B}]\,[\mathrm{Bfa1}^{\mathrm{P4}}:\mathrm{Tem1}^{\mathrm{GTP}}] - k_{\mathrm{off}}^{\mathrm{B4}}\,[\mathrm{B}:\mathrm{Bfa1}^{\mathrm{P4}}:\mathrm{Tem1}^{\mathrm{GTP}}]
\end{aligned}
$$

$$
\begin{aligned}
v_6 &= k_{\text{on}}^{\text{B}}\,[\text{B}]\,[\text{Bfa1}^{\text{P5}}:\text{Tem1}^{\text{GTP}}] - k_{\text{off}}^{\text{B}}\,[\text{B}:\text{Bfa1}^{\text{P5}}:\text{Tem1}^{\text{GTP}}]\\
v_7 &= k_{\text{on}}^{\text{B}}\,[\text{B}]\,[\text{Bfa1}:\text{Tem1}^{\text{GDP}}] - k_{\text{off}}^{\text{B}}\,[\text{B}:\text{Bfa1}:\text{Tem1}^{\text{GDP}}]\\
v_8 &= k_{\text{on}}^{\text{B4}}\,[\text{B}]\,[\text{Bfa1}^{\text{P4}}:\text{Tem1}^{\text{GDP}}] - k_{\text{off}}^{\text{B4}}\,[\text{B}:\text{Bfa1}^{\text{P4}}:\text{Tem1}^{\text{GDP}}]\\
v_9 &= k_{\text{on}}^{\text{B}}\,[\text{B}]\,[\text{Bfa1}^{\text{P5}}:\text{Tem1}^{\text{GDP}}] - k_{\text{off}}^{\text{B}}\,[\text{B}:\text{Bfa1}^{\text{P5}}:\text{Tem1}^{\text{GDP}}]\\
v_{10} &= k_{\text{on}}^{\text{BT}}\,[\text{B}:\text{Bfa1}]\,[\text{Tem1}^{\text{GTP}}] - k_{\text{off}}^{\text{BT}}\,[\text{B}:\text{Bfa1}:\text{Tem1}^{\text{GTP}}]\\
v_{11} &= k_{\text{on}}^{\text{B4T}}\,[\text{B}:\text{Bfa1}^{\text{P4}}]\,[\text{Tem1}^{\text{GTP}}] - k_{\text{off}}^{\text{BT}}\,[\text{B}:\text{Bfa1}^{\text{P4}}:\text{Tem1}^{\text{GTP}}]\\
v_{12} &= k_{\text{on}}^{\text{B5T}}\,[\text{B}:\text{Bfa1}^{\text{P5}}]\,[\text{Tem1}^{\text{GTP}}] - k_{\text{off}}^{\text{BT}}\,[\text{B}:\text{Bfa1}^{\text{P5}}:\text{Tem1}^{\text{GTP}}]\\
v_{13} &= k_{\text{on}}^{\text{BT}}\,[\text{B}:\text{Bfa1}]\,[\text{Tem1}^{\text{GDP}}] - k_{\text{off}}^{\text{BT}}\,[\text{B}:\text{Bfa1}:\text{Tem1}^{\text{GDP}}]\\
v_{14} &= k_{\text{on}}^{\text{B4T}}\,[\text{B}:\text{Bfa1}^{\text{P4}}]\,[\text{Tem1}^{\text{GDP}}] - k_{\text{off}}^{\text{BT}}\,[\text{B}:\text{Bfa1}^{\text{P4}}:\text{Tem1}^{\text{GDP}}]\\
v_{15} &= k_{\text{on}}^{\text{B5T}}\,[\text{B}:\text{Bfa1}^{\text{P5}}]\,[\text{Tem1}^{\text{GDP}}] - k_{\text{off}}^{\text{BT}}\,[\text{B}:\text{Bfa1}^{\text{P5}}:\text{Tem1}^{\text{GDP}}]\\
v_{16} &= \alpha k_{\text{on}}^{\text{BT}}\,[\text{Bfa1}]\,[\text{Tem1}^{\text{GTP}}] - k_{\text{off}}^{\text{BT}}\,[\text{Bfa1}:\text{Tem1}^{\text{GTP}}]\\
v_{17} &= \alpha k_{\text{on}}^{\text{B4T}}\,[\text{Bfa1}^{\text{P4}}]\,[\text{Tem1}^{\text{GTP}}] - k_{\text{off}}^{\text{BT}}\,[\text{Bfa1}^{\text{P4}}:\text{Tem1}^{\text{GTP}}]\\
v_{18} &= \alpha k_{\text{on}}^{\text{B5T}}\,[\text{Bfa1}^{\text{P5}}]\,[\text{Tem1}^{\text{GTP}}] - k_{\text{off}}^{\text{BT}}\,[\text{Bfa1}^{\text{P5}}:\text{Tem1}^{\text{GTP}}]\\
v_{19} &= \alpha k_{\text{on}}^{\text{BT}}\,[\text{Bfa1}]\,[\text{Tem1}^{\text{GDP}}] - k_{\text{off}}^{\text{BT}}\,[\text{Bfa1}:\text{Tem1}^{\text{GDP}}]\\
v_{20} &= \alpha k_{\text{on}}^{\text{B4T}}\,[\text{Bfa1}^{\text{P4}}]\,[\text{Tem1}^{\text{GDP}}] - k_{\text{off}}^{\text{BT}}\,[\text{Bfa1}^{\text{P4}}:\text{Tem1}^{\text{GDP}}]\\
v_{21} &= \alpha k_{\text{on}}^{\text{B5T}}\,[\text{Bfa1}^{\text{P5}}]\,[\text{Tem1}^{\text{GDP}}] - k_{\text{off}}^{\text{BT}}\,[\text{Bfa1}^{\text{P5}}:\text{Tem1}^{\text{GDP}}]\\
v_{22} &= k_{\text{on}}^{\text{T}}\,[\text{T}]\,[\text{Tem1}^{\text{GTP}}] - k_{\text{off}}^{\text{T}}\,[\text{T}:\text{Tem1}^{\text{GTP}}]\\
v_{23} &= k_{\text{on}}^{\text{T}}\,[\text{T}]\,[\text{Tem1}^{\text{GDP}}] - k_{\text{off}}^{\text{T}}\,[\text{T}:\text{Tem1}^{\text{GDP}}]\\
v_{24} &= u k_{+}^{\text{Kin4}}\,[\text{B}:\text{Bfa1}]\\
v_{25} &= u k_{+}^{\text{Kin4}}\,[\text{B}:\text{Bfa1}:\text{Tem1}^{\text{GTP}}]\\
v_{26} &= u k_{+}^{\text{Kin4}}\,[\text{B}:\text{Bfa1}:\text{Tem1}^{\text{GDP}}]\\
v_{27} &= k_{+}^{\text{Cdc5}}\,[\text{B}:\text{Bfa1}]\\
v_{28} &= k_{+}^{\text{Cdc5}}\,[\text{B}:\text{Bfa1}:\text{Tem1}^{\text{GTP}}]\\
v_{29} &= k_{+}^{\text{Cdc5}}\,[\text{B}:\text{Bfa1}:\text{Tem1}^{\text{GDP}}]\\
v_{30} &= u k_{+}^{\text{Kin4}}\,[\text{Bfa1}]\\
v_{31} &= u k_{+}^{\text{Kin4}}\,[\text{Bfa1}:\text{Tem1}^{\text{GTP}}]\\
v_{32} &= u k_{+}^{\text{Kin4}}\,[\text{Bfa1}:\text{Tem1}^{\text{GDP}}]\\
v_{33} &= k_{-}^{\text{Kin4}}\,[\text{Bfa1}^{\text{P4}}]\\
v_{34} &= k_{-}^{\text{Kin4}}\,[\text{Bfa1}^{\text{P4}}:\text{Tem1}^{\text{GTP}}]\\
v_{35} &= k_{-}^{\text{Kin4}}\,[\text{Bfa1}^{\text{P4}}:\text{Tem1}^{\text{GDP}}]
\end{aligned}
$$

$$
\begin{aligned}
v_{36} &= uk_{-}^{\mathrm{Cdc5}}\,[\mathrm{Bfa1}^{\mathrm{P5}}] \\
v_{37} &= uk_{-}^{\mathrm{Cdc5}}\,[\mathrm{Bfa1}^{\mathrm{P5}}\!:\mathrm{Tem1}^{\mathrm{GTP}}] \\
v_{38} &= uk_{-}^{\mathrm{Cdc5}}\,[\mathrm{Bfa1}^{\mathrm{P5}}\!:\mathrm{Tem1}^{\mathrm{GDP}}] \\
v_{39} &= k_{\mathrm{hyd}}\,[\mathrm{Tem1}^{\mathrm{GTP}}] \\
v_{40} &= k_{\mathrm{nex}}\,[\mathrm{Tem1}^{\mathrm{GDP}}] \\
v_{41} &= k_{\mathrm{hyd}}\,[\mathrm{T}\!:\mathrm{Tem1}^{\mathrm{GTP}}] \\
v_{42} &= k_{\mathrm{nex}}\,[\mathrm{T}\!:\mathrm{Tem1}^{\mathrm{GDP}}] \\
v_{43} &= k_{\mathrm{hyd}}^{\mathrm{BT}}\,[\mathrm{Bfa1}\!:\mathrm{Tem1}^{\mathrm{GTP}}] \\
v_{44} &= k_{\mathrm{hyd}}^{\mathrm{B4T}}\,[\mathrm{Bfa1}^{\mathrm{P4}}\!:\mathrm{Tem1}^{\mathrm{GTP}}] \\
v_{45} &= k_{\mathrm{hyd}}\,[\mathrm{Bfa1}^{\mathrm{P5}}\!:\mathrm{Tem1}^{\mathrm{GTP}}] \\
v_{46} &= k_{\mathrm{hyd}}^{\mathrm{BT}}\,[\mathrm{B}\!:\mathrm{Bfa1}\!:\mathrm{Tem1}^{\mathrm{GTP}}] \\
v_{47} &= k_{\mathrm{hyd}}^{\mathrm{B4T}}\,[\mathrm{B}\!:\mathrm{Bfa1}^{\mathrm{P4}}\!:\mathrm{Tem1}^{\mathrm{GTP}}] \\
v_{48} &= k_{\mathrm{hyd}}\,[\mathrm{B}\!:\mathrm{Bfa1}^{\mathrm{P5}}\!:\mathrm{Tem1}^{\mathrm{GTP}}]
\end{aligned}
$$

The three model variants are implemented in terms of kinetic parameters (cf. Table 4.4) and the structural parameter $\alpha \in \{0, 1\}$, which is used to prevent cytosolic association of Bfa1 and Tem1 ($\alpha = 0$) in the "hot-spot association" model.

Var.	Conc.	Num.	Notes	References
[B]	8.3×10^{-5}	150	Unidentified Bfa1-binding site at the SPB. Adds up to 300 binding sites in total together with [B : $Bfa1^{P5}$].	Caydasi *et al.*, 2012
[B:$Bfa1^{P5}$]	8.3×10^{-5}	150		Caydasi *et al.*, 2012
[Bfa1]	2.04×10^{-8}	1230	Adds up to 1380 together with [B:$Bfa1^{P5}$].	Ghaemmaghami *et al.*, 2003
[$Tem1^{GTP}$]	4.93×10^{-8}	2967	Adds up to 3450 together with [$Tem1^{GDP}$] (2.5-fold of total Bfa1). Ratio of [$Tem1^{GTP}$] and [$Tem1^{GDP}$] according to section 3.2.3.	Caydasi *et al.*, 2012; Ghaemmaghami *et al.*, 2003
[$Tem1^{GDP}$]	8.02×10^{-9}	483	Adds up to 3450 together with [$Tem1^{GTP}$] (2.5-fold of total Bfa1). Ratio of [$Tem1^{GTP}$] and [$Tem1^{GDP}$] according to section 3.2.3.	Caydasi *et al.*, 2012; Ghaemmaghami *et al.*, 2003
[T]	1.66×10^{-4}	300	Unidentified Tem1-binding site at the SPB.	Caydasi *et al.*, 2012
all others	0			

Table 4.3: Initial conditions of the ordinary differential equations. *Table adapted from Caydasi et al. (2012).* The following abbreviations were used in the column headings: **Var.**, Model variable; **Conc.**, Initial concentration in molar; **Num.**, Initial number of molecules (corresponds to concentration).

Table 4.4: Parameters used for the simulations of the models. *Table adapted from Caydasi et al. (2012).*

Param.	Value			Unit	Notes	Reactions	References
	Ubiquitous association	*Hot-spot association*	*Ubiquitous inactive*				
k_{on}^{B}	1.25×10^{6}	1.25×10^{6}	1.25×10^{6}	$\text{M}^{-1}\text{s}^{-1}$	Association of Bfa1 with the SPB.[a]	1, 3, 4, 6, 7, 9	Caydasi *et al.*, 2012
$k_{\text{off}}^{\text{B}}$	1.2×10^{-3}	1.2×10^{-3}	1.2×10^{-3}	s^{-1}	Dissociation of Bfa1 from the SPB. Corresponding to a half-life of $t_{1/2} = 300$ s.[b,c]	1, 3, 4, 6, 7, 9	Caydasi *et al.*, 2009
$k_{\text{on}}^{\text{B4}}$	2×10^{4}	2×10^{4}	2×10^{4}	$\text{M}^{-1}\text{s}^{-1}$	Association of Bfa1 with the SPB, low affinity after phosphorylation by Kin4.[a]	2, 5, 8	Caydasi *et al.*, 2012
$k_{\text{off}}^{\text{B4}}$	3.65×10^{-2}	3.65×10^{-2}	3.65×10^{-2}	s^{-1}	Dissociation of Bfa1 from the SPB, low affinity after phosphorylation by Kin4. Corresponding to a half-life of $t_{1/2} \approx 19$ s in cells with misaligned spindle.[b]	2, 5, 8	Caydasi *et al.*, 2009
$k_{\text{on}}^{\text{BT}}$	3.65×10^{7}	3.65×10^{7}	3.65×10^{7}	$\text{M}^{-1}\text{s}^{-1}$	Association of Tem1 and Bfa1.[a]	10, 13, 16, 19	Caydasi *et al.*, 2012
$k_{\text{on}}^{\text{B4T}}$	3.65×10^{7}	3.65×10^{7}	3.65×10^{7}	$\text{M}^{-1}\text{s}^{-1}$	Association of Tem1 and Bfa1^{P4}.[a]	11, 14, 17, 20	Caydasi *et al.*, 2012
$k_{\text{on}}^{\text{B5T}}$	7×10^{6}	5.5×10^{6}	7×10^{6}	$\text{M}^{-1}\text{s}^{-1}$	Association of Tem1 and Bfa1^{P5}.[a]	12, 15, 18, 21	Caydasi *et al.*, 2012
$k_{\text{off}}^{\text{BT}}$	1.83×10^{-1}	1.83×10^{-1}	1.83×10^{-1}	s^{-1}	Dissociation of Bfa1:Tem1 complex. Estimated from Tem1 half-life at the SPB of $t_{1/2} \approx 3.8$ s in WT cells with normal anaphase spindle, where Bfa1 is the primary binding site.[b]	10 – 21	Caydasi *et al.*, 2009
k_{on}^{T}	1.9×10^{6}	1.25×10^{6}	1.9×10^{6}	$\text{M}^{-1}\text{s}^{-1}$	Association of Tem1 with the GAP-independent binding site.[a]	22, 23	Caydasi *et al.*, 2012

Continued on the next page

Table 4.4: continued

Param.	Value			Unit	Notes	Reactions	References
	Ubiquitous association	*Hot-spot association*	*Ubiquitous inactive*				
$k_{\text{off}}^{\text{T}}$	1.83×10^{-1}	1.83×10^{-1}	1.83×10^{-1}	s^{-1}	Dissociation of Tem1 from the GAP-independent binding site. Estimated from Tem1 at the SPB of $t_{1/2} \approx 3.8$ s in cells with misapligned spindle.[b]	22, 23	Caydasi *et al.*, 2009
k_{+}^{Kin4}	10^3	10^3	10^3	s^{-1}	Pseudo first-order rate coefficient for the phosphorylation of Bfa1 by Kin4 at the SPB.	24 – 26	Caydasi *et al.*, 2012
$k_{+,\text{cyto}}^{\text{Kin4}}$	0.09	0.09	0.09	s^{-1}	Pseudo first-order rate coefficient for the phosphorylation of Bfa1 by Kin4.	30 – 32	Caydasi *et al.*, 2012
k_{-}^{Kin4}	2.51×10^{-2}	2.51×10^{-2}	2.51×10^{-2}	s^{-1}	Effective rate coefficient for the dephosphorylation of Bfa1 by the unknown phosphatase counteracting Kin4.	33 – 35	Caydasi *et al.*, 2012
k_{+}^{Cdc5}	1	1	1	s^{-1}	Effective rate coefficient for the phosphorylation of Bfa1 by Cdc5.	27 – 29	Caydasi *et al.*, 2012
k_{-}^{Cdc5}	10^{-2}	10^{-2}	10^{-2}	s^{-1}	Effective rate coefficient for the dephosphorylation of Bfa1 by the unknown phosphatase counteracting Kin4.	36 – 38	Caydasi *et al.*, 2012
k_{hyd}	2.24×10^{-3}	2.24×10^{-3}	2.24×10^{-3}	s^{-1}	Effective intrinsic GTP-hydrolysis by Tem1. See equation (3.2.9) and table 3.1 in section 3.2.5.	39, 41, 45, 48	Chapter 3
k_{nex}	1.36×10^{-2}	1.36×10^{-2}	1.36×10^{-2}	s^{-1}	Effective intrinsic GDP-GTP-exchange rate by Tem1. See equation (3.2.9) and table 3.1 in section 3.2.5.	40, 42	Chapter 3

Continued on the next page

Table 4.4: continued

Param.	Value			Unit	Notes	Reactions	References
	Ubiquitous association	*Hot-spot association*	*Ubiquitous inactive*				
$k_{\mathrm{hyd}}^{\mathrm{BT}}$	2	2	2.24×10^{-3}	s^{-1}	GAP-accelerated GTP-hydrolysis by Tem1. See Table 3.1 in section 3.2.5 and (3.2.12) in section 3.2.7. Fold-acceleration $\lambda = 1000$, $\rho = 0$. Unphosphorylated Bfa1 considered inactive in the Bfa1-control model, thus value computed with $\lambda = \rho = 1$.	43, 46	Chapter 3
$k_{\mathrm{hyd}}^{\mathrm{B4T}}$	2	2	2	s^{-1}	GAP-accelerated GTP-hydrolysis by Tem1. See Table 3.1 in section 3.2.5 and (3.2.12) in section 3.2.7. Fold-acceleration $\lambda = 1000$, $\rho = 0$.	44, 47	Chapter 3
α	1	0	1		Structural parameter preventing association of Bfa1 and Tem1 in the cytosol if 0.		
u	0 or 1	0 or 1	0 or 1		Input signal modeling correct spindle alignment $u = 0$ or spindle misalignment $u = 1$. All simulations start with $u = 1$ at $t = 0$ min and switch to $u = 0$ at $t = 30$ min.		
V_{S}	3×10^{-18}	3×10^{-18}	3×10^{-18}	l	Volume of the SPB compartment by overestimating the SPB as a cylindrical volume element approximately 100 nm high and 200 nm in diameter		Jaspersen *et al.*, 2004
V_{S}	1×10^{-13}	1×10^{-13}	1×10^{-13}	l	Volume of the cytosol compartment considered similar to the whole cell volume		Bryan *et al.*, 2010

Continued on the next page

Table 4.4: continued

Param.	Value		Unit	Notes	Reactions	References
Ubiquitous association	*Hot-spot association*	*Ubiquitous inactive*				

[a] Association rate was manually adjusted to match the molecule numbers at the SPB, given the respective dissociation rate.
[b] Dissociation rate coefficient estimated according to $k_{\text{off}} = \ln(2)/t_{1/2}$ where $t_{1/2}$ is the average half-life at the SPB.
[c] Bfa1 is tightly bound to SPBs of correctly aligned anaphase spindles Caydasi *et al.*, 2009. However, in order to allow Cdc5 to deactivate also the cytosolic Bfa1 pool, we assume a more rapid half-life of 600s.

4.2.3 Observable Quantities of the Dynamical Model

Bfa1 and Tem1 are modeled with a combinatorial number of variables to account for their different states and complexes. Thus, the amounts of active and inactive Bfa1 and Tem1, respectively, are not directly represented as model variables and must be derived by summing up the respective variables appropriately. In the following, GTP-bound Tem1 is considered active, regardless of whether it is bound to Bfa1 or not. Thus, equations

$$\begin{aligned}
[\mathrm{Tem1}^{\mathrm{active}}_{\mathrm{SPB}}] &= [\mathrm{T}:\mathrm{Tem1}^{\mathrm{GTP}}] + [\mathrm{B}:\mathrm{Bfa1}:\mathrm{Tem1}^{\mathrm{GTP}}] \\
&\quad + [\mathrm{B}:\mathrm{Bfa1}^{\mathrm{P4}}:\mathrm{Tem1}^{\mathrm{GTP}}] + [\mathrm{B}:\mathrm{Bfa1}^{\mathrm{P5}}:\mathrm{Tem1}^{\mathrm{GTP}}]\,, \\
[\mathrm{Tem1}^{\mathrm{active}}_{\mathrm{Cyto}}] &= [\mathrm{Tem1}^{\mathrm{GTP}}] + [\mathrm{Bfa1}:\mathrm{Tem1}^{\mathrm{GTP}}] \\
&\quad + [\mathrm{Bfa1}^{\mathrm{P4}}:\mathrm{Tem1}^{\mathrm{GTP}}] + [\mathrm{Bfa1}^{\mathrm{P5}}:\mathrm{Tem1}^{\mathrm{GTP}}]
\end{aligned}$$

define the observables for active Tem1 at the SPB or in the cytosol, respectively. Similarly, Tem1 bound to GDP is always considered inactive, therefore equations

$$\begin{aligned}
[\mathrm{Tem1}^{\mathrm{inactive}}_{\mathrm{SPB}}] &= [\mathrm{T}:\mathrm{Tem1}^{\mathrm{GDP}}] + [\mathrm{B}:\mathrm{Bfa1}:\mathrm{Tem1}^{\mathrm{GDP}}] \\
&\quad + [\mathrm{B}:\mathrm{Bfa1}^{\mathrm{P4}}:\mathrm{Tem1}^{\mathrm{GDP}}] + [\mathrm{B}:\mathrm{Bfa1}^{\mathrm{P5}}:\mathrm{Tem1}^{\mathrm{GDP}}]\,, \\
[\mathrm{Tem1}^{\mathrm{inactive}}_{\mathrm{Cyto}}] &= [\mathrm{Tem1}^{\mathrm{GDP}}] + [\mathrm{Bfa1}:\mathrm{Tem1}^{\mathrm{GDP}}] \\
&\quad + [\mathrm{Bfa1}^{\mathrm{P4}}:\mathrm{Tem1}^{\mathrm{GDP}}] + [\mathrm{Bfa1}^{\mathrm{P5}}:\mathrm{Tem1}^{\mathrm{GDP}}]
\end{aligned}$$

define the observables for inactive Tem1 at the SPB or in the cytosol.

The activity of Bfa1 is regulated by its phosphorylation status, irrespectively of being in complex with Tem1. However, dependent upon the model variant, unphosphorylated Bfa1 is considered active ("ubiquitous association" and "hot-spot association" models) while it is considered inactive in the "ubiquitous inactive" variant. With $q = 1$ for "ubiquitous association" and "hot-spot association" variants, and $q = 0$ for the "ubiquitous inactive" variant, the observables for active Bfa1 at SPB and in the cytosol read

$$\begin{aligned}
[\mathrm{Bfa1}^{\mathrm{active}}_{\mathrm{SPB}}] &= q\left\{[\mathrm{B}:\mathrm{Bfa1}] + [\mathrm{B}:\mathrm{Bfa1}:\mathrm{Tem1}^{\mathrm{GTP}}] + [\mathrm{B}:\mathrm{Bfa1}:\mathrm{Tem1}^{\mathrm{GDP}}]\right\} \\
&\quad + [\mathrm{B}:\mathrm{Bfa1}^{\mathrm{P4}}] + [\mathrm{B}:\mathrm{Bfa1}^{\mathrm{P4}}:\mathrm{Tem1}^{\mathrm{GTP}}] + [\mathrm{B}:\mathrm{Bfa1}^{\mathrm{P4}}:\mathrm{Tem1}^{\mathrm{GDP}}]\,, \\
[\mathrm{Bfa1}^{\mathrm{active}}_{\mathrm{Cyto}}] &= q\left\{[\mathrm{Bfa1}] + [\mathrm{Bfa1}:\mathrm{Tem1}^{\mathrm{GTP}}] + [\mathrm{Bfa1}:\mathrm{Tem1}^{\mathrm{GDP}}]\right\} \\
&\quad + [\mathrm{Bfa1}^{\mathrm{P4}}] + [\mathrm{Bfa1}^{\mathrm{P4}}:\mathrm{Tem1}^{\mathrm{GTP}}] + [\mathrm{Bfa1}^{\mathrm{P4}}:\mathrm{Tem1}^{\mathrm{GDP}}]\,.
\end{aligned}$$

Accordingly, the respective observables for inactive Bfa1 are

$$\begin{aligned}[\mathrm{Bfa1}^{\mathrm{inactive}}_{\mathrm{SPB}}] &= (1-q)\left\{[\mathrm{B:Bfa1}] + [\mathrm{B:Bfa1:Tem1}^{\mathrm{GTP}}] + [\mathrm{B:Bfa1:Tem1}^{\mathrm{GDP}}]\right\} \\ &\quad + [\mathrm{B:Bfa1}^{\mathrm{P5}}] + [\mathrm{B:Bfa1}^{\mathrm{P5}}\mathrm{:Tem1}^{\mathrm{GTP}}] + [\mathrm{B:Bfa1}^{\mathrm{P5}}\mathrm{:Tem1}^{\mathrm{GDP}}] \\ [\mathrm{Bfa1}^{\mathrm{inactive}}_{\mathrm{Cyto}}] &= (1-q)\left\{[\mathrm{Bfa1}] + [\mathrm{Bfa1:Tem1}^{\mathrm{GTP}}] + [\mathrm{Bfa1:Tem1}^{\mathrm{GDP}}]\right\} \\ &\quad + [\mathrm{Bfa1}^{\mathrm{P5}}] + [\mathrm{Bfa1}^{\mathrm{P5}}\mathrm{:Tem1}^{\mathrm{GTP}}] + [\mathrm{Bfa1}^{\mathrm{P5}}\mathrm{:Tem1}^{\mathrm{GDP}}]\,.\end{aligned}$$

4.2.4 Deterministic and Stochastic Simulation of the SPOC-Model

To reproduce the changes in Bfa1 and Tem1 SPB-localization upon changes of spindle orientation *in silico*, an arbitrarily chosen time period of 60 min in total was simulated for all three model variants. Simulations started from an early anaphase state with a misaligned spindle, that is, with phosphorylation of Bfa1 by Kin4 turned on (parameter $u = 1$, cf. Table 4.4). After simulated 30 min, the spindle was considered to align correctly and turn off SPOC signaling by inactivation of Kin4 (parameter $u = 0$). The model output shows the levels of Bfa1 and Tem1 in their respective active and inactive states at the SPBs and in the cytosol (see definition of the observables in the previous section).

For the deterministic simulations, the ODEs defined in section 4.2.2 were solved numerically using the build-in MATLAB function ode15s (MathWorks, 2009).

For the stochastic simulations, the well known "stochastic simulation algorithm" (SSA) by D. T. Gillespie (1976) was implemented in MATLAB (MathWorks, 2009). The propensity functions for all reactions were derived from their respective reactant stoichiometries and kinetic parameters. The trajectories resulting from simulations with the SSA are random samples from the chemical master-equation of the system. Thus, ensembles of 200 individual trajectories have been computed and snapshots of the ensemble have been recorded at regular intervals. For each snapshot, mean and standard deviation have been calculated.

In both cases, model variables were summed up according to the definition of the observables in section 4.2.3.

4.2.5 Scans of the GTPase-Parameters

The model variants were simulated deterministically as described in the previous section with the Tem1 GDP-dissociation rate coefficient and the fold-acceleration of GTP hydrolysis by the GAP varied in a wide range, that is $k^{\mathrm{D}}_{\mathrm{off}} \in [10^{-3}\mathrm{s}^{-1}, 10^{2}\mathrm{s}^{-1}]$ and $\lambda \in [1, 10^{4}]$, respectively. All other parameters remained at their nominal values.

For every combination of parameter values for $k_{\text{off}}^{\text{D}}$ and λ, the following quantities were recorded:

1. the number of Tem1^{GTP} molecules remaining at the SPB at $t = 30$ min (x_{30})
2. the number of Tem1^{GTP} molecules accumulated at the SPB at $t = 40$ min (x_{40}).

Furthermore, the constants $x_{\text{MEN}} = 65$ molecules and $x_{\max} = 255$ molecules were defined, where x_{MEN} is the amount of Tem1^{GTP} at the SPB sufficient for activation of MEN (cf. Caydasi *et al.*, 2012) and $x_{\max}$ is the total steady-state amount of Tem1 at the SPB, which is reached in all models. Thus, $x_{\max}$ is an upper bound of the level of Tem1^{GTP} at the SPB at $t = 40$ min. Importantly, x_{MEN} and $x_{\max}$ are independent from the scanned parameters and in all model variants.

4.2.5.1 Relative Inhibition and Recovery

From the recorded Tem1^{GTP} levels (x_{30} and x_{40}), the relative inhibition (I) and recovery (R) were computed, which are defined to be $I = \max\{0, 1 - x_{30}/x_{\text{MEN}}\}$ and $R = \max\{0, (x_{40} - x_{\text{MEN}})/(x_{\max} - x_{\text{MEN}})\}$, respectively. Relative inhibition measures the reduction of SPB-bound Tem1^{GTP} below the threshold x_{MEN}, 30 min after SPOC activation. Similarly, relative recovery measures the increment of SPB-bound Tem1^{GTP} above the threshold x_{MEN} reached 10 min after deactivation of SPOC.

4.2.5.2 Quality Level

The quality level of the checkpoint response (Q) is based on the relative inhibition (I) and recovery (R). The quality level is the minimum of both criteria, i.e., $Q = \min\{I, R\}$. It combines relative inhibition and recovery into a more rigorous measure: If one of relative inhibition or recovery is not sufficient, the quality level of the parameter combination is zero. Low-quality levels indicate that either inhibition or recovery (or both) is barely sufficient, whereas a quality level of 1 would mean that both inhibition and recovery are maximal.

4.2.5.3 Dynamic Range

The dynamic range is computed according to $DR = (x_4 - x_{30})/x_{\max}$. A high dynamic range is desirable because this property implies robustness of the checkpoint response. It is important to note that low quality levels can be associated with high dynamic ranges. This is particularly pronounced if low quality is a consequence of poor inhibition of Tem1, due to the asymmetry of maximal inhibition and maximal

recovery in terms of absolute molecule numbers, which is hidden in the normalized measures I and R. The dynamic range complements the non-differentiable- quality level with a smooth measure of robustness.

4.2.6 S:A:P-Model of Adapter-Mediated Complex Formation

Indirect binding of a protein P to its stationary binding-site S via an adapter-protein A can be described in sufficient detail with the chemical reaction equation

$$\begin{aligned} \mathrm{A} + \mathrm{P} &\underset{k_P^-}{\overset{u\,k^+}{\rightleftharpoons}} A{:}P \\ S{:}A + \mathrm{P} &\underset{k_P^-}{\overset{k^+}{\rightleftharpoons}} S{:}A{:}P \\ \mathrm{S} + \mathrm{A} &\underset{k_S^-}{\overset{k^+}{\rightleftharpoons}} S{:}A \\ \mathrm{S} + A{:}P &\underset{k_S^-}{\overset{k^+}{\rightleftharpoons}} S{:}A{:}P\,. \end{aligned} \tag{4.2.50}$$

Note that for simplicity the association rate constant is considered to be equal for all reactions, whereas the average life-time of the interactions between adapter and protein P are assumed to be different from those of the stationary binding site with the adapter. The structural parameter $u \in \{0, 1\}$ was integrated to control the association of protein P with free adapters A. If $u = 1$, both can bind without restrictions, otherwise ($u = 0$) binding of P is limited to adapters already bound to the stationary binding site S.

4.2.6.1 Ordinary Differential Equations of the S:A:P-Model

Under the assumption of mass action kinetics, the ordinary differential equation system corresponding to equation (4.2.50) is given by

$$\begin{aligned} \mathrm{d}[P]/\mathrm{d}t &= -(v_1 + v_2) \\ \mathrm{d}[A]/\mathrm{d}t &= -(v_1 + v_3) \\ \mathrm{d}[S]/\mathrm{d}t &= -(v_3 + v_4) \\ \mathrm{d}[A{:}P]/\mathrm{d}t &= v_1 - v_4 \\ \mathrm{d}[S{:}A]/\mathrm{d}t &= v_3 + v_2 \\ \mathrm{d}[S{:}A{:}P]/\mathrm{d}t &= v_2 + v_4 \end{aligned} \tag{4.2.51}$$

Kinetic Parameters		
Parameter	*Value (a.u.)*	*Remark*
k^+	1	
k_P^-	0.005	Dissociation of the interaction between A and P was chosen five times as fast as dissociation of A and S to reflect the different turnover times of Bfa1 and Tem1 at the SPB.
k_S^-	0.001	See k_P^-.
u	0 or 1	Structural parameter controlling association of P with free A.
Initial conditions		
Species	*Conc. (a.u.)*	*Remark*
$[P]_0$	10	
$[A]_0$	$r[P]_0$	The relative amount r of the adapter A with respect to protein P is varied in the range $[10^{-1}, 10^1]$.
$[S]_0$	1	
$[A{:}P]$, $[S{:}A]$, $[S{:}A{:}P]$	0	

Table 4.5: Parameters and initial conditions of the $S{:}A{:}P$-model.

with net reaction fluxes $v_i = v_i^+ - v_i^-$ using the uni-directional reaction rates

$$\begin{aligned} v_1^+ &= uk^+[A][P] \\ v_1^- &= k_P^-[A{:}P] \\ v_2^+ &= k^+[S{:}A][P] \\ v_2^- &= k_P^-[S{:}A{:}P] \\ v_3^+ &= k^+[S][A] \\ v_3^- &= k_S^-[S{:}A] \\ v_4^+ &= k^+[S][A{:}P] \\ v_4^- &= k_S^-[S{:}A{:}P]\,. \end{aligned} \tag{4.2.52}$$

The parameters and initial conditions are summarized in Table 4.5.

4.2.6.2 Relative Saturation and Association Rate

The relative saturation

$$\sigma := \frac{[S{:}A{:}P]}{[S] + [S{:}A] + [S{:}A{:}P]} \tag{4.2.53}$$

is the percentage of stationary binding sites S which are associated to a protein P. This measure is normalized to $[0, 1]$ such that $\sigma = 1$ if all S-molecules have a P-molecule attached. In contrast, the relative association rate of S and P

$$\nu := \frac{v_2^+ + v_4^+}{\sum_{i=1}^4 v_i^+} \tag{4.2.54}$$

relates the cumulative rate of the reactions increasing saturation σ to the cumulative rate of all reactions involving S or P. Thus, ν is 0 if P-molecules never associate with S, whereas it approaches 1 if almost every reaction links a P-molecule to a stationary binding site.

4.2.6.3 Scan of the Total Ratio of A and P

To investigate the dependency of protein P accumulation at the stationary binding site S upon the total ratio of adapter A and protein P, the ODE system was simulated using the matlab built-in function ode15s (MathWorks, 2009) for an arbitrary time period of $t \in [0, 10^4]$ with parameters and initial conditions a listed in Table 4.5 with ratio r varied in $[10^{-1}, 10^1]$. The temporal evolution of measures σ and ν were then computed from the simulation results.

4.3 Results

4.3.1 Molecular Amounts of Bfa1, Bub2 and Tem1 at the SPBs

Anaphase levels of Bfa1, Bub2 and Tem1 at the SPBs were determined employing a method that uses GFP-tagged structural kinetochore proteins with known stoichiometry as reference standard (Joglekar *et al.*, 2006, 2008; Lawrimore *et al.*, 2011). The 32 kinetochores form two clusters with 16 kinetochores each in the vicinity of the SPBs (Coffman *et al.*, 2011). Molecular amounts of GFP-tagged SPB-associated proteins can thus be estimated by comparing their fluorescence with the fluorescence of the GFP-tagged reference from the kinetochore clusters. The statistical analysis of the experimental results is described in section 4.2.1, the experimental setup and results are detailed in (Caydasi *et al.*, 2012). This section summarizes the results therein, the estimated mean molecule numbers at the SPBs are reported in Table 4.6.

Fluorescence intensities were recorded for Bfa1-GFP, Bub2-GFP, and Tem1-GFP in a yeast strain with a deletion of the KAR9 locus (kar9Δ). Yeast cells lacking

Table 4.6: Numbers of Bf1, Bub2 and Tem1 molecules at the SPBs. *Table adapted from Caydasi et al. (2012).*

Protein	Spindle[a]	SPB[b]	Mean	SD[c]	CV[d][%]	% of Total
Bfa1	misaligned	m, d	50	32	64	4
	aligned	m	57	39	68	4
	aligned	d	287	96	34	21
Bub2	misaligned	m, d	37	24	65	3
	aligned	m	32	21	68	2
	aligned	d	199	89	45	14
Tem1[e]	misaligned	m, d	125	35	28	3
	aligned	m	112	41	37	3
	aligned	d	255	98	38	7
Tem1[f]	short (< 4 μm)	m, d	75	29	39	2
	long (≥ 4 μm)	m, d	96	32	32	3

[a] Spindle alignment status or spindle length in case of Tem1 in absence of Bfa1 and Bub2 [b] Measured at mother SPB (m) or daughter SPB (d)
[c] Standard deviation [d] Coefficient of variation [e] in presence of Bfa1 and Bub2
[f] in absence of Bfa1 and Bub2 (bfa1Δ bub2Δ)

Kar9 frequently fail to properly orient the anaphase spindle, so deletion of KAR9 provides a strain background suitable for measuring fluorescence at normally aligned and misaligned spindles as well. Levels of Bfa1, Bub2 and Tem1 at the SPBs are not constant during anaphase (Caydasi *et al.*, 2009; Molk *et al.*, 2004), thus fluorescence intensities show a considerable variation around the mean. In cells with normally aligned spindle, Bfa1, Bub2 and Tem1 localize asymmetrically to mSPB and dSPB, reaching 5-6 times higher levels at the dSPB. In contrast, their levels do not differ significantly between the SPBs in cells with misaligned spindle. Thus, molecule numbers were estimated separately for mSPB and dSPB in case of normal spindle alignment, whereas a common molecule number was computed for both SPBs in case of spindle misalignment.

In addition to the molecule numbers at the SPBs, whole cell molecule numbers were estimated by linearly relating the mean whole cell fluorescence of Bfa1-GFP, Bub2-GFP, and Tem1-GFP to the respective mean fluorescence at the SPB. For Bfa1, this resulted in a total molecule number of 1374 ± 292. The total molecule number of Bub2 was similar. Because the ratio of Bfa1 and Tem1 is particularly important for numerical simulation of the SPOC, total molecule numbers of Tem1 were estimated by computing the ratio of Tem1 and Bfa1 whole cell fluorescence. This ratio was

about 2.5, resulting in an estimation of 3435 ± 730 Tem1 molecules per cell.

Most of Tem1 binds to the SPBs in a Bfa1-Bub2-dependent manner and follows the asymmetric binding pattern of the GAP-complex. However, a small pool of Tem1 binds symmetrically to both SPBs even in the absence of Bfa1 and Bub2 (Caydasi *et al.*, 2009; Pereira *et al.*, 2002; Valerio-Santiago *et al.*, 2011). This "GAP-independent pool" was measured by recording fluorescence intensities of Tem1-GFP of cells with deleted Bfa1 and Bub2 loci (bfa1Δ bub2Δ), confirming that that the GAP-independent pool is small compared to the GAP-dependent pool. Fluorescence was measured separately for short and long anaphase spindles, and Tem1-amounts at the SPBs turned out to be significantly lower in cells with short spindles.

4.3.2 A Dynamical Model of the SPOC

To analyze the systemic capability of the SPOC to inhibit Tem1 at the SPBs, a dynamical model of the SPOC was developed focusing on the regulation of Tem1 by the GAP complex Bfa1:Bub2 according to the wiring diagram outlined in Figure 4.4. The model was build around the GTPase-model developed in chapter 3. The details of the model and its implementation are described in section 4.2. To limit the complexity of the resulting model, the monomeric forms of Bfa1 and Bub2 were neglected, assuming that both proteins occur always in form of the GAP-complex Bfa1:Bub2. Bfa1 was used shorthand for Bfa1:Bub2 in the model, because Bfa1 is the regulatory subunit of the GAP complex whereas Bub2 does likely contribute the catalytic site (Geymonat *et al.*, 2002, 2003). The model was designed such that it could reproduce the binding pattern of Bfa1 and Tem1 at the dSPB in both situations, when the SPOC is active, and when it is inactive. To this end, molecules at the dSPB and molecules in the cytosol were distinguished (Figure 4.4A), allowing them to exchange with kinetics compatible with previous FRAP analysis (Caydasi *et al.*, 2009). Tem1 was considered to associate with the SPBs in a GAP-dependent (Figure 4.4C) and -independent manner (Figure 4.4B). The minimal model of the intrinsic GTPase-cycle of Tem1 was embedded into this framework (Figure 4.4B; chapter 3), together with the acceleration of GTP hydrolysis by the Bfa1Bub2 GAP complex (Figure 4.4C) (Geymonat *et al.*, 2002). Bfa1 regulation was accounted for through counteracting phosphorylation by Cdc5 and Kin4. Kin4 is essential for the activation of the SPOC in response to spindle misalignment; hence Kin4 was used to switch between active and inactive SPOC by allowing or disallowing it to phosphorylate Bfa1, respectively (Figure 4.4A).

An important question which should be addresses *in silico* was whether the GAP

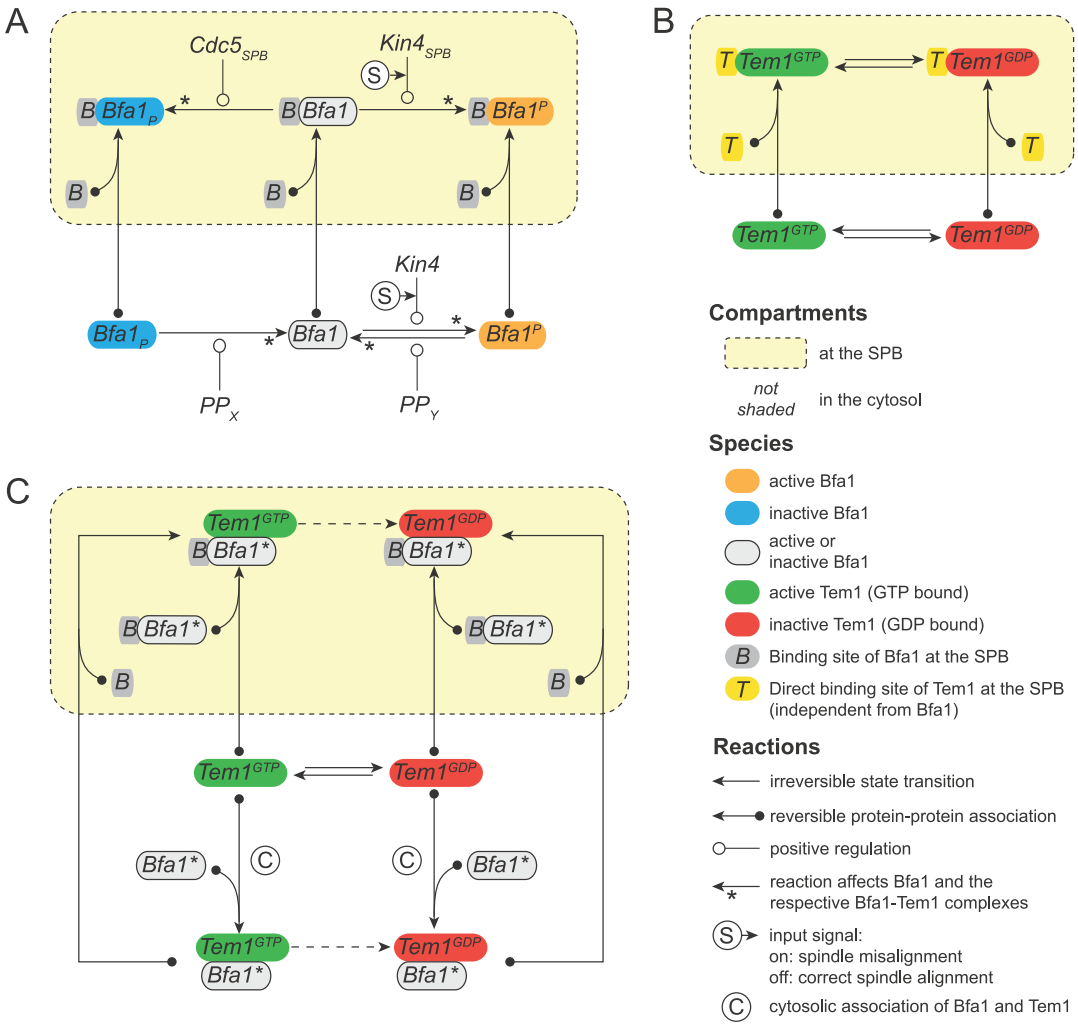

Figure 4.4: Wiring diagram of the dynamical model. *Figure published in Caydasi et al. (2012).* Yellow boxes indicate the SPB compartment. Reactions crossing the compartment boundary represent the reversible SPB association of the respective species or complexes. (**A**) Regulation of Bfa1 by Kin4, Cdc5 and their opposing phosphatases PP_X and PP_Y. In reactions marked with an asterisk, corresponding : complexes participate too. Kin4-mediated phosphorylation depends on spindle misalignment (input signal; encircled 'S'). Rate coefficients of Bfa1 association with the SPB differ with respect to the state of Bfa1. (**B**) Intrinsic Tem1 GTPase-cycle and reversible SPB association. Tem1 bound directly to the SPB does not interact with Bfa1; however, hydrolysis and nucleotide exchange take place. (**C**) Interaction of Tem1 and Bfa1. The scheme applies to all states of Bfa1, that is, there is one instance of the scheme for Bfa1* replaced by either Bfa1 ('unphosphorylated'), $Bfa1^P$ (phosphorylated by Kin4) or $Bfa1_P$ (phosphorylated by Cdc5). GTP hydrolysis by the respective Bfa1:$Tem1^{GTP}$ complexes (dashed arrows) is or is not accelerated depending on the GAP activity of the respective state of Bfa1.

Model variant	Key assumptions		Outcomes	
	Tem1 and Bfa1 interaction	*Unphosphorylated Bfa1*	*Tem1 inhibition*	*Tem1 activation*
Ubiquitous-association	SPB and cytosol	Active	Sufficient	Slow
Hot-spot-association	SPB only	Active	Insufficient	Rapid
Ubiquitous-inactive	SPB and cytosol	Inactive/Inhibited	Sufficient	Rapid

Table 4.7: Key assumptions and outcomes of the of the SPOC model variants. Attribution of sufficiency of inhibition or recovery according to the level of SPB-bound $\mathrm{Tem1^{GTP}}$ in relation to the $\mathrm{Tem1^{GTP}}$-threshold for activation of MEN.

inhibits Tem1 solely at the SPBs or also in the cytosol. Therefore, the two possibilities were implemented by two model variants, named as "hot-spot-association" and "ubiquitous-association" models. In the hot-spot-association model, binding of Bfa1 and Tem1 takes place exclusively at the SPB. This restriction was removed in the ubiquitous-association model, allowing for cytosolic association of Bfa1 and Tem1 (reactions marked with encircled "C" in Figure 4.4C). Comparison of the results of *in silico* and *in vivo* overexpression of Bfa1 supports the ubiquitous-association model and suggests that the hot-spot association model disagrees with biological reality. Thus, no further efforts were spent investigating the hot-spot-association model.

It is unclear whether the GAP complex containing unphosphorylated Bfa1 (Bfa1 which is neither phosphorylated by Cdc5 nor by Kin4) is active or inactive *in vivo*. In the ubiquitous-association model, unphosphorylated Bfa1 is considered active. To investigate the opposite situation, the additional "ubiquitous-inactive" model variant considers unphosphorylated Bfa1 to be inactive or inhibited.

Table 4.7 summarizes the key assumptions and outcomes for all model variants.

4.3.3 Threshold of SPB-bound $\mathrm{Tem1^{GTP}}$ for Activation of MEN

To evaluate the ability of the model variants to regulate Tem1 activity in response to spindle alignment status, a threshold for the SPB-bound $\mathrm{Tem1^{GTP}}$ level was defined such that this level is with high certainty sufficient for initiation of MEN signaling. The threshold is based on the number of Tem1 molecules at the SPBs of bfa1Δ bub2Δ cells (75 molecules; Table 4.6). Analysis of the mathematical model of the intrinsic Tem1 GTPase-cycle results in an estimated steady state of 86% $\mathrm{Tem1^{GTP}}$ and 14% $\mathrm{Tem1^{GDP}}$ in absence of a GAP. Because most likely only the active, GTP-bound form of Tem1 is able to activate MEN, the threshold was set to $0.86 \times 75 \approx 65$

molecules of SPB-bound $Tem1^{GTP}$. Thus, exceeding 65 molecules of $Tem1^{GTP}$ at the SPB was assumed to be a necessary and sufficient condition for triggering the MEN cascade. In the contrary, maintaining the $Tem1^{GTP}$-level at the SPB significantly below this threshold was assumed to prevent activation of MEN. Every reasonable model must, without violating the constraints imposed by the molecule numbers at the SPB, maintain the level of $Tem1^{GTP}$ well below 65 molecules if the SPOC is active, and allow rapid recovery of $Tem1^{GTP}$ to the level of or above this threshold upon deactivation of the SPOC to initiate MEN signaling.

4.3.4 Model Dynamics

In vivo, Bfa1 and Tem1 levels rapidly decreased at the SPBs upon spindle misalignment, whereas they accumulated at the dSPB concomitantly with the establishment of correct spindle alignment during anaphase (Caydasi *et al.*, 2012). To reproduce such behavior in silico, an arbitrary time period of 60 min in total was simulated (see section 4.2.4), starting from an early anaphase state with a misaligned spindle (phosphorylation of Bfa1 by Kin4 switched on). After 30 min, the spindle was considered to align correctly and turn off the SPOC (phosphorylation of Bfa1 by Kin4 switched off) (indicated by vertical lines in Figure 4.5). The model output shows the levels of Bfa1 and Tem1 in their respective active and inactive states at the SPBs and in the cytosol (Figure 4.5; cf. section 4.2.3).

4.3.4.1 Dynamics of the Ubiquitous-Association Model

In the ubiquitous-association model, in which Tem1 and Bfa1 can interact both at the SPB and in the cytosol, Bfa1 becomes rapidly activated and depleted from the SPB in response to spindle misalignment (Figure 4.5A, orange areas). The level of Tem1 decreases at the SPB along with Bfa1 and at the same time inactive Tem1 in the cytosol as well as at the SPB (Figure 4.5, red areas). The amount of remaining GTP-bound Tem1 is well below 65 molecules at the SPB (horizontal line in Figure 4.5A); hence inhibition of mitotic exit was considered to be reliable. In contrast, recovery of active Tem1 after SPOC deactivation does barely reach the threshold within 30 minutes (Figure 4.5A, $t > 30$). Slow recovery is a consequence of the slow deactivation of cytosolic Bfa1 by Cdc5, which is limited by the turnover of Bfa1 at the SPBs.

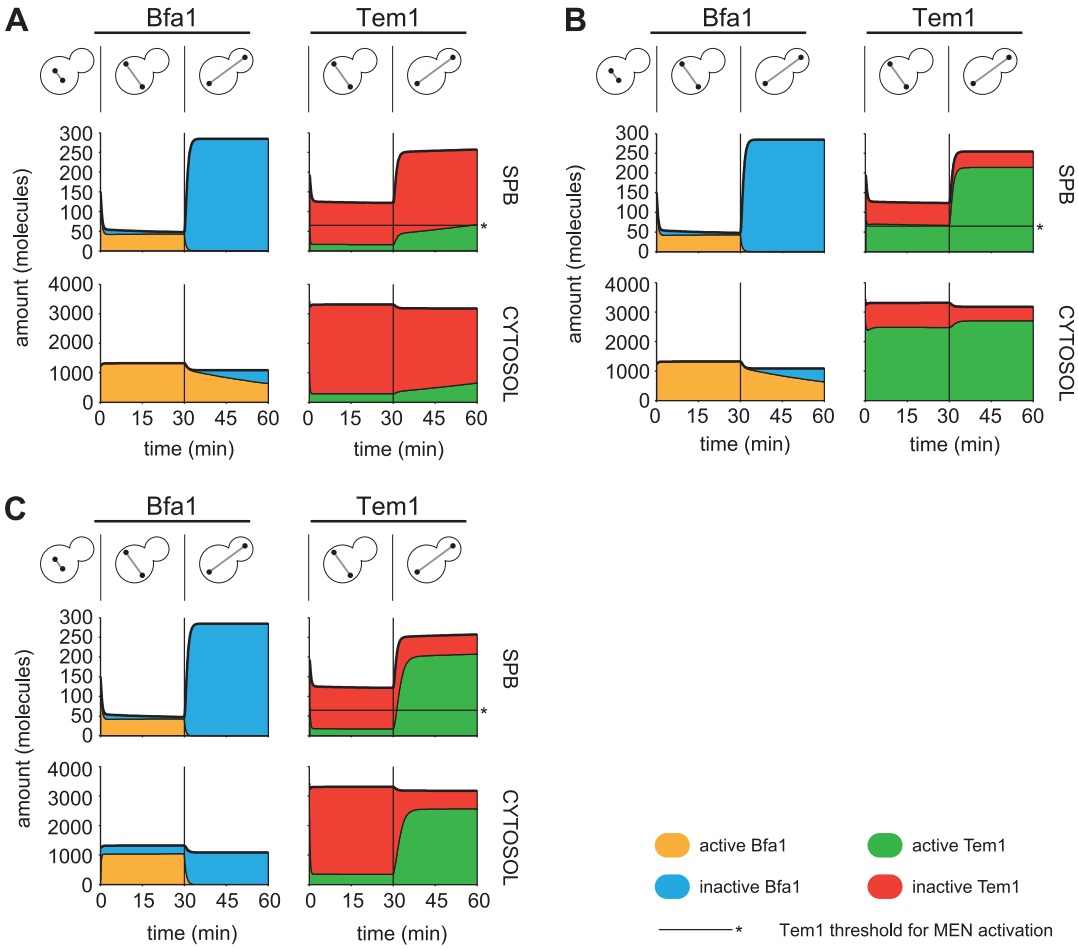

Figure 4.5: Deterministic simulations. *Figure adapted from Caydasi et al. (2012).* Dynamics of ubiquitous-association (**A**), hot-spot-association (**B**) and ubiquitous-inactive (**C**) models are shown. Amounts of Bfa1 and Tem1 in active and inactive forms are shown at the SPB and in the cytosol. Simulations start with activation of the SPOC from a metaphase-like state ($t = 0$ min). Vertical lines indicate the time point of proper spindle alignment ($t = 30$ min), resulting in deactivation of the SPOC. Dashed horizontal lines mark the number of active Tem1 molecules at the SPB sufficient for MEN activation.

4.3.4.2 Dynamics of the Hot-Spot-Association Model

If association of Tem1 and Bfa1 is restricted to the SPB, the dynamics of the total SPB bound Bfa1 and Tem1 levels at the SPB are virtually the same as in the ubiquitous-association model (Figure 4.5B). Although the level of SPB-bound

$Tem1^{GTP}$ decreases rapidly upon checkpoint activation, it does barely reach the threshold for activation of MEN (Figure 4.5B). Thus, the hot-spot-association model is not capable of preventing premature mitotic exit. On the other hand, active Tem1 accumulates rapidly at the SPB after spindle realignment, reaching about 84% of the total SPB-bound Tem1(Figure 4.5B, $t > 30$), which is close to the theoretical limit of 86% in the absence of the GAP (cf. section 3.2.3).

In contrast to the ubiquitous-association model, the cytosolic level of $Tem1^{GTP}$ remains high throughout the simulation. This is expected, because the substantial acceleration of GTP-hydrolysis by the GAP (the model assumes a 1000-fold) is impaired by the requirement of Tem1 turnover at a very limited pool of Bfa1 molecules.

4.3.4.3 Dynamics of the Ubiquitous-Inactive Model

The ubiquitous-inactive model combines ubiquitous association of Bfa1 and Tem1 with the assumption that unphosphorylated Bfa1 is inactive or inhibited upon proper spindle alignment. Tem1 is rapidly and efficiently inhibited upon spindle misalignment(Figure 4.5C), whereas the GTP-bound form reach levels sufficient for activation of MEN soon after spindle alignment (Figure 4.5C, $t > 30$). The ubiquitous-inactive model unites the effective inhibition of Tem1 from the ubiquitous-association model and the rapid recovery of $Tem1^{GTP}$ from the hot-spot-association model without adopting their weaknesses. It does therefore satisfy the previously defined criteria for the checkpoint mechanism controlling Tem1 and indicates that an additional Bfa1 inhibitor is required to fully control Tem1 activity.

4.3.5 Tem1 Interacts with Bfa1 in the Cytosol and at the SPBs

As a first step to identify an *in vivo* experiment which would discriminate between the hot-spot-association and the ubiquitous-association model variants, a simple, more abstract model of the binding process between a stationary binding site (S; corresponding to the Bfa1-binding site at the SPB), an adapter A (corresponding to Bfa1) and an associating protein P (corresponding to Tem1) was developed. This model, which is referred to as the $S{:}A{:}P$-model, is detailed in section 4.2.6. The $S:A:P$-model has one structural parameter which either enables or disables the association of P with free A. Here, free A is opposed to A which is bound to the stationary binding site S. Importantly, the $S{:}A{:}P$-model turns out to be sensitive to alterations of the total ratio of A and P molecules if association of P and free A is enabled ($u = 1$), whereas this sensitivity is significantly reduced in the opposite

situation ($u = 0$). Figure 4.6 shows the percentage of the saturation of stationary binding sites S with P molecules in both situations as a function of the total A to P ratio. When applied to the wild-type ratio of Bfa1 and Tem1 ($r \approx 0.35$; WT in Figure 4.6A and 4.6C), virtually full saturation is reached rapidly for $u = 0$ and $u = 1$. However, a 10-fold increase of the A to P ratio ($r \approx 3.5$, corresponding to 10-fold overexpression of BFA1) reduces saturation significantly (note the logarithmic color scale in Figure 4.6). Hence, an approximately 10-fold overexpression of BFA1 was an appealing candidate to distinguish the two variants of the SPOC model.

In silico overexpression of BFA1 by a factor of 10 translates the results from the S:A:P-model well to the full SPOC model. Tem1 levels at the SPB are reduced in the ubiquitous-association model while Tem1 levels at the SPB are even slightly elevated in the hot-spot-association model (Figure 4.7).

The previous results where eventually translated into an *in vivo* experiment to determine whether Bfa1 and Tem1 do actually interact in the cytosol. When BFA1 was overexpressed approximately 10-fold *in vivo*, SPB-bound Tem1 decreased in the majority of the cells, supporting the ubiquitous-association model and excluding the hot-spot-association model (Caydasi *et al.*, 2012).

What is the reason for this possibly counterintuitive result? In the wild type situation, the number of Tem1 molecules exceeds the number of Bfa1 molecules by far. Binding of Tem1 to the SPB is then limited by the amount of Bfa1 present as illustrated in Figure 4.8A. Obviously, free Bfa1 competes with SPB-bound Bfa1 for free Tem1. If the total amount of Bfa1 increases significantly, free Bfa1 prevents Tem1 from binding to the SPB as depicted in Figure 4.8B. This situation is comparable with the stoichiometric effects of scaffolded signal transduction cascades discussed by Ferrell, (2000) and Burack *et al.*, (2000).

This model is supported by the S:A:P-model with $u = 1$. This can be seen by inspecting the the relative association rate of S and P, which is defined in section 4.2.6. Reactions linking protein P with the stationary binding sites S are rather frequent events in the wild-type situation and even dominate during the transient phase at $t \approx 10^0$ (WT in Figure 4.6B). Upon overexpression, binding of P to S becomes rare (OE in Figure 4.6B). If interaction of protein P and adapters A is limited to the stationary binding sites ($u = 0$), this dependency does not exist (Figure 4.6D).

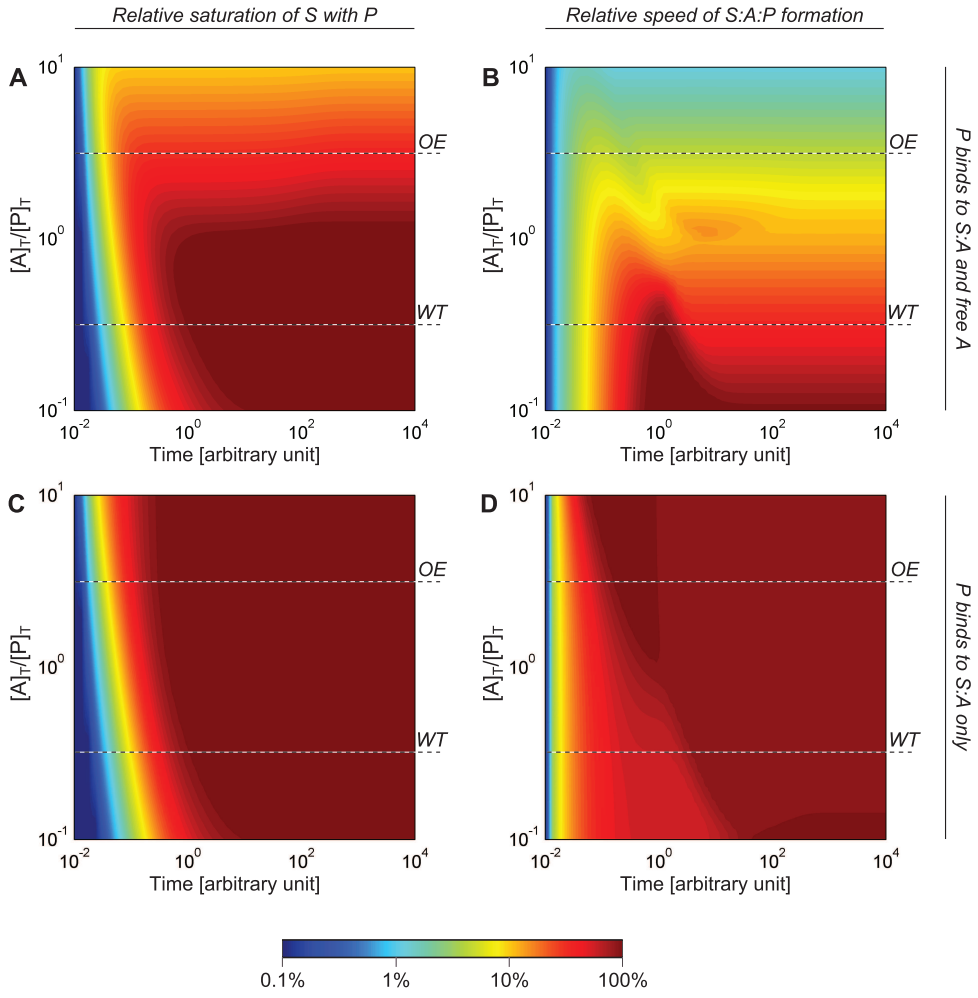

Figure 4.6: Dependency of $S{:}A{:}P$-concentration on the ratio of total A and P concentrations. Temporal evolution of relative saturation σ of stationary binding sites S with protein P and relative association rate ν of the ternary $S{:}A{:}P$ complex are shown as functions of the ratio $r = [A]_T/[P]_T$ of total concentrations of adapter A and protein P. Dashed lines indicate ratios r when the model is applied to Bfa1 (as adapter) and Tem1: *WT* indicates the wild type ratio $r \approx 0.35$, and *OE* corresponds to 10-fold overexpression of BFA1 ($r \approx 3.5$). (**A**) Relative saturation σ if adapter A can associate with protein P without restriction. (**B**) Relative association rate ν of protein P with the stationary binding site S corresponding to panel A. (**C**) Relative saturation σ if association of adapter A and protein P is limited to adapter molecules A which are which are already bound to the stationary binding site S. (**D**) Relative association rate ν of protein P with the stationary binding site S corresponding to panel C.

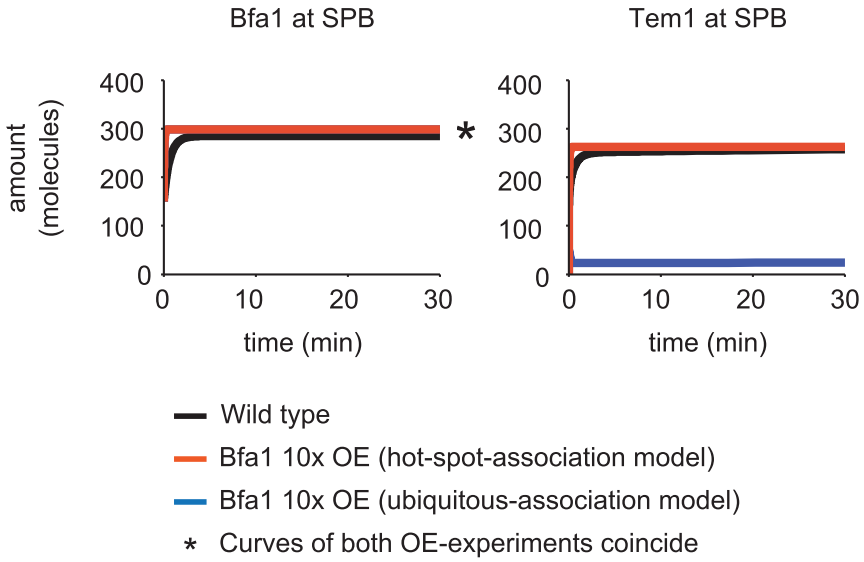

Figure 4.7: 10-fold overexpression of Bfa1 in silico. *Figure adapted from Caydasi et al. (2012).* Temporal evolution of the levels of Bfa1 and Tem1 at the SPBs with wild-type (black) and 10-fold increased Bfa1-levels (blue and orange curves). Virtually no difference exists between ubiquitous- and hot-spot-association models in the wild type situation. Upon overexpression of Bfa1, the level of SPB-bound Bfa1 increases to full saturation of the available binding sites for both models. In contrast, the level of Tem1 decreases significantly in the ubiquitous-association model whereas the it is even slightly elevated in the hot-spot-association model.

4.3.6 Checkpoint Reliability

Although the rate coefficients of the SPOC model were assumed to be constants, many external parameters like temperature or pH-value affect the rate of intracellular reactions *in vivo*. While sensitivity against changes of reaction rates due to alteration of environmental conditions enables some biochemical systems to act as sensors (Rudoni *et al.*, 2001), robustness against changes of reaction kinetics is a desirable feature of biochemical systems which have to function reliably under a wide range of conditions. In this section, robustness of the SPOC against intrinsic noise and changes of the key kinetic parameter is evaluated.

4.3.6.1 Robustness to Perturbations of the GDP-Dissociation Rate

The ability of the SPOC models to regulate Tem1 activity is largely dependent on the GDP-dissociation rate coefficient of Tem1 (see chapter 3). To assess the robust-

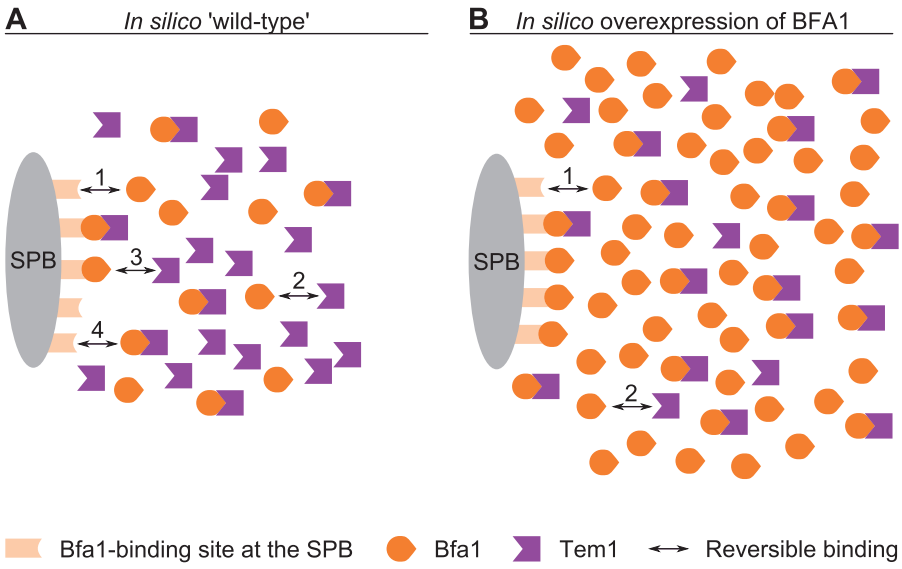

Figure 4.8: Effect of Bfa1-overexpression on Tem1 association with the SPB. (**A**) In the wild-type, the number Tem1 molecules exceeds the number of Bfa1 molecules, such that reactions (1-4) can frequently occur. In particular, Tem1 can bind to the SPB via two parallel pathways. On one hand, Bfa1 might bind to the SPB first (Reaction 1) and provide an anchor at the SPB to which Tem1 can subsequently bind (Reaction 3). On the other hand, Bfa1 and Tem1 might form a complex in the cytosol (Reaction 2) which then binds to the SPB via Bfa1 (Reaction 4). (**B**) In contrast, Bfa1 overexpression creates a situation where most free Tem1 is already bound to Bfa1 through reaction (2). In this situation, reaction (3) does rarely occur. Reaction (1) outcompetes reaction (4) if the excess of Bfa1 is high enough such that the ratio of free Bfa1 and Bfa1-Tem1 is high.

ness of the ubiquitous-association and ubiquitous-inactive models to perturbations of the GDP-dissociation rate, the ability of both models to inhibit Tem1 upon spindle misalignment ("relative inhibition") and to activate Tem1 upon spindle realignment ("relative recovery") were examined for a range of GDP-dissociation rate coefficients (Figure 4.9; see section 4.2.5 for details). In terms of relative inhibition, both models behave similarly and require a low GDP-dissociation rate coefficient to allow inhibition of Tem1 below the levels sufficient for MEN activation (Figure 4.9A, red curves). In contrast, GDP-release must be significantly faster in the ubiquitous-association model to reach the same relative recovery as the ubiquitous-inactive model (Figure 4.9A, green curves). SPOC can only work reliably if both inhibition and recovery are sufficient. Thus, relative inhibition and recovery were combined into the "quality

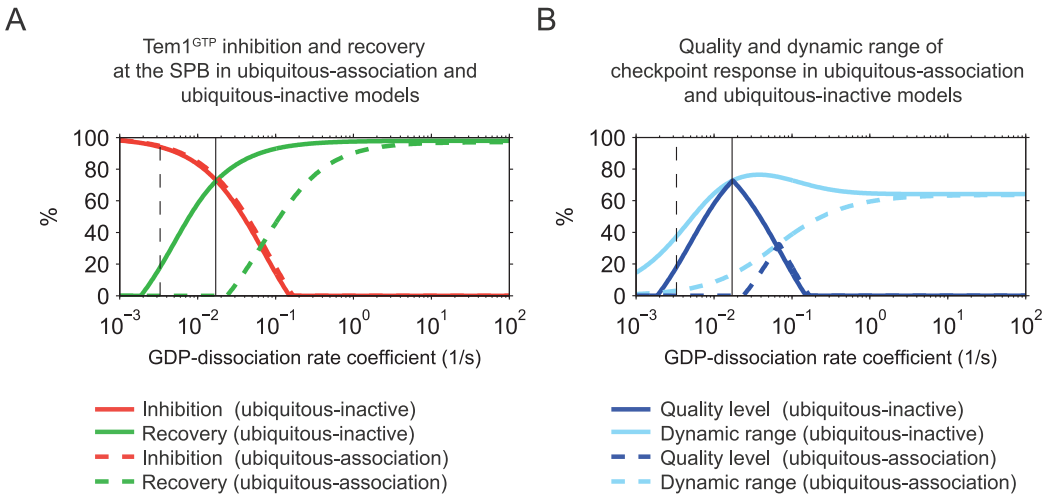

Figure 4.9: Scan of the GDP-dissociation rate coefficient. *Figure adapted from (Caydasi et al., 2012).* Comparison of 'ubiquitous-association' (solid curves) and 'ubiquitous-inactive' (dashed curves) models with respect to the regulation of $\mathrm{Tem1}^{\mathrm{GTP}}$ at the SPB as a function of the GDP-dissociation rate coefficient. The GDP-dissociation rate coefficient was scanned in the range from 0.001 to 100 s^{-1}, assuming a fold-acceleration by the GAP of $\lambda = 10^3$ (see Materials and methods). For each parameter value, both models were simulated and the respective levels of $\mathrm{Tem1}^{\mathrm{GTP}}$ were recorded at time points $t = 30$ min and $t = 40$ min (i.e., 30 min after SPOC activation and 10 min after subsequent spindle realignment). From these data, relative inhibition (red) and recovery (green) of Tem1, quality level (dark blue) and dynamic range of the checkpoint response (light blue) were computed. Vertical lines indicate the one-fold (dashed) and five-fold (solid) of the GDP-dissociation rate constant measured by (Geymonat *et al.*, 2002). Refer to the main text for details. (**A**) Relative inhibition and recovery of Tem1 as percentage of the theoretical limit. (**B**) Quality level and dynamic range as percentage of the theoretical limit.

level", which is zero if at least one of the two criteria (relative inhibition and recovery) is not satisfied. The quality level can only be high if both, relative inhibition and recovery, are high. Importantly, the quality level of the ubiquitous-inactive model is higher and covers considerably wider range of GDP-dissociation rates than the ubiquitous-association model (Figure 4.9B, dark blue curves).

For robust checkpoint response, a clear distinction between the checkpoint active and inactive states is desirable. As a measure of robustness, the "dynamic range" of the checkpoint response was calculated (Figure 4.9B, light blue curves). The dynamic range shows how distinct the SPOC active and inactive states are

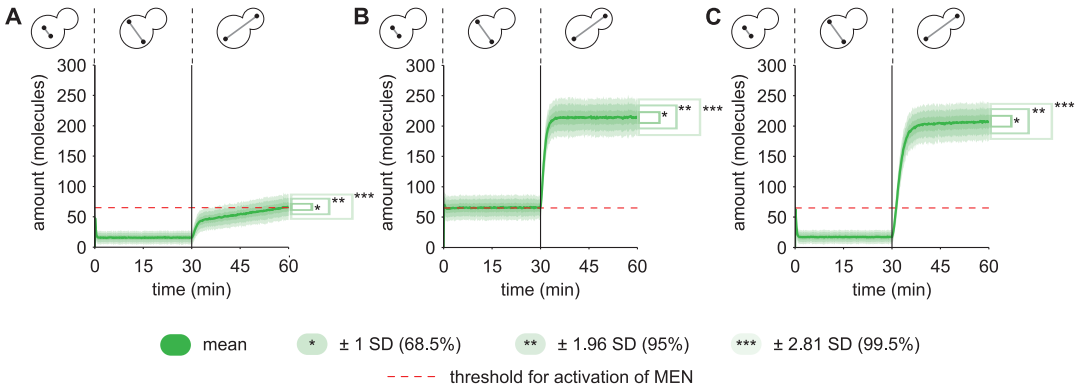

Figure 4.10: Stochastic simulations. *Figure adapted from Caydasi et al. (2012).* Tem1^{GTP} at the SPB from stochastic simulations of the ubiquitous-association (**A**), hot-spot-association (**B**), and ubiquitous-inactive (**C**) models with the same parameters as in Figure 4.5. Mean and 1 (*), 1.96 (**), and 2.81 (***) standard deviations (corresponding to 68.5%, 95%, and 99.5% of simulations within the indicated bounds) of ensembles of 200 individual stochastic simulations were indicated. Horizontal line indicates the number of active Tem1 molecules at the SPB sufficient for MEN activation.

in terms of SPB-bound amounts of active Tem1. Interestingly, the dynamic range of the ubiquitous-inactive model is identical or higher than the dynamic range of the ubiquitous-association model for all parameter values scanned. The maximum dynamic range of the ubiquitous-inactive model is reached near the maximal quality level of this model. In contrast, the maximum quality level of the ubiquitous-association model lies in a region of only moderate dynamic range. Importantly, quality level of the ubiquitous-inactive model is maximal for GDP-dissociation rate coefficients close to the estimated nominal value of 0.017 s^{-1} (vertical solid lines in Figure 4.9). Collectively, these measures show that the ubiquitous-inactive model is more robust against perturbations of the Tem1 GDP-dissociation rate.

4.3.6.2 Stochastic Simulation of the SPOC Models

Because of the discrete and stochastic nature of chemical reactions, considerable intrinsic noise can be present if the molecule numbers are low. Thus, a discrete stochastic simulation method (D. T. Gillespie, 1976) was employed to assess the robustness of the checkpoint response with respect to intrinsic noise (see section 4.2.4). The states of 200 trajectories were read out and averaged in regular intervals. For

each interval, the standard deviation was computed and served as a measure for assessing the likelihood of individual trajectories crossing the $Tem1^{GTP}$ threshold at the SPB. Averages of trajectories resulting from simulations of the chemical master equation (CME) do not necessarily match with deterministic reaction rate equations (RRE), because the RRE-solutions approximate the mode of the CME-state distribution rather than its mean (Samoilov *et al.*, 2006). However, for the SPOC model, averages did match the RRE-solutions closely, indicating that the statistics of the relevant quantities can be considered representative of the stochastic variations. All three model variants were simulated starting from an early anaphase state with a misaligned spindle for an arbitrarily chosen period of 60 minutes. After 30 minutes of simulated time, the spindle was assumed to align properly. The results underline the results of the deterministic simulations. The ubiquitous-association model establishes reliable inhibition of MEN, but would fail to deactivate the SPOC timely in the majority of simulations (Figure 4.10A). The hot-spot-association model is generally not capable of MEN-inhibition but does rapidly recover $Tem1^{GTP}$ (Figure 4.10B). Finally, the ubiquitous-inactive model variant combines reliable inhibition with rapid checkpoint deactivation (Figure 4.10C).

4.4 Discussion

Spatial and temporal control of mitotic exit in budding yeast requires elaborate regulatory mechanisms involving differential phosphorylation and binding to subcellular compartments. The inherent complexity of those mechanisms motivated several mathematical models which aimed at understanding of how the various components work together, but regulation of Tem1 activity is considered only crudely (K. C. Chen *et al.*, 2004; Hancioglu *et al.*, 2012; Queralt *et al.*, 2006; Tóth *et al.*, 2007). Tem1 constitutes the biochemical interface between SPOC and MEN, so regulation of Tem1 activity, in particular at the SPBs, is key to understanding delay of mitotic exit in response to spindle misalignment. The dynamical model presented in the course of this chapter is focused on the regulation of Tem1 activity through the GAP-complex Bfa1:Bub2. This model is the first comprehensive model of the SPOC core mechanism and closes the gap to the existing models by rationalizing regulation of Tem1 activity.

To put the model on a quantitatively solid foundation, the molecule numbers of Bfa1, Bub2 and Tem1 proteins at the SPBs and in the cytosol were estimated by a comparative fluorescence microscopy approach (Caydasi *et al.*, 2012). Taking con-

straints imposed by previously collected data on Bfa1, Bub2 and Tem1 binding kinetics (Caydasi *et al.*, 2009; Molk *et al.*, 2004) into account, reasonable binding parameters could be determined.

Investigation of Tem1 activity *in vivo* is hampered by the lack of a tool to discriminate between its GTP- and GDP-bound states. In *Schizosaccharomyces pombe*, antibodies binding preferentially to the GDP-bound form of the Tem1-homolog Spg1 allowed monitoring of inactive Spg1 during mitotic exit *in vivo* (Sohrmann *et al.*, 1998), whereas no adequate method has been established to differentiate between active and inactive Tem1 in budding yeast (Caydasi *et al.*, 2012). To position the dynamical model as a reasonable substitute for *in vivo* analysis, the intrinsic GTPase-cycle of Tem1 was integrated into the dynamical model with great care.

Together, the SPOC model captures the observed localization dynamics of Bfa1 and Tem1 and further enables analysis of the ratio of active and inactive GAP and GTPase amounts at the SPBs and in the cytosol in response to events regulating GAP activity and SPB-binding kinetics.

Combining the theoretical steady state distribution of Tem1 GTP- and GDP-bound states (cf. section 3.2.3) with the estimates of the *in vivo* molecule numbers of SPB-bound Tem1 in absence of Bfa1 and Bub2 indicated that only 65 molecules of SPB-bound Tem1^{GTP} are sufficient for activation of MEN. This threshold also enabled evaluation of model variants with respect to their ability to reversibly delay mitotic exit.

Two important phenomena are predicted by comparison of model variants with respect to their ability to robustly reduce and maintain SPB-bound Tem1^{GTP} below aforementioned threshold when the SPOC is active and the time required for establishing a Tem1^{GTP}-level sufficient for triggering MEN upon SPOC silencing.

First, robust checkpoint arrest is only achieved if Tem1 inhibition takes place in the cytoplasm and at the SPBs. This is a consequence of the Tem1 pool that binds to the SPBs in a GAP-independent manner. This pool cannot be inhibited by the GAP if the association of the GAP and GTPase is restricted to the SPBs (Figure 4.11A). However, Tem1 binds to the GAP-independent binding site with sufficiently fast binding dynamics to efficiently exchange between the cytosolic and the SPB associated pools (Caydasi *et al.*, 2009). Thus, the distribution of GTP- and GDP-bound states of Tem1 is essentially the same in the cytoplasm and at the GAP-independent binding sites at the SPB. Consequently, if cytosolic association of Tem1 with its GAP were allowed, regulation of Tem1 activity in the cytosol were directly translated to regulation of Tem1 activity at the GAP-independent binding

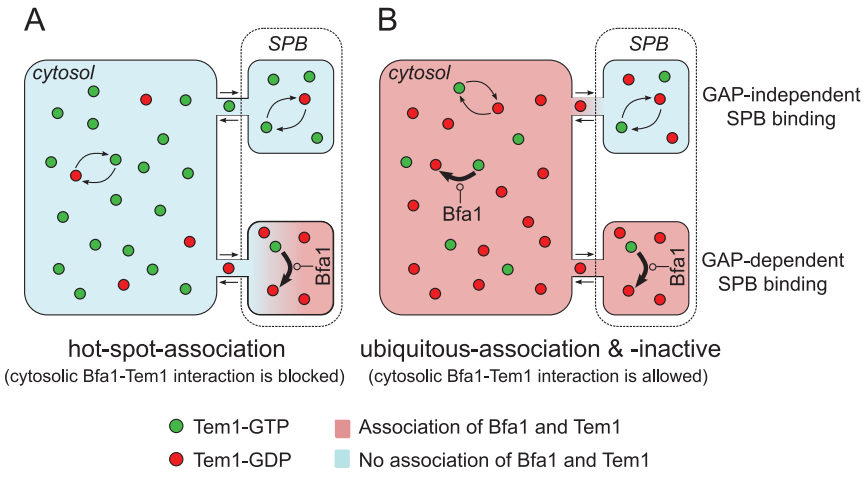

Figure 4.11: Regulation of SPB-bound Tem1 through cytoplasmic Bfa1-Tem1-interactions. *Figure from Caydasi et al. (2012).* Tem1 inhibition in the cytoplasm improves Tem1 inhibition at the SPB. Tem1 undergoes an intrinsic GTPase-cycle (bent arrows), resulting in a balance between Tem1 active (Tem1GTP) and inactive (Tem1GDP) states. The active GAP complex Bfa1Bub2 binds to Tem1 and shifts the balance effectively towards Tem1GDP. Tem1-association with the SPB can be compared with a vessel (cytosol) with two chambers connected by a narrow tube. The chambers represent the GAP-dependent (bottom) and GAP-independent (top) Tem1 pools. If association of Bfa1 and Tem1 is spatially restricted to the bottom chamber like in the hot-spot-association model (A), the balance is affected only locally due to the narrow passage to the cytosol. Because Bfa1 does not affect Tem1 in the top chamber, the balance there is the same as in the cytosol. If Bfa1 can additionally associate with Tem1 in the cytosol, which is the situation in the ubiquitous-association and ubiquitous-inactive models (B), the balance in the cytosol is affected, too. Because the inflow into this chamber is then dominated by inactive Tem1, the concentration in the small chamber shifts towards inactive Tem1 despite the absence of the GAP complex. The outflow of active Tem1 in turn hardly affects the cytosol due to the huge difference of the volumes.

site at the SPBs (Figure 4.11B). In fact, cytoplasmic interaction of Bfa1 and Tem1 was supported by an *in vivo* experiment where high cellular levels of Bfa1 kept Tem1 away from the SPBs as predicted by the model.

Second, for rapid activation of MEN upon spindle re-alignment *in silico*, Bfa1 must be inactivated quickly at the SPB and in the cytosol. Considering that deactivation of Bfa1 through phosphorylation by Cdc5 takes place only at the SPB (Maekawa *et al.*, 2007), it is clear that phosphorylation of the cytosolic pool is limited by the

turnover-rate of Bfa1 at the SPB (Caydasi *et al.*, 2009). Unphosphorylated Bfa1, if active, would continue to down-regulate Tem1 activity in the cytosol even after spindle re-alignment and therefore prevent mitotic exit. *In silico*, deactivation of the cytosolic pool of Bfa1 by Cdc5 is too slow to enable sufficiently fast recovery of $Tem1^{GTP}$ at the SPB, even though the phosphatase counteracting Cdc5 was shut off immediately after spindle re-alignment. According to previous reports the Bfa1-11A mutant, which cannot be phosphorylated by Cdc5 (Hu *et al.*, 2001), is sufficient to provide SPOC arrest even in the absence of Kin4 (Pereira *et al.*, 2005). This suggests that unphosphorylated Bfa1 is active if the spindle is misaligned. However, the same mutant does not promote a mitotic arrest if the anaphase spindle is normally aligned; implying that unphosphorylated Bfa1 is not fully active in this case (Hu *et al.*, 2001). Thus, GAP complexes containing unphosphorylated Bfa1 need to be inactivated efficiently whenever correct spindle alignment is achieved. The mechanisms which achieve this proposed inhibition of Bfa1 upon spindle re-alignment remain to be identified, though. Evidence exists that the bud cortex associated Cdc42-effector Gic1 inhibits the interaction of Bfa1:Bub2 with Tem1 and promotes mitotic exit (Höfken *et al.*, 2004). Interestingly, Gic1 is released from the bud cortex into the cytoplasm when the dSPB enters the bud, and tethering Gic1 to the bud cortex prevents its ability to promote mitotic exit (Höfken *et al.*, 2004). Furthermore, Gic1 becomes essential in cells expressing temperature sensitive cdc5-10 mutants at the restrictive temperature (Höfken *et al.*, 2004). ΔGIC1 ΔGIC2 deletion mutants did not show a prominent phenotype on its own (Höfken *et al.*, 2004), thus Gic1 might serve as a backup mechanism for Bfa1:Bub2-inhibition if phosphorylation of Bfa1 by Cdc5 cannot be achieved sufficiently fast. Gic1 is therefore an appealing candidate for inhibition of Bfa1:Bub2 GAP activity towards Tem1 by preventing GAPGTPase interaction upon dSPB entrance into the bud. Alternatively, additional regulation might be at the level of Bub2 as it is also subject to phosphorylation (Hu *et al.*, 2002).

SPB localization of $Tem1^{GTP}$ is essential for mitotic exit (Monje-Casas *et al.*, 2009; Valerio-Santiago *et al.*, 2011). Furthermore, Cdc5 inhibits GAP-activity of SPB-bound Bfa1:Bub2 through phosphorylation, such that active Tem1 binding to SPB-bound Bfa1:Bub2 will likely remain active. Thus, reduction of the Bfa1:Bub2 amount at the SPBs is an important response to spindle misalignment (Caydasi *et al.*, 2009), because it prevents accumulation of active Tem1 beyond the level dictated by the GAP-independent binding site if the cytoplasmic concentration of $Tem1^{GTP}$ is still high. However, the level of Tem1 binding to the SPB independently of the GAP-

complex is so high that cytosolic control of Tem1-activity and thus cytosolic control of Bfa1:Bub2-activity is kinetically indispensable to shift the equilibrium of SPB-bound Tem1 towards the inactive GDP-bound state.

SPOC might translate the information about spindle orientation into Bfa1:Bub2 activity, which can be considered a "WAIT"-signal propagating throughout the cytosol. This mechanism might be analogous to the spindle assembly checkpoint (SAC; reviewed in Musacchio *et al.*, 2007), which senses spindle attachment at individual kinetochores and broadcasts a nucleoplasmic WAIT-signal from unattached kinetochores until proper bipolar attachment to the spindle is established. Modeling of SAC helped to pinpoint advantages and problems of putative regulatory mechanisms (J. Chen *et al.*, 2014; Doncic *et al.*, 2005, 2006; Ibrahim *et al.*, 2008; Mistry *et al.*, 2008; Sear *et al.*, 2006; Simonetta *et al.*, 2009). Similarly, mathematical modeling of SPOC can serve as a basis to integrate future findings and evaluate novel hypothesis related to checkpoint architecture and regulation.

5 Conclusion

5.1 Summary

The eukaryotic cell cycle is a highly complex dynamical system which robustly coordinates order, timing, and completion of many interlinked processes. The underlying mechanisms communicate through biochemical signal transduction networks, which integrate, amplify, or attenuate signals in response to various inputs. Signal transduction networks do often involve feedback mechanisms and hence resemble closed-loop control systems. In simple cases, a keen mind might be able to deduce the logic behind their functioning from network topology. Signaling, however, is also about temporal dynamics of the system state. Even simple networks can exhibit significant nonlinear behavior, which often eludes intuition for all but the most divine minds. Mathematical modeling can add substance to our intuitive understanding of biochemical networks, even if they comprise many different molecular species and interactions. There are many different approaches to choose from, each with its particular advantages and shortcomings. Qualitative approaches can help to understand the topology of a network, particularly if the number of different components is large. Quantitative models promote comprehension of the dynamic properties of a signaling pathway, but the level of detail can vary greatly, even within the very same model. Avoiding the pitfalls associated with choosing and integrating the right degree of abstraction for each component is a delicate task. Particular attention must be paid to preserve the features which lead to a desired emergent property – it is easy to create

a model of an oscillatory system by a sum of sinusoids, but even though this might mimic the original system perfectly, it would not elucidate its underlying mechanisms. In this thesis, I developed quantitative models of the core mechanisms of SAC and SPOC. Both checkpoints are intricate signaling cascades coupling the physiological state of the mitotic spindle with cell cycle progression. Their core mechanisms appear to be simple at first glance because only a handful of components interact, but significant complexity is added by dynamic localization to subcellular structures, multi-state-components, and the reversible formation of protein complexes thereof. Despite the superficial similarity of SAC and SPOC with respect to their role in cell cycle regulation, the scope of the models was quite different, though. The analysis of the SAC core mechanism focused on the kinetic consequences of dynamic subcellular localization and limiting effects through finite numbers of binding sites. In turn, the SPOC model was designed specifically to enable *in silico*-analysis of the regulation of Tem1-activity. To this end I elaborated a minimal but nevertheless physically sound model of the Tem1-GTPase-cycle, which was then integrated into the regulatory framework of SPOC. As a side note, the model of the GTPase-cycle is very general and can be adapted to other small GTPases with minimal effort. The SPOC model made it eventually possible to draw important, non-trivial conclusions about the mode of operation of SPOC *in vivo*.

5.2 Spatial organization of mitotic signal transduction networks

Regulation of cell cycle progression by SAC and SPOC involves a high degree of localized information processing. Specific sites integrate information about the physiological state of the spindle locally into their respective regulatory networks, which cause biochemical responses also at distal sites of the cell. Localization might be necessary to guarantee specificity of the biochemical signal flow (Good *et al.*, 2011). Tethering of signaling molecules to a scaffold can impede signal amplification because the cascaded components are present in stoichiometric amounts (Good *et al.*, 2011; Heinrich *et al.*, 2002), however. In SPOC and SAC signaling this situation is complicated by the particular nature of the signal integration sites. Not only are kinetochores and centrosomes particularly small assemblies with only several 100nm in diameter, their abundance is also low. In the extreme case, only a single unattached kinetochore must suffice to maintain the cell cycle arrest. Thus it is interesting to ask how SAC and SPOC propagate their signals reliably from the site of information

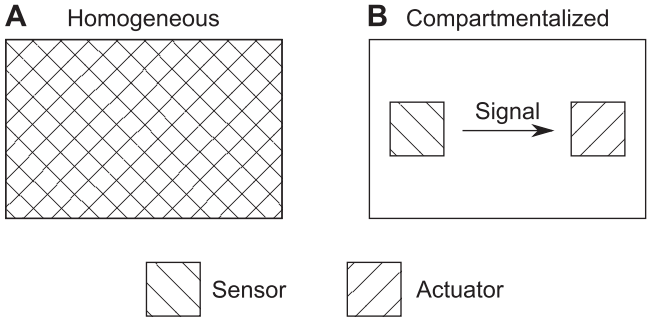

Figure 5.1: Compartmentalization in biochemical signal transduction networks. The most general biochemical signal transduction cascade consists of a sensor which is activated through the presence of an external stimulus, and an actuator whose activity depends on the activity of the sensor. (**A**) In a spatially homogeneous system, sensor and actuator molecules are evenly distributed throughout the reactor volume. Sensor molecules can directly activate actuator molecules or might even be identical to them. (**B**) A compartmentalized signaling system separates sensor and actuator molecules spatially, so activation of the actuator requires translocation of a signaling molecule from the sensor compartment to the actuator compartment.

integration to their respective sites of actuation.

Spatial separation of sensors and actuators in biochemical networks has non-trivial consequences. When compared to the assumption of a well stirred signaling system (Figure 5.1A), spatial separation imposes several constraints on the signaling networks. Most obvious is the need for a signaling molecule which translocates from the sensor to the actuator (Figure 5.1B). More subtle is the rate limiting effect of binding kinetics of the signaling molecule to sensor or actuator. The first limits the signal accumulation rate while the latter limits efficiency of actuator activation. Those potential limitations have been overlooked in most models of cell cycle regulation, and it would be interesting to know to which extend their integration would change model dynamics.

Goldbeter *et al.* (1981) analyzed reversible activation of a substrate through covalent modification by two antagonistic converting enzymes, so-called push-pull networks. This regulatory pattern is prevalent in cell cycle regulation, which builds largely on phosphorylation and dephosphorylation. Goldbeter *et al.* coined the term zeroth-order ultrasensitivity for the effect that steady state activity of the substrate can switch from none to full through only a slight change in the effectiveness of one of the enzymes, provided that both enzymes are virtually saturated. Many

cell cycle models employed zeroth-order ultrasensitivity to simplify regulatory interactions (K. C. Chen *et al.*, 2004; Goldbeter, 1991; Tóth *et al.*, 2007). However, spatial separation of the antagonistic enzymes can significantly alter the switch like dynamics, particularly at lower diffusion rates (Albada *et al.*, 2007). Furthermore, micro-compartments like kinetochores or centrosomes can accumulate extremely high concentrations of signaling proteins. However, due to their tiny volumes, the respective molecule numbers can be low. In budding yeast, for instance, kinetochores or centrosomes bind only a very limited number of individual proteins, at most a few hundred in most cases. In such a situation, sensitivity and accuracy of the response to changes in the efficiencies of the converting enzymes can be considerably reduced (Berg *et al.*, 2000).

Finally there are considerable differences between membrane-bound compartments and scaffold-based, open micro-compartments like kinetochores or centrosomes. Generally there is no uncontrolled exchange of matter between topologically adjacent membrane-bound compartments. Instead, flow of matter is tightly regulated by pore complexes or active transport mechanisms. Thus, reactions can proceed in a protected biochemical environment which may differ vastly from its surroundings. Reactions in open micro-compartments, in turn, are immediately affected by all changes to the embedding environment. A particularly important difference is that the biochemical composition within a membrane-bound compartment can be held constant by active transport. In contrast, concentration changes through reactions restricted to micro-compartments do directly feed back, and reactions affecting binding affinities of proteins and the micro-compartment's scaffold can dramatically and rapidly affect the composition and function of the whole micro-compartment.

Taken together, I am convinced that thorough understanding of intracellular signaling, and signal-processing through networks like SAC and SPOC in particular, can only be achieved if the spatio-temporal arrangement of the underlying mechanisms is considered properly.

5.3 Combinatorial complexity in modeling SPOC

Formation of protein complexes is a ubiquitous mechanism in biochemical signal transduction networks, which, together with post-translational modification of the individual subunits, leads to an exponential number of possible states for each individual macromolecular species (Hlavacek *et al.*, 2003; Weng *et al.*, 1999). Many proteins are constructed in a modular fashion from functionally independent do-

mains, suggesting that a natural description of the interactions in biochemical networks considers individual domains rather than individual molecules (Hlavacek *et al.*, 2003). Assuming that reaction kinetics depend largely upon the participating domains and are independent from the states of the whole proteins, rules can be formulated from which the complete set of kinetic equations can be automatically constructed (Hlavacek *et al.*, 2003, 2006). This rule-based approach sounds promising for formulating the SPOC network with few simple rules which cover the multiple combinations of Bfa1, Bub2, Tem1, and their binding sites at the SPBs. In fact, such a model would be appealing because its canonical form would facilitate analysis and enable integration of further network components with low effort. Why was this approach apparently ignored? Unfortunately, the kinetic coefficients of most reactions appear to be dependent on the particular states of the whole reactant proteins such that they cannot be modeled independently from one another (e.g., dissociation rates of Bfa1 from the SPB binding site Caydasi *et al.*, 2009). This is not necessarily a contradiction to the modular paradigm of protein structure, it might merely point out that not sufficient molecular detail is known on the considered interactions. However, a rule-set representing the SPOC network with sufficient kinetic detail to observe the measured protein levels would require a specialized rule for most reactions, rendering the rule-based approach pointless.

In my opinion, rule-based modeling is a useful approach for systems with high combinatorial complexity, provided that the independent domains have been identified. If proteins with uncertain secondary structure must be modeled, this approach might result in severe oversimplification and unnoticed distortion of the results, though. In simple cases, this limitation might be overcome by substituting an ansatz interpolating between defined rate coefficients for the constant rate coefficient in reaction rules. I presume that such an approach could be particularly useful to apply rule-based modeling to highly cooperative systems, for instance if multiple phosphorylation gradually alters the affinity of proteins for one another. With respect to modeling SPOC, this might help to analyze how hyperphosphorylation of Bfa1 by Cdc5 affects the stability of its complexes with Bub2 and Tem1 (cf. Hu *et al.*, 2001, and Geymonat *et al.*, 2003).

5.4 Outlook

5.4.1 Modeling of the SAC

In the SAC models presented in chapter 2, particular attention was paid to the kinetics of protein association with the kinetochores and it turned out that binding kinetics and stoichiometry can dramatically affect checkpoint function. This notion is supported by a recent model of the SAC which considers stripping off SAC constituents upon microtubule attachment (J. Chen *et al.*, 2014). The model suggested that regulation of kinetochore-binding kinetics is crucial for reliable checkpoint activity. However, the model focused on contribution of the spindle to signaling, incorporating only a very abstract model of the SAC biochemistry. Future work should aim to integrate this model with the most comprehensive available model of the SAC biochemistry (Ibrahim *et al.*, 2009) in a way ensuring that the resulting model is kinetically sound. As a further extension, the model geometry should be made dynamic and integrated with a biophysically viable model of the spindle apparatus (Nedelec *et al.*, 2007; Wollman *et al.*, 2005). Such an integrative model could constitute a virtual wet-lab suitable for guiding further research to reveal the detailed mechanism behind SAC regulation.

5.4.2 Modeling of the SPOC

A particular challenge in the development of the first dynamical model of the molecular mechanism underlying SPOC function (chapter 4) was the scarcity of available kinetic data. Only Bfa1 and Tem1 binding to the SPB have been characterized in sufficient detail to constrain model kinetics (Caydasi *et al.*, 2009; Molk *et al.*, 2004). This is one of the main reasons behind the model-assumption that Bfa1 and Bub2 form a persistent complex. However, the dynamics of Bfa1-Bub2 complex formation might be crucial for the regulation of GAP-activity (Geymonat *et al.*, 2003; Hu *et al.*, 2001). Furthermore, Bfa1 bound to Tem1 in absence of Bub2 might prevent GTP-dissociation and hydrolysis (Geymonat *et al.*, 2002). A consequent extension of the SPOC model should consider the Bfa1-Bub2-interaction explicitly to explore potential roles of this particularity of Bfa1. Additional efforts should be made to integrate possible regulatory mechanisms for SPB-binding dynamics of Bfa1 to model cell-cycle-dependent effects properly. Bmh1 has been found to convert Kin4-activity into increased Bfa1-mobility at the SPB, likely through constituting a highly dynamic shuttle-mechanism between SPB and cytosol (Caydasi *et al.*, 2014b). This might be a good starting point to develop working hypothesis which can be tested *in vivo*.

However, modeling such detailed binding dynamics is challenging and requires dedicated work in the wet-lab. A preliminary, handcrafted SPOC model with a 4-state Bfa1-binding site and explicit Bfa1-Bub2 interactions consisted of 84 state variables connected by 590 elementary reactions with 75 kinetic parameters. While the overall dynamics could be preserved, it was apparent that the model is pointless without further experimentally determined constraints on the parameter space.

Independent from any model extension it would be interesting to integrate a nondimensionalized version of the current model into the model by K. C. Chen *et al.* (2004). This way, the SPOC model would be challenged to not interfere with the cell cycle engine during normal cell cycle progression but prevent exit from mitosis in case of spindle defects.

Bibliography

Albada, S. B. van and P. R. ten Wolde (2007). "Enzyme localization can drastically affect signal amplification in signal transduction pathways". In: *PLoS Computational Biology* 3.10 (2007), pp. 1925–34.

Aldridge, B. B., J. M. Burke, D. a. Lauffenburger, and P. K. Sorger (2006). "Physicochemical modelling of cell signalling pathways". In: *Nature Cell Biology* 8.11 (2006), pp. 1195–203.

Alexandru, G., W. Zachariae, A. Schleiffer, and K. Nasmyth (1999). "Sister chromatid separation and chromosome re-duplication are regulated by different mechanisms in response to spindle damage." In: *The EMBO Journal* 18.10 (1999), pp. 2707–21.

Amon, A., M. Tyers, B. Futcher, and K. Nasmyth (1993). "Mechanisms that help the yeast cell cycle clock tick: G2 cyclins transcriptionally activate G2 cyclins and repress G1 cyclins". In: *Cell* 74 (1993), pp. 993–1007.

Asakawa, K., S. Yoshida, F. Otake, and A. Toh-E (2001). "A novel functional domain of Cdc15 kinase is required for its interaction with Tem1 GTPase in Saccharomyces cerevisiae". In: *Genetics* 157.4 (2001), pp. 1437–50.

Ashyraliyev, M., Y. Fomekong-Nanfack, J. A. Kaandorp, and J. G. Blom (2009). "Systems biology: parameter estimation for biochemical models". In: *The FEBS Journal* 276.4 (2009), pp. 886–902.

Bardin, A. J. and A. Amon (2001). "Men and sin: what's the difference?" In: *Nature Reviews Molecular Cell Biology* 2.11 (2001), pp. 815–26.

Barik, D., W. T. Baumann, M. R. Paul, B. Novak, and J. J. Tyson (2010). "A model of yeast cell-cycle regulation based on multisite phosphorylation". In: *Molecular Systems Biology* 6 (2010), p. 405.

Berg, O. G. and P. H. von Hippel (1985). "Diffusion-controlled macromolecular interactions". In: *Annual Review of Biophysics & Biophysical Chemistry* 14 (1985), pp. 131–60.

Berg, O. G., J. Paulsson, and M. Ehrenberg (2000). "Fluctuations and quality of control in biological cells: zero-order ultrasensitivity reinvestigated". In: *Biophysical Journal* 79.3 (2000), pp. 1228–36.

Bertazzi, D. T., B. Kurtulmus, and G. Pereira (2011). "The cortical protein Lte1 promotes mitotic exit by inhibiting the spindle position checkpoint kinase Kin4". In: *Journal of Cell Biology* 193.6 (2011), pp. 1033–48.

Blinov, M. L., J. Yang, J. R. Faeder, and W. S. Hlavacek (2006). "Graph Theory for Rule-Based Modeling of Biochemical Networks". In: *Transactions on Computational Systems Biology VII*. Ed. by C. Priami, A. Ingolfsdottir, B. Mishra, and H. R. Nielson. Berlin/Heidelberg: Springer, 2006, pp. 89–106.

Bornholdt, S. (2008). "Boolean network models of cellular regulation: prospects and limitations". In: *Journal of the Royal Society Interface* 5 (2008), S85–94.

Bos, J. L., H. Rehmann, and A. Wittinghofer (2007). "GEFs and GAPs: Critical Elements in the Control of Small G Proteins". In: *Cell* 129 (2007), pp. 865–77.

Bourne, H. R., D. A. Sanders, and F. McCormick (1991). "The GTPase superfamily: conserved structure and molecular mechanism". In: *Nature* 349 (1991).

Branzei, D. and M. Foiani (2008). "Regulation of DNA repair throughout the cell cycle". In: *Nature Reviews Molecular Cell Biology* 9.4 (2008), pp. 297–308.

Bryan, A. K., A. Goranov, A. Amon, and S. R. Manalis (2010). "Measurement of mass, density, and volume during the cell cycle of yeast". In: *Proceedings of the National Academy of Sciences of the United States of America* 107.3 (2010), pp. 999–1004.

Buffin, E., C. Lefebvre, J. Huang, M. E. Gagou, and R. E. Karess (2005). "Recruitment of Mad2 to the kinetochore requires the Rod/Zw10 complex". In: *Current Biology* 15 (2005), pp. 856–61.

Burack, W. R. and A. S. Shaw (2000). "Signal transduction: hanging on a scaffold". In: *Current Opinion in Cell Biology* 12.2 (2000), pp. 211–6.

Cao, Y., D. T. Gillespie, and L. R. Petzold (2007). "Adaptive explicit-implicit tau-leaping method with automatic tau selection". In: *The Journal of Chemical Physics* 126.22 (2007), p. 224101.

Casamayor, A. and M. Snyder (2002). "Bud-site selection and cell polarity in budding yeast". In: *Current Opinion in Microbiology* 5.2 (2002), pp. 179–186.

Caydasi, A. K., B. Ibrahim, and G. Pereira (2010). "Monitoring spindle orientation: Spindle position checkpoint in charge". In: *Cell Division* 5 (2010), p. 28.

Caydasi, A. K., B. Kurtulmus, M. I. L. Orrico, A. Hofmann, B. Ibrahim, and G. Pereira (2010). "Elm1 kinase activates the spindle position checkpoint kinase Kin4". In: *Journal of Cell Biology* 190.6 (2010), pp. 975–89.

Caydasi, A. K., M. Lohel, G. Grünert, P. Dittrich, G. Pereira, and B. Ibrahim (2012). "A dynamical model of the spindle position checkpoint." In: *Molecular systems biology* 8 (2012), p. 582.

Caydasi, A. K., Y. Micoogullari, B. Kurtulmus, S. Palani, and G. Pereira (2014a). "The 14-3-3 protein Bmh1 functions in the spindle position checkpoint by breaking Bfa1 asymmetry at yeast centrosomes". In: *Molecular Bology of the Cell* 25.14 (2014), pp. 2143–51.

— (2014b). "The 14-3-3 protein Bmh1 functions in the spindle position checkpoint by breaking Bfa1 asymmetry at yeast centrosomes". In: *Molecular biology of the cell* 25.14 (2014), pp. 2143–51.

Caydasi, A. K. and G. Pereira (2009). "Spindle alignment regulates the dynamic association of checkpoint proteins with yeast spindle pole bodies". In: *Developmental Cell* 16.1 (2009), pp. 146–56.

Cenamor, R., J. Jimenez, V. J. Cid, C. Nombela, and M. Sanchez (1999). "The budding yeast Cdc15 localizes to the spindle pole body in a cell-cycle-dependent manner". In: *Molecular Cell Biology Research Communications* 2.3 (1999), pp. 178–84.

Chan, L. Y. and A. Amon (2009). "The protein phosphatase 2A functions in the spindle position checkpoint by regulating the checkpoint kinase Kin4". In: *Genes & Development* 23.14 (2009), pp. 1639–49.

Chao, W. C. H., K. Kulkarni, Z. Zhang, E. H. Kong, and D. Barford (2012). "Structure of the mitotic checkpoint complex". In: *Nature* 484 (2012), pp. 208–13.

Chaouiya, C. (2007). "Petri net modelling of biological networks". In: *Briefings in Bioinformatics* 8.4 (2007), pp. 210–9.

Cheeseman, I. M. and A. Desai (2008). "Molecular architecture of the kinetochore-microtubule interface". In: *Nature Reviews Molecular Cell Biology* 9.1 (2008), pp. 33–46.

Chen, J. and J. Liu (2014). "Spatial-temporal model for silencing of the mitotic spindle assembly checkpoint". In: *Nature Communications* 5 (2014), p. 4795.

Chen, K. C., L. Calzone, A. Csikasz-Nagy, F. R. Cross, B. Novak, and J. J. Tyson (2004). "Integrative Analysis of Cell Cycle Control in Budding Yeast". In: *Molecular Biology of the Cell* 15.August (2004), pp. 3841–62.

Chen, K. C., A. Csikasz-Nagy, B. Gyorffy, J. Val, B. Novak, and J. J. Tyson (2000). "Kinetic analysis of a molecular model of the budding yeast cell cycle". In: *Molecular Bology of the Cell* 11.1 (2000), pp. 369–91.

Chen, W. W., M. Niepel, and P. K. Sorger (2010). "Classic and contemporary approaches to modeling biochemical reactions". In: *Genes & Development* 24 (2010), pp. 1861–75.

Ciliberto, A. and J. V. Shah (2009). "A quantitative systems view of the spindle assembly checkpoint". In: *The EMBO journal* 28 (2009), pp. 2162–73.

Cimini, D. and F. Degrassi (2005). "Aneuploidy: a matter of bad connections". In: *Trends in Cell Biology* 15.8 (2005), pp. 442–51.

Coffman, V. C., P. Wu, M. R. Parthun, and J.-Q. Wu (2011). "CENP-A exceeds microtubule attachment sites in centromere clusters of both budding and fission yeast". In: *Journal of Cell Biology* 195.4 (2011), pp. 563–72.

D'Aquino, K. E., F. Monje-Casas, J. Paulson, V. Reiser, G. M. Charles, L. Lai, K. M. Shokat, and A. Amon (2005). "The protein kinase Kin4 inhibits exit from mitosis in response to spindle position defects". In: *Molecular Cell* 19.2 (2005), pp. 223–34.

Daum, J. R., N. Gomez-Ospina, M. Winey, and D. J. Burke (2000). "The spindle checkpoint of Saccharomyces cerevisiae responds to separable microtubule-dependent events". In: *Current Biology* 10 (2000), pp. 1375–1378.

Davidich, M. I. and S. Bornholdt (2008). "Boolean network model predicts cell cycle sequence of fission yeast". In: *PLoS one* 3.2 (2008), e1672.

De Antoni, A. *et al.* (2005). "The Mad1/Mad2 complex as a template for Mad2 activation in the spindle assembly checkpoint". In: *Current Biology* 15.3 (2005), pp. 214–25.

Deribe, Y. L., T. Pawson, and I. Dikic (2010). "Post-translational modifications in signal integration". In: *Nature Structural & Molecular Biology* 17.6 (2010), pp. 666–72.

Desai, A. and T. J. Mitchison (1997). "Microtubule polymerization dynamics". In: *Annual Review of Cell and Developmental Biology* 13 (1997), pp. 83–117.

Di Talia, S., J. M. Skotheim, J. M. Bean, E. D. Siggia, and F. R. Cross (2007). "The effects of molecular noise and size control on variability in the budding yeast cell cycle". In: *Nature* 448.7156 (2007), pp. 947–51.

Di Ventura, B., C. Lemerle, K. Michalodimitrakis, and L. Serrano (2006). "From in vivo to in silico biology and back". In: *Nature* 443 (2006), pp. 527–33.

Díaz-Martínez, L. a. and H. Yu (2007). "Running on a treadmill: dynamic inhibition of APC/C by the spindle checkpoint". In: *Cell division* 2 (2007), p. 23.

Dirick, L., T. Böhm, and K. Nasmyth (1995). "Roles and regulation of Cln-Cdc28 kinases at the start of the cell cycle of Saccharomyces cerevisiae". In: *The EMBO journal* 14.19 (1995), pp. 4803–13.

Doncic, A., E. Ben-Jacob, and N. Barkai (2005). "Evaluating putative mechanisms of the mitotic spindle checkpoint". In: *Proceedings of the National Academy of Sciences of the United States of America* 102.18 (2005), pp. 6332–7.

— (2006). "Noise resistance in the spindle assembly checkpoint". In: *Molecular Systems Biology* (2006), p. 2006.0027.

Doncic, A., E. Ben-Jacob, S. Einav, and N. Barkai (2009). "Reverse engineering of the spindle assembly checkpoint". In: *PLoS one* 4.8 (2009), e6495.

Enserink, J. M. and R. D. Kolodner (2010). "An overview of Cdk1-controlled targets and processes". In: *Cell Division* 5 (2010), p. 11.

Evans, T., E. T. Rosenthal, J. Youngblom, D. Distel, and T. Hunt (1983). "Cyclin: a protein specified by maternal mRNA in sea urchin eggs that is destroyed at each cleavage division". In: *Cell* 33.2 (1983), pp. 389–96.

Falk, J. E., L. Y. Chan, and A. Amon (2011). "Lte1 promotes mitotic exit by controlling the localization of the spindle position checkpoint kinase Kin4". In: *Proceedings of the National Academy of Sciences of the United States of America* 108.31 (2011), pp. 12584–90.

Faure, A., A. Naldi, F. Lopez, C. Chaouiya, A. Ciliberto, and D. Thieffry (2009). "Modular logical modelling of the budding yeast cell cycle". In: *Molecular BioSystems* 5 (2009), pp. 1787–96.

Ferrell, J. E. (2000). "What do scaffold proteins really do?" In: *Science's STKE* 2000.52 (2000), pe1.

Ferrell, J. E., T. Y.-C. Tsai, and Q. Yang (2011). "Modeling the cell cycle: why do certain circuits oscillate?" In: *Cell* 144 (2011), pp. 874–85.

Fesquet, D., P. J. Fitzpatrick, A. L. Johnson, K. M. Kramer, J. H. Toyn, and L. H. Johnston (1999). "A Bub2p-dependent spindle checkpoint pathway regulates the Dbf2p kinase in budding yeast". In: *EMBO Journal* 18.9 (1999), pp. 2424–34.

Fraschini, R., E. Formenti, G. Lucchini, and S. Piatti (1999). "Budding yeast Bub2 is localized at spindle pole bodies and activates the mitotic checkpoint via a different pathway from Mad2". In: *Journal of Cell Biology* 145.5 (1999), pp. 979–91.

Fraschini, R., M. Venturetti, E. Chiroli, and S. Piatti (2008). "The spindle position checkpoint: how to deal with spindle misalignment during asymmetric cell division in budding yeast." In: *Biochemical Society Transactions* 36.3 (2008), pp. 416–20.

Furge, K. A., K. Wong, J. Armstrong, M. Balasubramanian, and C. F. Albright (1998). "Byr4 and Cdc16 form a two-component GTPase-activating protein for the Spg1 GTPase that controls septation in fission yeast". In: *Current Biology* 8.17 (1998), pp. 947–54.

Gadde, S. and R. Heald (2004). "Mechanisms and molecules of the mitotic spindle". In: *Current Biology* 14 (2004), R797–805.

Gentry, M. S. and R. L. Hallberg (2002). "Localization of Saccharomyces cerevisiae Protein Phosphatase 2A Subunits throughout Mitotic Cell Cycle". In: 13.October (2002), pp. 3477–92.

Georgatos, S. D., A. Pyrpasopoulou, and P. A. Theodoropoulos (1997). "Nuclear envelope breakdown in mammalian cells involves stepwise lamina disassembly and microtubule-drive deformation of the nuclear membrane". In: *Journal of Cell Science* 110 (1997), pp. 2129–40.

Geymonat, M., A. Spanos, S. J. M. Smith, E. Wheatley, K. Rittinger, L. H. Johnston, and S. G. Sedgwick (2002). "Control of mitotic exit in budding yeast. In vitro regulation of Tem1 GTPase by Bub2 and Bfa1". In: *Journal of Biological Chemistry* 277.32 (2002), pp. 28439–28445.

Geymonat, M., A. Spanos, P. A. Walker, L. H. Johnston, and S. G. Sedgwick (2003). "In vitro regulation of budding yeast Bfa1/Bub2 GAP activity by Cdc5". In: *Journal of Biological Chemistry* 278.17 (2003), pp. 14591–4.

Geymonat, M., A. Spanos, G. de Bettignies, and S. G. Sedgwick (2009). "Lte1 contributes to Bfa1 localization rather than stimulating nucleotide exchange by Tem1". In: *Journal of Cell Biology* 187.4 (2009), pp. 497–511.

Geymonat, M., A. Spanos, S. Jensen, and S. G. Sedgwick (2010). "Phosphorylation of Lte1 by Cdk prevents polarized growth during mitotic arrest in S. cerevisiae". In: *Journal of Cell Biology* 191.6 (2010), pp. 1097–112.

Ghaemmaghami, S., W.-K. Huh, K. Bower, R. W. Howson, A. Belle, N. Dephoure, E. K. O'Shea, and J. S. Weissman (2003). "Global analysis of protein expression in yeast". In: *Nature* 425.6959 (2003), pp. 737–41.

Gideon, P., J. John, M. Frech, A. Lautwein, R. Clark, J. E. Scheffler, and A. Wittinghofer (1992). "Mutational and kinetic analyses of the GTPase-activating pro-

tein (GAP)-p21 interaction: the C-terminal domain of GAP is not sufficient for full activity". In: *Molecular Cell Biology* 12.5 (1992), pp. 2050–6.

Gillespie, D. T. (1976). "A general method for numerically simulating the stochastic time evolution of coupled chemical reactions". In: *Journal of Computational Physics* 22 (1976), pp. 403–34.

— (1992). "A rigorous derivation of the chemical master equation". In: *Physica A: Statistical Mechanics and its Applications* 188 (1992), pp. 404–425.

Gillespie, D. (2000). "The chemical Langevin equation". In: *The Journal of Chemical Physics* 113.1 (2000), pp. 297–306.

— (2001). "Approximate accelerated stochastic simulation of chemically reacting systems". In: *The Journal of Chemical Physics* 115.4 (2001), pp. 1716–1733.

Glaser, R. (2001). *Biophysics*. Berlin/Heidelberg: Springer, 2001.

Goldbeter, A. and D. Koshland (1981). "An amplified sensitivity arising from covalent modification in biological systems". In: *Proceedings of the National Academy of Sciences of the United States of America* 78.11 (1981), pp. 6840–6844.

Goldbeter, A. (1991). "A minimal cascade model for the mitotic oscillator involving cyclin and cdc2 kinase". In: *Proceedings of the National Academy of Sciences of the United States of America* 88 (1991), pp. 9107–11.

Good, M. C., J. G. Zalatan, and W. A. Lim (2011). "Scaffold proteins: hubs for controlling the flow of cellular information". In: *Science* 332 (2011), pp. 680–6.

Gordon, D. J., B. Resio, and D. Pellman (2012). "Causes and consequences of aneuploidy in cancer". In: *Nature Reviews Genetics* 13.3 (2012), pp. 189–203.

Gruneberg, U., K. Campbell, C. Simpson, J. Grindlay, and E. Schiebel (2000). "Nud1p links astral microtubule organization and the control of exit from mitosis." In: *The EMBO journal* 19.23 (2000), pp. 6475–88.

Grünert, G., B. Ibrahim, T. Lenser, M. Lohel, T. Hinze, and P. Dittrich (2010). "Rule-based spatial modeling with diffusing, geometrically constrained molecules." In: *BMC Bioinformatics* 11 (2010), p. 307.

Hancioglu, B. and J. J. Tyson (2012). "A mathematical model of mitotic exit in budding yeast: the role of Polo kinase". In: *PloS one* 7.2 (2012), e30810.

Hardy, S. and P. N. Robillard (2004). "Modeling and simulation of molecular biology systems using petri nets: modeling goals of various approaches". In: *Journal of Bioinformatics and Computational Biology* 2.4 (2004), pp. 619–637.

Haseltine, E. L. and J. B. Rawlings (2002). "Approximate simulation of coupled fast and slow reactions for stochastic chemical kinetics". In: *The Journal of Chemical Physics* 117.15 (2002), p. 6959.

Hattori, S., L. S. Ulsh, K. Halliday, and T. Y. Shih (1985). "Biochemical Properties of a Highly Purified v-rasH p21 Protein Overproduced in Escherichia coli and Inhibition of Its Activities by a Monoclonal Antibody". In: *Molecular and Cellular Biology* 5.6 (1985), pp. 1449–55.

He, E., O. Kapuy, R. a. Oliveira, F. Uhlmann, J. J. Tyson, and B. Novák (2011). "System-level feedbacks make the anaphase switch irreversible". In: *Proceedings of the National Academy of Sciences of the United States of America* 108.24 (2011), pp. 10016–21.

Heinrich, R., B. G. Neel, and T. A. Rapoport (2002). "Mathematical Models of Protein Kinase Signal Transduction". In: *Molecular Cell* 9.5 (2002), pp. 957–970.

Hirano, T. (2000). "Chromosome cohesion, condensation, and separation". In: *Annual Review of Biochemistry* 69 (2000), pp. 115–44.

Hlavacek, W. S., J. R. Faeder, M. L. Blinov, A. S. Perelson, and B. Goldstein (2003). "The complexity of complexes in signal transduction". In: *Biotechnology and Bioengineering* 84.7 (2003), pp. 783–94.

Hlavacek, W. S., J. R. Faeder, M. L. Blinov, R. G. Posner, M. Hucka, and W. Fontana (2006). "Rules for modeling signal-transduction systems". In: *Science's STKE* 2006.344 (2006), re6.

Höfken, T. and E. Schiebel (2004). "Novel regulation of mitotic exit by the Cdc42 effectors Gic1 and Gic2". In: *The Journal of Cell Biology* 164.2 (2004), pp. 219–31.

Holland, A. J. and D. W. Cleveland (2009). "Boveri revisited: chromosomal instability, aneuploidy and tumorigenesis". In: *Nature Reviews Molecular Cell Biology* 10.7 (2009), pp. 478–87.

Holy, T. E. and S. Leibler (1994). "Dynamic instability of microtubules as an efficient way to search in space". In: *Proceedings of the National Academy of Sciences of the United States of America* 91.12 (1994), pp. 5682–5.

Howell, A. S. and D. J. Lew (2012). "Morphogenesis and the Cell Cycle". In: *Genetics* 190 (2012), pp. 51–77.

Howell, B. J., B. F. McEwen, J. C. Canman, D. B. Hoffman, E. M. Farrar, C. L. Rieder, and E. D. Salmon (2001). "Cytoplasmic dynein/dynactin drives kinetochore protein transport to the spindle poles and has a role in mitotic spindle checkpoint inactivation". In: *Journal of Cell Biology* 155.7 (2001), pp. 1159–72.

Hu, F. and S. J. Elledge (2002). "Bub2 is a cell cycle regulated phospho-protein controlled by multiple checkpoints". In: *Cell Cycle* 1.5 (2002), pp. 351–5.

Hu, F., Y. Wang, D. Liu, Y. Li, J. Qin, and S. J. Elledge (2001). "Regulation of the Bub2/Bfa1 GAP complex by Cdc5 and cell cycle checkpoints". In: *Cell* 107.5 (2001), pp. 655–65.

Ibrahim, B., S. Diekmann, E. Schmitt, and P. Dittrich (2008). "In-silico modeling of the mitotic spindle assembly checkpoint." In: *PLoS one* 3.2 (2008), e1555.

Ibrahim, B., P. Dittrich, S. Diekmann, and E. Schmitt (2007). "Stochastic effects in a compartmental model for mitotic checkpoint regulation". In: *Journal of Integrative Bioinformatics* 4.3 (2007), p. 66.

— (2008). "Mad2 binding is not sufficient for complete Cdc20 sequestering in mitotic transition control (an in silico study)". In: *Biophysical Chemistry* 134 (2008), pp. 93–100.

Ibrahim, B., E. Schmitt, P. Dittrich, and S. Diekmann (2009). "In silico study of kinetochore control, amplification, and inhibition effects in MCC assembly". In: *BioSystems* 95 (2009), pp. 35–50.

Ideker, T. E., V. Thorsson, and R. M. Karp (2000). "Discovery of regulatory interactions trough perturbation: inference and experimental design". In: *Pacific Symposium on Biocomputing* 5 (2000), pp. 302–313.

Ideker, T., T. Galitski, and L. Hood (2001). "A New Approach to Decoding Life: Systems Biology". In: *Annual Review of Genomics and Human Genetics* 2 (2001), pp. 343–72.

Ideker, T. and D. Lauffenburger (2003). "Building with a scaffold: emerging strategies for high- to low-level cellular modeling". In: *Trends in Biotechnology* 21.6 (2003), pp. 255–62.

Jaqaman, K. and G. Danuser (2006). "Linking data to models: data regression". In: *Nature Reviews Molecular Cell Biology* 7.11 (2006), pp. 813–9.

Jaspersen, S. L., J. F. Charles, R. L. Tinker-Kulberg, and D. O. Morgan (1998). "A late mitotic regulatory network controlling cyclin destruction in Saccharomyces cerevisiae". In: *Molecular Biology of the Cell* 9.10 (1998), pp. 2803–17.

Jaspersen, S. L. and M. Winey (2004). "The budding yeast spindle pole body: structure, duplication, and function". In: *Annual Review of Cell and Developmental Biology* 20 (2004), pp. 1–28.

Joglekar, A. P., D. C. Bouck, J. N. Molk, K. S. Bloom, and E. D. Salmon (2006). "Molecular architecture of a kinetochore-microtubule attachment site." In: *Nature Cell Biology* 8.6 (2006), pp. 581–585.

Joglekar, A. P., E. D. Salmon, and K. S. Bloom (2008). "Counting kinetochore protein numbers in budding yeast using genetically encoded fluorescent proteins". In: *Methods in Cell Biology* 85 (2008), pp. 127–51.

Jordan, J. D., E. M. Landau, and R. Iyengar (2000). "Signaling networks: the origins of cellular multitasking". In: *Cell* 103 (2000), pp. 193–200.

Kar, S., W. T. Baumann, M. R. Paul, and J. J. Tyson (2009). "Exploring the roles of noise in the eukaryotic cell cycle". In: *Proceedings of the National Academy of Sciences of the United States of America* 106.16 (2009), pp. 6471–6.

Kauffman, S., C. Peterson, B. Samuelsson, and C. Troein (2003). "Random Boolean network models and the yeast transcriptional network". In: *Proceedings of the National Academy of Sciences of the United States of America* 100.25 (2003), pp. 14796–9.

Khodjakov, A. and J. Pines (2010). "Centromere tension: a divisive issue". In: *Nature cell biology* 12.10 (2010), pp. 919–23.

Kholodenko, B. N. (2006). "Cell-signalling dynamics in time and space". In: *Nature Reviews Molecular Cell Biology* 7.3 (2006), pp. 165–76.

King, R. W., J. M. Peters, S. Tugendreich, M. Rolfe, P. Hieter, and M. W. Kirschner (1995). "A 20S complex containing CDC27 and CDC16 catalyzes the mitosis-specific conjugation of ubiquitin to cyclin B". In: *Cell* 81.2 (1995), pp. 279–88.

King, R. W., R. J. Deshaies, J.-M. Peters, and M. W. Kirschner (1996). "How proteolysis drives the cell cycle". In: *Science* 274 (1996), pp. 1652–9.

Kitano, H. (2002). "Computational systems biology". In: *Nature* 420 (2002), pp. 206–10.

Kops, G. J. P. L., B. A. Weaver, and D. W. Cleveland (2005). "On the road to cancer: aneuploidy and the mitotic checkpoint". In: *Nature Reviews Cancer* 5.10 (2005), pp. 773–85.

Kulukian, A., J. S. Han, and D. W. Cleveland (2009). "Unattached kinetochores catalyze production of an anaphase inhibitor that requires a Mad2 template to prime Cdc20 for BubR1 binding". In: *Developmental Cell* 16.1 (2009), pp. 105–17.

Labbé, J.-C., J.-P. Capony, D. Caput, J.-C. Cavadore, J. Derancourt, M. Kaghad, J.-M. Lelias, A. Picard, and M. Dorée (1989). "MPF from starfish oocytes at first meiotic metaphase is a heterodimer containing one molecule of cdc2 and one molecule of cyclin B". In: *The EMBO Journal* 8.10 (1989), pp. 3053–8.

Lawrimore, J., K. S. Bloom, and E. D. Salmon (2011). "Point centromeres contain more than a single centromere-specific Cse4 (CENP-A) nucleosome". In: *The Journal of Cell Biology* 195.4 (2011), pp. 573–82.

Lee, S. E., S. Jensen, L. M. Frenz, A. L. Johnson, D. Fesquet, and L. H. Johnston (2001). "The Bub2-dependent mitotic pathway in yeast acts every cell cycle and regulates cytokinesis". In: *Journal of Cell Science* 114.12 (2001), pp. 2345–54.

Lew, D. J. (2003). "The morphogenesis checkpoint: how yeast cells watch their figures". In: *Current Opinion in Cell Biology* 15 (2003), pp. 648–53.

Li, F., T. Long, Y. Lu, Q. Ouyang, and C. Tang (2004). "The yeast cell-cycle network is robustly designed". In: *Proceedings of the National Academy of Sciences of the United States of America* 101.14 (2004), pp. 4781–6.

Li, R. (1999). "Bifurcation of the mitotic checkpoint pathway in budding yeast". In: *Proceedings of the National Academy of Sciences of the United States of America* 96.9 (1999), pp. 4989–94.

Lohel, M., B. Ibrahim, S. Diekmann, and P. Dittrich (2009). "The role of localization in the operation of the mitotic spindle assembly checkpoint". In: *Cell Cycle* 8.16 (2009), pp. 2650–60.

López-Avilés, S., O. Kapuy, B. Novák, and F. Uhlmann (2009). "Irreversibility of mitotic exit is the consequence of systems-level feedback". In: *Nature* 459 (2009), pp. 592–5.

Luo, X., Z. Tang, G. Xia, K. Wassmann, T. Matsumoto, J. Rizo, and H. Yu (2004). "The Mad2 spindle checkpoint protein has two distinct natively folded states". In: *Nature Structural & Molecular Biology* 11.4 (2004), pp. 338–45.

Maekawa, H., C. Priest, J. Lechner, G. Pereira, and E. Schiebel (2007). "The yeast centrosome translates the positional information of the anaphase spindle into a cell cycle signal". In: *Journal of Cell Biology* 179.3 (2007), pp. 423–36.

Maiato, H., J. DeLuca, E. D. Salmon, and W. C. Earnshaw (2004). "The dynamic kinetochore-microtubule interface". In: *Journal of Cell Science* 117.23 (2004), pp. 5461–77.

Malumbres, M. and M. Barbacid (2005). "Mammalian cyclin-dependent kinases". In: *Trends in Biochemical Sciences* 30.11 (2005), pp. 630–41.

— (2009). "Cell cycle, CDKs and cancer: a changing paradigm". In: *Nature Reviews Cancer* 9.3 (2009), pp. 153–66.

Maresca, T. J. and E. D. Salmon (2010). "Welcome to a new kind of tension: translating kinetochore mechanics into a wait-anaphase signal." In: *Journal of cell science* 123.Pt 6 (2010), pp. 825–35.

Martin, S., Z. Zhang, A. Martino, and J.-L. Faulon (2007). "Boolean dynamics of genetic regulatory networks inferred from microarray time series data". In: *Bioinformatics* 23.7 (2007), pp. 866–74.

MathWorks (2009). *MATLAB*. Natick, Massachusetts, 2009.

McAinsh, A. D., J. D. Tytell, and P. K. Sorger (2003). "Structure, function, and regulation of budding yeast kinetochores". In: *Annual Review of Cell and Developmental Biology* 19 (2003), pp. 519–39.

Mendenhall, M. D. and A. E. Hodge (1998). "Regulation of Cdc28 cyclin-dependent protein kinase activity during the cell cycle of the yeast Saccharomyces cerevisiae". In: *Microbiology and Molecular Biology Reviews* 62.4 (1998), pp. 1191–243.

Mistry, H. B., D. E. MacCallum, R. C. Jackson, M. A. J. Chaplain, and F. A. Davidson (2008). "Modeling the temporal evolution of the spindle assembly checkpoint and role of Aurora B kinase". In: *Proceedings of the National Academy of Sciences of the United States of America* 105.51 (2008), pp. 20215–20.

Molk, J. N., S. C. Schuyler, J. Y. Liu, J. G. Evans, E. D. Salmon, D. Pellman, and K. Bloom (2004). "The differential roles of budding yeast Tem1p, Cdc15p, and Bub2p protein dynamics in mitotic exit". In: *Molecular biology of the cell* 15.4 (2004), pp. 1519–32.

Monje-Casas, F. and A. Amon (2009). "Cell polarity determinants establish asymmetry in MEN signaling". In: *Developmental cell* 16.1 (2009), pp. 132–45.

Moore, J. K. and J. A. Cooper (2010). "Coordinating mitosis with cell polarity: Molecular motors at the cell cortex". In: *Seminars in Cell and Developmental Biology* 21 (2010), pp. 283–9.

Morgan, D. O. (2007). *The Cell Cycle: Principles of Control*. Ed. by E. Lawrence and K. Freeland. Corby, Northants: Oxford University Press, 2007.

Munsky, B. and M. Khammash (2006). "The finite state projection algorithm for the solution of the chemical master equation". In: *The Journal of Chemical Physics* 124 (2006), p. 044104.

Murray, A. W. (1992). "Creative blocks: cell-cycle checkpoints and feedback controls". In: *Nature* 359 (1992), pp. 599–604.

— (1995). "The genetics of cell cycle checkpoints". In: *Current Opinion in Genetics & Development* 5 (1995), pp. 5–11.

— (2004). "Recycling the cell cycle: cyclins revisited". In: *Cell* 116 (2004), pp. 221–34.

Murray, A. W. and M. W. Kirschner (1989). "Dominoes and Clocks: The Union of Two Views of the Cell Cycle". In: *Science* 246.4930 (1989), pp. 614–621.

Musacchio, A. and K. G. Hardwick (2002). "The spindle checkpoint: structural insights into dynamic signalling". In: *Nature Reviews Molecular Cell Biology* 3.10 (2002), pp. 731–41.

Musacchio, A. and E. D. Salmon (2007). "The spindle-assembly checkpoint in space and time". In: *Nature Reviews Molecular Cell Biology* 8.5 (2007), pp. 379–93.

Nedelec, F. and D. Foethke (2007). "Collective Langevin dynamics of flexible cytoskeletal fibers". In: *New Journal of Physics* 9.11 (2007), pp. 427–427.

Nezi, L. and A. Musacchio (2009). "Sister chromatid tension and the spindle assembly checkpoint". In: *Current Opinion in Cell Biology* 21 (2009), pp. 785–95.

Nigg, E. A. (2001). "Mitotic kinases as regulators of cell division and its checkpoints". In: *Nature reviews. Molecular cell biology* 2.1 (2001), pp. 21–32.

Nilsson, J., M. Yekezare, J. Minshull, and J. Pines (2008). "The APC/C maintains the spindle assembly checkpoint by targeting Cdc20 for destruction". In: *Nature Cell Biology* 10.12 (2008), pp. 1411–20.

Norel, R. and Z. Agur (1991). "A model for the adjustment of the mitotic clock by cyclin and MPF levels". In: *Science* 251 (1991), pp. 1076–8.

Novak, B. and J. J. Tyson (1993). "Numerical analysis of a comprehensive model of M-phase control in Xenopus oocyte extracts and intact embryos". In: *Journal of Cell Science* 106 (1993), pp. 1153–68.

— (2008). "Design principles of biochemical oscillators". In: *Nature Reviews Molecular Cell Biology* 9.12 (2008), pp. 981–91.

Novak, B., J. J. Tyson, B. Gyorffy, and A. Csikasz-Nagy (2007). "Irreversible cell-cycle transitions are due to systems-level feedback". In: *Nature Cell Biology* 9.7 (2007), pp. 724–8.

Nurse, P. (1990). "Universal control mechanism regulating onset of M-phase". In: *Nature* 344.4 (1990), pp. 503–7.

Nurse, P., P. Thuriaux, and K. Nasmyth (1976). "Genetic control of the cell division cycle in the fission yeast Schizosaccharomyces pombe". In: *Molecular and General Genetics* 146.2 (1976), pp. 167–78.

O'Connell, C. B. and A. L. Khodjakov (2007). "Cooperative mechanisms of mitotic spindle formation". In: *Journal of Cell Science* 120 (2007), pp. 1717–22.

Pardee, A. B. (1974). "A restriction point for control of normal animal cell proliferation". In: *Proceedings of the National Academy of Sciences of the United States of America* 71.4 (1974), pp. 1286–90.

Park, J.-E., C. J. Park, K. Sakchaisri, T. Karpova, S. Asano, J. McNally, Y. Sunwoo, S.-H. Leem, and K. S. Lee (2004). "Novel functional dissection of the localization-specific roles of budding yeast polo kinase Cdc5p." In: *Molecular and cellular biology* 24.22 (2004), pp. 9873–86.

Pereira, G., T. Hoefken, J. Grindlay, C. Manson, and E. Schiebel (2000). "The Bub2p spindle checkpoint links nuclear migration with mitotic exit". In: *Molecular Cell* 6.1 (2000), pp. 1–10.

Pereira, G., C. Manson, J. Grindlay, and E. Schiebel (2002). "Regulation of the Bfa1p-Bub2p complex at spindle pole bodies by the cell cycle phosphatase Cdc14p". In: *Journal of Cell Biology* 157.3 (2002), pp. 367–79.

Pereira, G. and E. Schiebel (2005). "Kin4 kinase delays mitotic exit in response to spindle alignment defects". In: *Molecular Cell* 19.2 (2005), pp. 209–21.

Pereira, G., T. U. Tanaka, K. Nasmyth, and E. Schiebel (2001). "Modes of spindle pole body inheritance and segregation of the Bfa1p-Bub2p checkpoint protein complex". In: *EMBO Journal* 20.22 (2001), pp. 6359–70.

Pereira, G. and Y. M. Yamashita (2012). "Fly meets yeast: Checking correct orientation of cell division". In: *Trends in Cell Biology* 21.9 (2012), pp. 526–533.

Phillips, R. A., J. L. Hunter, J. F. Eccleston, and M. R. Webb (2003). "The mechanism of Ras GTPase activation by neurofibromin". In: *Biochemistry* 42.13 (2003), pp. 3956–65.

Planas-Silva, M. D. and R. A. Weinberg (1997). "The restriction point and control of cell proliferation". In: *Current Opinion in Cell Biology* 9 (1997), pp. 768–72.

Pruyne, D. and A. Bretscher (2000). "Polarization of cell growth in yeast. I. Establishment and maintenance of polarity states". In: *Journal of Cell Science* 11 (2000), pp. 365–75.

Queralt, E., C. Lehane, B. Novak, and F. Uhlmann (2006). "Downregulation of PP2A-Cdc55 phosphatase by separase initiates mitotic exit in budding yeast". In: *Cell* 125 (2006), pp. 719–32.

Rao, C. V., D. M. Wolf, and A. P. Arkin (2002). "Control, exploitation and tolerance of intracellular noise". In: *Nature* 420 (2002), pp. 231–7.

Rudoni, S., S. Colombo, P. Coccetti, and E. Martegani (2001). "Role of guanine nucleotides in the regulation of the Ras/cAMP pathway in Saccharomyces cerevisiae". In: *Biochimica et biophysica acta* 1538 (2001), pp. 181–9.

Sackmann, A., M. Heiner, and I. Koch (2006). "Application of Petri net based analysis techniques to signal transduction pathways". In: *BMC Bioinformatics* 7 (2006), p. 482.

Samoilov, M. S. and A. P. Arkin (2006). "Deviant effects in molecular reaction pathways". In: *Nature Biotechnology* 24.10 (2006), pp. 1235–40.

Scheffzek, K., M. R. Ahmadian, and A. Wittinghofer (1998). "GTPase-activating proteins: helping hands to complement an active site." In: *Trends in Biochemical Sciences* 23.7 (1998), pp. 257–62.

Schlosshauer, M. and D. Baker (2004). "Realistic protein-protein association rates from a simple diffusional model neglecting long-range interactions, free energy barriers, and landscape ruggedness". In: *Protein Science* 13.6 (2004), pp. 1660–69.

Schreiber, G. (2002). "Kinetic studies of protein-protein interactions". In: *Current Opinion in Structural Biology* 12.1 (2002), pp. 41–47.

Sear, R. P. and M. Howard (2006). "Modeling dual pathways for the metazoan spindle assembly checkpoint". In: *Proceedings of the National Academy of Sciences of the United States of America* 103.45 (2006), pp. 16758–63.

Segal, M. and K. Bloom (2001). "Control of spindle polarity and orientation in Saccharomyces cerevisiae". In: *Trends in Cell Biology* 11.4 (2001), pp. 160–166.

Shah, J. V. and D. W. Cleveland (2000). "Waiting for Anaphase : Mad2 and the Spindle Assembly Checkpoint". In: *Cell* 103 (2000), pp. 997–1000.

Shirayama, M., Y. Matsui, K. Tanaka, and A. Toh-E (1994). "Isolation of a CDC25 family gene, MSI2/LTE1, as a multicopy suppressor of ira1". In: *Yeast* 10.4 (1994), pp. 451–61.

Shirayama, M., Y. Matsui, and A. Toh-E (1994). "The Yeast TEM1 Gene, Which Encodes a GTP-Binding Protein, Is Involved in Termination of M Phase". In: *Molecular and Cellular Biology* 14.11 (1994), pp. 7476–82.

Siller, K. H. and C. Q. Doe (2009). "Spindle orientation during asymmetric cell division". In: *Nature Cell Biology* 4.11 (2009), pp. 365–73.

Simanis, V. (2003). "Events at the end of mitosis in the budding and fission yeasts". In: *Journal of Cell Science* 116 (2003), pp. 4263–4275.

Simonetta, M., R. Manzoni, R. Mosca, M. Mapelli, L. Massimiliano, M. Vink, B. Novak, A. Musacchio, and A. Ciliberto (2009). "The influence of catalysis on Mad2 activation dynamics". In: *PLoS Biol* 7.1 (2009), e10.

Singhania, R., R. M. Sramkoski, J. W. Jacobberger, and J. J. Tyson (2011). "A hybrid model of mammalian cell cycle regulation." In: *PLoS Computational Biology* 7.2 (2011), e1001077.

Sironi, L., M. Mapelli, S. Knapp, A. De Antoni, K.-T. Jeang, and A. Musacchio (2002). "Crystal structure of the tetrameric Mad1-Mad2 core complex: implica-

tions of a 'safety belt' binding mechanism for the spindle checkpoint". In: *The EMBO Journal* 21.10 (2002), pp. 2496–506.

Siu, K. T., M. R. Rosner, and A. C. Minella (2012). "An integrated view of cyclin E function and regulation". In: *Cell Cycle* 11.1 (2012), pp. 57–64.

Sivaram, M. V. S., T. L. Wadzinski, S. D. Redick, T. Manna, and S. J. Doxsey (2009). "Dynein light intermediate chain 1 is required for progress through the spindle assembly checkpoint". In: *The EMBO Journal* 28.7 (2009), pp. 902–14.

Sohrmann, M., S. Schmidt, I. Hagan, and V. Simanis (1998). "Asymmetric segregation on spindle poles of the Schizosaccharomyces pombe septum-inducing protein kinase Cdc7p". In: *Genes & Development* 12.1 (1998), pp. 84–94.

Sprang, S. R. (1997). "G proteins, effectors and GAPs: structure and mechanism". In: *Current Opinion in Structural Biology* 7 (1997), pp. 849–56.

Stegmeier, F. and A. Amon (2004). "Closing mitosis: the functions of the Cdc14 phosphatase and its regulation". In: *Annual Review of Genetics* 38 (2004), pp. 203–32.

Stern, B. M. and A. W. Murray (2001). "Lack of tension at kinetochores activates the spindle checkpoint in budding yeast". In: *Current Biology* 11 (2001), pp. 1462–7.

Steuer, R. (2004). "Effects of stochasticity in models of the cell cycle: from quantized cycle times to noise-induced oscillations". In: *Journal of Theoretical Biology* 228.3 (2004), pp. 293–301.

Straight, A. F. and C. M. Field (2000). "Microtubules, membranes and cytokinesis". In: *Current Biology* 10.20 (2000), R760–R770.

Sudakin, V., G. K. T. Chan, and T. J. Yen (2001). "Checkpoint inhibition of the APC/C in HeLa cells is mediated by a complex of BUBR1, BUB3, CDC20, and MAD2". In: *Journal of Cell Biology* 154.5 (2001), pp. 925–36.

Sudakin, V., D. Ganoth, A. Dahan, H. Heller, J. Hershko, F. C. Luca, J. V. Ruderman, and A. Hershko (1995). "The cyclosome, a large complex containing cyclin-selective ubiquitin ligase activity, targets cyclins for destruction at the end of mitosis." In: *Molecular biology of the cell* 6 (1995), pp. 185–97.

Sullivan, M. and D. O. Morgan (2007). "Finishing mitosis, one step at a time". In: *Nature Reviews Molecular Cell Biology* 8.11 (2007), pp. 894–903.

Tanaka, T. U., M. J. R. Stark, and K. Tanaka (2005). "Kinetochore capture and bi-orientation on the mitotic spindle." In: *Nature Reviews Molecular Cell Biology* 6.12 (2005), pp. 929–42.

Tóth, A., E. Queralt, F. Uhlmann, and B. Novák (2007). "Mitotic exit in two dimensions". In: *Journal of Theoretical Biology* 248 (2007), pp. 560–73.

Tucker, J., G. Sczakiel, J. Feuerstein, J. John, R. S. Goody, and A. Wittinghofer (1986). "Expression of p21 proteins in Escherichia coli and stereochemistry of the nucleotide-binding site". In: *The EMBO journal* 5.6 (1986), pp. 1351–8.

Tyson, J. J. (1991). "Modeling the cell division cycle: cdc2 and cyclin interactions". In: *Proceedings of the National Academy of Sciences of the United States of America* 88 (1991), pp. 7328–32.

Tyson, J. J., K. C. Chen, and B. Novak (2003). "Sniffers, buzzers, toggles and blinkers: dynamics of regulatory and signaling pathways in the cell". In: *Current Opinion in Cell Biology* 15.2 (2003), pp. 221–31.

Tyson, J. J. and B. Novák (2010). "Functional motifs in biochemical reaction networks." In: *Annual Review of Physical Chemistry* 61 (2010), pp. 219–40.

Valerio-Santiago, M. and F. Monje-Casas (2011). "Tem1 localization to the spindle pole bodies is essential for mitotic exit and impairs spindle checkpoint function". In: *The Journal of Cell Biology* 192.4 (2011), pp. 599–614.

Vetter, I. R. and A. Wittinghofer (2001). "The guanine nucleotide-binding switch in three dimensions". In: *Science (New York, N.Y.)* 294.5545 (2001), pp. 1299–304.

Vink, M. *et al.* (2006). "In vitro FRAP identifies the minimal requirements for Mad2 kinetochore dynamics". In: *Current Biology* 16.8 (2006), pp. 755–66.

Vinod, P. K., P. Freire, A. Rattani, A. Ciliberto, F. Uhlmann, and B. Novák (2011). "Computational modeling of mitotic exit in budding yeast: the role of separase and Cdc14 endocycles". In: *Journal of the Royal Society Interface* 8.61 (2011), pp. 1128–41.

Visintin, R. and A. Amon (2001). "Regulation of the Mitotic Exit Protein Kinases Cdc15 and Dbf2". In: *Mol. Biol. Cell* 12.10 (2001), pp. 2961–2974.

Wang, Y., F. Hu, and S. J. Elledge (2000). "The Bfa1/Bub2 GAP complex comprises a universal checkpoint required to prevent mitotic exit". In: *Current Biology* 10.21 (2000), pp. 1379–1382.

Weaver, B. A. and D. W. Cleveland (2008). "The aneuploidy paradox in cell growth and tumorigenesis". In: *Cancer Cell* 14.6 (2008), pp. 431–3.

Weinberg, R. A. (1995). "The retinoblastoma protein and cell cycle control". In: *Cell* 81 (1995), pp. 323–30.

Weng, G., U. S. Bhalla, and R. Iyengar (1999). "Complexity in Biological Signaling Systems". In: *Science* 284.April (1999), pp. 92–96.

Westerhoff, H. V. and B. O. Palsson (2004). "The evolution of molecular biology into systems biology". In: *Nature biotechnology* 22.10 (2004), pp. 1249–52.

Westermann, S., D. G. Drubin, and G. Barnes (2007). "Structures and functions of yeast kinetochore complexes". In: *Annual Review of Biochemistry* 76 (2007), pp. 563–91.

Willems, A. R., T. Goh, L. Taylor, I. Chernushevich, A. Shevchenko, and M. Tyers (1999). "SCF ubiquitin protein ligases and phosphorylation-dependent proteolysis". In: *Philosophical Transactions of the Royal Society of London B* 354 (1999), pp. 1533–50.

Wittmann, T., A. Hyman, and A. Desai (2001). "The spindle: a dynamic assembly of microtubules and motors". In: *Nature cell biology* 3.1 (2001), E28–34.

Wollman, R., E. N. Cytrynbaum, J. T. Jones, T. Meyer, J. M. Scholey, and A. Mogilner (2005). "Efficient chromosome capture requires a bias in the 'search-and-capture' process during mitotic-spindle assembly". In: *Current Biology* 15.9 (2005), pp. 828–32.

Yeong, F. M., H. H. Lim, Y. Wang, and U. Surana (2001). "Early Expressed Clb Proteins Allow Accumulation of Mitotic Cyclin by Inactivating Proteolytic Machinery during S Phase". In: *Molecular and Cellular Biology* 21 (2001), pp. 5071–81.

Yoshida, S., R. Ichihashi, and A. Toh-e (2003). "Ras recruits mitotic exit regulator Lte1 to the bud cortex in budding yeast." In: *The Journal of cell biology* 161.5 (2003), pp. 889–97.

Yu, H. (2002). "Regulation of APC-Cdc20 by the spindle checkpoint". In: *Current Opinion in Cell Biology* 14.6 (2002), pp. 706–14.

Zhou, B.-B. S. and S. J. Elledge (2000). "The DNA damage response: putting checkpoints in perspective". In: *Nature* 408 (2000), pp. 433–439.